Characterization and Modeling of the Ionomer-Conductor Interface in Ionic Polymer Transducers

by

Barbar J. Akle

Dissertation submitted to the Faculty of the
Virginia Polytechnic Institute and State University
in partial fulfillment of the requirements for the degree of

Doctor of Philosophy

in

Mechanical Engineering

Donald J. Leo, Chair
Daniel Inman
James E. McGrath
Timothy E. Long
Pavlos Vlachos
Zoubeida Ounaies

July 2005

Blacksburg, Virginia

Keywords: Ionic Polymer, Transducer, Actuator, Sensor, Electric double layer, Capacitor.

Copyright 2005

Characterization and Modeling of the Ionomer-Conductor Interface in Ionic Polymer Transducers

Barbar J. Akle, Ph.D.
Virginia Polytechnic Institute and State University, 2005
Advisor: Donald J. Leo

Abstract

Ionomeric polymer transducers consist of an ion-exchange membrane plated with conductive metal layers on its outer surfaces. Such materials are known to exhibit electromechanical coupling under the application of electric fields and imposed deformation (Oguro et al., 1992; Shahinpoor et al., 1998). Compared to other types of electromechanical transducers, such as piezoelectric materials, ionomeric transducers have the advantage of high-strain output ($> 9\%$ is possible), low-voltage operation (typically less than 5 V), and high sensitivity in the charge-sensing mode.

A series of experiments on actuators with various ionic polymers such as Nafion and novel poly(Arylene ether disulphonate) systems (BPS and PATS) and electrode composition demonstrated the existence of a linear correlation between the strain response and the capacitance of the material. This correlation was shown to be independent of the polymer composition and the plating parameters. Due to the fact that the low-frequency capacitance of an ionomer is strongly related to charge accumulation at the electrodes, this correlation suggests a strong relationship between the surface charge accumulation and the mechanical deformation in ionomeric actuators. The strain response of water-hydrated transducers varies from 50 μstrain/V to 750 μstrain/V at 1Hz, while the strain-to-charge response is between 9 $\frac{\mu strain}{\frac{C}{m^2}}$ and 15

$\frac{\mu strain}{\frac{C}{m^2}}$. This contribution suggests a strong correlation between cationic motion and the strain in the polymer at the ionomer-conductor interface.

A novel fabrication technique for ionic polymer transducers was developed for this dissertation for the purpose of quantifying the relationship between electrode composition and transducer performance. It consists of mixing an ionic polymer dispersion (or solution) with a fine conducting powder and attaching it to the membrane as an electrode. The Direct Assembly Process (DAP) allows the use of any type of ionomer, diluent, conducting powder, and counter ion in the transducer, and permits the exploration of any novel polymeric design. Several conducting powders have been incorporated in the electrode including single-walled carbon nanotubes (SWNT), polyaniline (PANI) powders, high surface area RuO_2, and carbon black electrodes. The DAP provided the tool which enabled us to study the effect of electrode architecture on performance of ionic polymer transducers. The DAP allows the variation in the electrode architecture which enabled us to fabricate dry transducers with 50x better performance compared to transducers made using the state of the art impregnation-reduction technique. DAP fabricated transducers achieved a strain of 9.4% at a strain rate of 1%/s. Each electrode material had an optimal concentration in the electrode. For RuO_2, the optimal loading was approximately 45% by volume. This study also demonstrated that carbon nanotubes electrodes have an optimal performance at loadings around 30 vol%, while PANI electrodes are optimized at 95 vol%.

Extensional actuation in ionic polymer transducers was first reported and characterized in this dissertation. An electromechanical coupling model presented by Leo et al. (2005) defined the strain in the active areas as a function of the charge. This model assumed a linear and a quadratic term that produces a nonlinear response for a sine wave actuation input. The quadratic term in the strain generates a zero net bending moment for ionic polymer transducers with symmetric electrodes, while the linear term is canceled in extensional actuation for symmetric electrodes. Experimental results demonstrated strains on the order of 110 μstrain in the thickness direction compared to 1700 μstrain peak to peak on the external fibers for the same

transducer, could be achieved when it is allowed to bend under +/-2V potential at 0.5 Hz. Extensional and bending actuation in ionic polymer transducers were explained using a bimorph active area model. Several experiments were performed to compare the bending actuation with the extensional actuation capability. The active area in the model was assumed to be the high surface area electrode. Electric double layer theory states that ions accumulate in a thin boundary layer close to the metal-polymer interface. Since the metal powders are evenly dispersed in the electrode area of the transducer, this area is expected to actuate evenly upon voltage application. This active area model emphasizes the importance the boundary layer on the conductor-ionomer interfacial area.

Computing model parameters based on experimental results demonstrated that the active areas model collapses the bending data from a maximum variation of 200% for the strain per charge, to less than 68% for the model linear term. Furthermore, the model successfully predicted bending response from parameters computed using thickness experimental results. The prediction was particularly precise in estimating the trends of non-linearity as a function of the amount of asymmetry between the two electrodes.

To my parents,

Jawad and Nazira,

my brothers Etienne and Simon,

and my sister and brother in law Angele and Jose Antonio

Acknowledgments

First I would like to thank my advisor, Dr. Donald J. Leo, for his help and patience throughout my graduate studies. His guidance and complete support made my working and learning experience, a very special one. Also, I want to extend my thanks to Dr. Daniel Inman, Dr. James McGrath, Dr. Timothy Long, Dr. Pavlos Vlachos, and Dr. Zoubeida Ounaies for their support and enthusiasm as members of my advisory committee. In addition, I want to thank my colleagues in the Center for Intelligent Material Systems and Structures. Also my great thanks to my research partners Matt Bennett, Kevin Farinholt, Curt Cothera. Also special thanks for Dr. Kenton Wiles, Dr. Michael Hickner, and Ali Etebary for the valuable collaborations. The Direct Assembly Process presented in this work is developed in collaboration with Dr. Kenton Wiles and the BPS and PATS were supplied by Dr. Michael Hickner. Both are members of Dr. James McGrath Group. I appreciate the support of the U.S. Army Research Laboratory and the U.S. Army Research Office under contract/grant number DAAD19-02-1-0275 Macromolecular Architecture for Performance (MAP) MURI.

Finally, I would like to express my deep gratitude to the support I received from my friends and my greatest appreciation to the love and support provided by my parents, my brothers, my sister and brother in law during my years at Virginia Tech.

Barbar J. Akle

Contents

Abstract ii

Acknowledgments vi

List of Tables xi

List of Figures xiii

Chapter 1 Introduction and Literature Review 1

1.1 Introduction 1

1.2 Smart Materials: The Big Picture 2

1.3 Ionic Polymer Transducers 7

1.3.1 Background 7

1.3.2 Actuation Mechanisms and Models 8

1.4 Electroactive Polymers and the Need for Large Displacement Actuators 11

1.5 Potential Applications of Ionic Polymer Transducers 12

1.6 Motivation 13

1.7 Percolation Process 14

1.8 Electric Double Layer 15

1.8.1 The Helmholtz model 16

1.8.2 The Gouy-Chapman model 17

1.8.3 Stern and Grahame models 18

1.8.4 Bockris, Devanathan, and Muller (BDM) models 19

1.9 Pseudocapacitance 19

1.9.1 Adsorption 20
1.9.2 Redox pseudocapacitance 21
1.10 Electromechanical Coupling Models 22
1.11 Objectives 22
1.12 Contributions 23
1.13 Document Organization 24

Chapter 2 Experimental Methodologies **27**
2.1 Electromechanical Characterization: Bending 28
2.2 Electromechanical Characterization: Extensional 32
2.2.1 Extensional Test Fixture Calibration 33
2.3 Ionic and Electric Conductivity Measurements 34
2.3.1 Complex Plane Frequency Response 34
2.4 Ionomers 34
2.5 Traditional Fabrication Methods of Ionic Polymer Transducers 36
2.5.1 Impregnation-Reduction Process 37
2.5.2 Variations to the Impregnation-Reduction Method 39
2.6 Direct Assembly Process (DAP) 39
2.6.1 Direct Assembly Process with Dry Membranes 40
2.6.2 Direct Assembly Process with Solvated Membranes 44
2.7 Electrode Materials 45
2.7.1 Carbon black 46
2.7.2 Single-Walled Carbon Nanotubes 47
2.7.3 Conducting polymers 48
2.7.4 Metal oxides 49
2.7.5 Platinum 50
2.7.6 Gold Flakes 51
2.8 Electrode Morphology 51
2.9 Conclusion 53

Chapter 3 Correlation of Capacitance and Actuation in Ionic Polymer Transducers **55**

3.1 Surface Charge Accumulation in Ionomeric Materials 56

3.1.1 Transducer Preparation 59

3.2 Experimental Results 61

3.3 Discussion of Results 62

3.4 Conclusions 67

Chapter 4 Optimization of the Direct Assembly Process **69**

4.1 Ionic liquids and Organic diluents 70

4.2 Effect of Electrode Thickness on Actuation Response 72

4.3 Conducting Electrode Material 74

4.4 Ruthenium dioxide - Gold hybrids 74

4.4.1 Variation of Metal Content by Weight 75

4.4.2 Variation of Metal Content by Volume 76

4.4.3 RuO_2 - Gold Electrode Optimization 78

4.5 Optimization of Conductor Powder Concentration in the Electrode . 80

4.5.1 Hybrid Conductors/Ionic Polymer Actuators 84

4.6 Electrical and Mechanical Property Characterization 86

4.6.1 Electrical Properties Characterization 86

4.6.2 Mechanical Damping 87

4.7 Reliability of the DAP Method 88

4.8 Conclusions 90

Chapter 5 Extensional and Bending Model **92**

5.1 Modeling 93

5.1.1 Active Areas Model: Simplified Bending 94

5.1.2 Active Areas Model: Extensional model 97

5.1.3 Active Areas Model: Bending with Electrostatic Expansion Term 99

5.2 Model Simulations 100

5.3 Experimental Results 102

5.3.1 Simplified Bending Model: FRF Analysis 102
5.3.2 Extensional Actuation Results 104
5.3.3 Bending with Electrostatic Expansion Term 106
5.4 Discussion and Model Verification 108
5.4.1 Dependency on the Potential 108
5.4.2 Model Discussion and Trends 109
5.5 Conclusions 111

Chapter 6 Summary and Conclusions **113**
6.1 Dissertation Summary 113
6.2 Contributions 116
6.3 Future Work 117
6.4 Conclusions 117

Bibliography **119**

Vita **129**

List of Tables

1.1 Summary of the advantages and disadvantages of each model with the corresponding capacitance. 20

2.1 Diluent uptake as a function of diluent composition, temperature, and duration. The composition present the volume of N-methylformmaide to the total volume of EmI-Tf and N-methylformamide. The last column presents the formamide vol% of the mixture in the membrane before evaporating the co-diluent. 43

3.1 Properties of Nafion, BPS, and PATS Copolymers. 59

3.2 Fully hydrated transducer thickness, optimal reducing agent concentration, and platinum layers surface conductivity before and after electroplating for each ionomer. 60

3.3 Values for the stiffness and the Young Modulus estimated using equation 2.9. 62

3.4 Microstrain per normalized charge for various ionomer actuators. 68

4.1 Strain rate of ionic polymer transducers with different diluents. Physical properties of the diluents are provided. 72

4.2 Physical and electrochemical properties of electrode conducting materials . 74

4.3 Weights of Au and RuO_2 mixed with 0.5 g of 5% Nafion solution and 0.5g Glycerol. It also presents the durations of sample hot-pressing. The densities of Au and RuO_2 are assumed to be 19300 Kg/m^3 and 7050Kg/m^3 respectively. 78

4.4 Weights of Au and RuO_2 mixed with 0.5g of 5% Nafion^{TM} solution and 0.5g Glycerol for electrode optimization. 79
4.5 Conductor/ionomer surface area in th electrode, and the corresponding peak strain. 83
4.6 Peak strain and strain rate of five actuators built for the SWNT/RuO_2 hybrid experiment. 85
4.7 Mechanical properties of five actuators fabricated for the SWNT/RuO_2 hybrid experiment. 89

5.1 Thickness measurements of the upper electrode, polymer substrate, and lower electrode for samples S1 through S7. 103
5.2 Stiffness of four samples computed from the natural frequencies and directly from the fixed-sliding beam experiment. 104
5.3 Thickness measurements of the upper electrode, polymer substrate, and lower electrode for samples L1 through L6. 107

List of Figures

1.1 Schematic representation of the transduction mechanisms in ionic polymer transducers, also shown is the cluster of anions (-) and the cations (+) free to move. 2

1.2 Energy density plot of several electroactive polymers. 3

1.3 Unimorph and bimorph induced strain actuation. 4

1.4 Actuation of a dielectric elastomer under the application of large electric potential 5

1.5 Ionomer-Conductor interface, (a) SEM of an ionic polymer transducer electrode, (b)Diffusion of electrons through the conductive particles, (c)Diffusion of cations through the ionomer electrolyte, and (d)Formation of the electric double layer around the particles. 10

1.6 Electric double layer models (a)Helmholtz model, (b)Gouy-Chapman, (c)Stern, and (d)Bockris, Devanathan, and Muller (BDM) model . . . 17

2.1 The experimental setup used to for the electromechanical measurements. . 28

2.2 Experimental setup used for the extensional electromechanical measurements. 32

2.3 (a) Stress amplitude generated by the piezoceramic transducer under 75kV/m electric field. time response of the piezoceramic under 75kV/m sine wave of 0.5Hz frequency. 33

2.4 The complex plane representation of a simple electrostatic double layer, and a double layer with leakage resistance. 35

2.5 The complex plane representation of a simple electrostatic double layer, and a double layer with leakage resistance. 36

2.6 (a)Chemical Structure of Nafion, (b)Chemical Structure of BPS, (c)Chemical Structure of PATS. 37
2.7 Schematic showing the reduction of platinum on the surface forming the electrode of the ionic polymer transducer 38
2.8 Schematic showing the four steps Direct Assembly Process (DAP) for building dry transducers. 41
2.9 Schematic showing the four steps Direct Assembly Process (DAP) for building solvated transducers. 46
2.10 Charge and discharge redox mechanism of conducting polymers . . . 49
2.11 Scanning electron microscopy (SEM) showing (a) the top cross-section of a Nafion 117 plated with platinum following 6 layers of impregnation-reduction, and (b) the top cross-section of a Nafion 117 ionomer painted with 6 layers of RuO_2 and Nafion mix . Also shown in (b) is the platinum interface between the painted layer and the electroplated gold overlayer. 52
2.12 Scanning electron microscopy (SEM) showing (a) the top cross-section of a Nafion 117 ionomer painted with a 9.5 μm RuO_2 / Nafion electrode. (b) shows the top cross-section of a Nafion 117 ionomer painted with a 38 μm RuO_2 / Nafion electrode. 53
2.13 Scanning electron microscopy (SEM) SEM images of the high surface area RuO_2 electrode with (a) 22, (b) 30, (c) 36, and (d) 66 Vol % metal. 54

3.1 Real and complex permitivities of a typical Nafion-based ionic polymer transducer. 57
3.2 Blocking electrode model using a resistor and two capacitors in series. 58
3.3 Stain per unit volt of the BPS and PATS transducers compared to Nafion. 61
3.4 Blocked force per unit volt of the BPS and PATS polymers compared to Nafion. 63
3.5 Impedance of the novel polymers compared to Nafion. 64
3.6 Real and imaginary FRF of the capacitance per cm^2 of the different BPS and PATS actuators to Nafion. 65

3.7 Normalized microstrain per unit charge and normalized microstrain per unit volt for several ionomer transducers. 66
3.8 MicroStrain vs. capacitance/cm^2 of each polymer a) at 1Hz, b) at 5Hz, c) at 10 Hz, and d) at 15Hz. 67

4.1 (a) Measured response due to a 2V step change in potential for actuators with RuO_2 electrodes and Formamide or EmI-Tf diluents. (b) Strain rate as a function volume uptake ionic liquid. 71
4.2 Capacitance per area FRF of 3 transducers with 10, 20, and 30 layers of 2.5:1 RuO_2 electrode. 73
4.3 (a) Strain response of four samples with different electrode thickness due to a 2V step input. (b) Peak strain as a function of electrode thickness. . . . 73
4.4 (a) Strain response as a function of electrode composition by weight, (b) Electrical impedance as a function of electrode composition by weight, (c) Strain response as a function of electrode composition by volume, and (d) Electrical impedance as a function of electrode composition by volume. . . 76
4.5 (a) Strain per unit charge/area for the samples produced by variation in the metal content with consistent volume, (b) Strain output to the application of square wave potentials of +/- 2 V. 77
4.6 Strain per volt frequency response for three RuO_2 samples. 79
4.7 Deflected shapes as a function of amplitude for a square wave potential input. 80
4.8 (a) Strain rate as a function of RuO_2 volume % in the electrode. Conductivity of the electrode as a function of RuO_2 volume % in the electrode. . 81
4.9 Strain rate as a function of carbon nanotube and polyaniline loading (volume %) in the electrode. 82
4.10 (a) Strain response due to a 2V step change in potential for samples with 10% RuO_2 and 10% SWNT. (b) Strain response due to a 2V step change in potential for samples with 40% RuO_2 and 40% SWNT. 83
4.11 Strain response due to a 2V step change in potential for samples with 45% RuO_2, 45% SWNT, and 85% PANI. 84

4.12 (a) Strain response due to a 2V step change in potential for samples with 10% SWNT, 45% SWNT, 35% RuO_2, 45% RuO_2 and a mix of 10% SWNT with 35% RuO_2. (b) Strain response due to a 2V step change in potential for samples with 85% PANI, 50% PANI with 35% RuO_2, and 50% PANI with 35% SWNT. 85
4.13 (a) Response to a 2V step for transducers with 45vol % RuO_2 and 45vol% SWNT. (b) Corresponding current response. 86
4.14 (a) Capacitance frequency response functions of transducers with 45vol % RuO_2 and 45vol% SWNT. (b) Capacitance frequency response functions of transducers with 85vol% PANI, 50%vol PANI + 35vol % RuO_2, and 50vol% PANI + 35vol% SWNT. 87
4.15 (a) Strain per volt frequency response functions of transducers with 45vol % RuO_2 and 45vol% SWNT. (b) Micro-Strain per charge per area frequency response functions of transducers with 45vol % RuO_2 and 45vol% SWNT. (c) Micro-Strain per volt frequency response functions of transducers with 85vol% PANI, 50%vol PANI + 35vol % RuO_2, and 50vol% PANI + 35vol% SWNT. (d) Strain per charge per area frequency response functions of transducers with 85vol% PANI, 50%vol PANI + 35vol % RuO_2, and 50vol% PANI + 35vol% SWNT. 88
4.16 microstrain per volt frequency response for three pure RuO_2 samples. . . 89
4.17 Reliability test on the three samples with +/-1V, +/-2V, +/-3V 1Hz sine wave applied on samples 1, 2, and 3 respectively. 90

5.1 Bending and extensional actuation in a bimorph model of ionic polymer transducers. 93
5.2 Schematic of a typical electrode in an ionic polymer transducer showing the particles surrounded by a charged sphere of ionomer. 94
5.3 Schematic of an asymmetric transducer with an electrode on one side, where y_b represents the distance toward the neutral axis 95

5.4 Schematic of the three-layered ionic polymer transducer in thickness configuration. 98
5.5 (a) Model simulation of the microstrain time response of three samples with different electrode configurations in bending mode. (b) Power spectrum of the time response. 100
5.6 (a) Model simulation of the forcing time response of three samples with different electrode configurations in extensional mode. (b) Power spectrum of the time response. 101
5.7 1st Harmonic/ Fundamental frequency response as a function of electrode symmetry in bending and extensional modes. 102
5.8 Modulus calibration of samples 103
5.9 (a) FRF of the strain per volt, (b) FRF of the strain per charge per area, and (c) FRF of the α computed from the simplified bending moment model. 105
5.10 Values of the α and β for the model to fit the experimental data for seven different ionic polymer transducers in the frequency range of 0.5 to 10Hz. . 106
5.11 (a) Typical blocked pressure response and model fit for a sample with 25μm electrodes on each side on a 180 μm membrane, actuated with a 2V 0.5Hz sine wave. (b) Measured and model prediction psd for the same sample. . 107
5.12 (a) Experimental ratio of the 1st harmonic to the fundamental frequency in the strain response under 2V sine waves (b) The distortion ratio in extensional actuation (c) Model prediction of this ratio 108
5.13 Experimental and modeling of a two sided transducer time response due to 2V 0.5Hz sine wave in bending. 109
5.14 (a)Values for α under 1V (b) Values for β under 1V (c) Values for α under 2V (d) Values for β under 2V 110
5.15 (a) Ratio of the 1st harmonic to the fundamental frequency in the strain response under 1V sine wave, and (b) 2V sine wave 111
5.16 Charge density profile in a cross section of an ionic polymer transducer at low frequency and high frequency. 111

Chapter 1

Introduction and Literature Review

1.1 Introduction

Smart materials are a class of materials that exhibit coupling between two or more physical domains. Electromechanical transducers are a subset of smart materials that exhibit coupling between the electrical and mechanical domains as sensors or actuators. Electromechanically coupled polymers also known as ElectroActive Polymers (EAP) are a soft and flexible class of transducers. In this dissertation we have studied a specific type of EAP, the ionic polymer transducer.

Also known as ionomeric polymer transducers, they consist of an ion-exchange membrane plated with conductive metal layers on the outer surfaces. Such materials are known to exhibit electromechanical coupling under the application of electric fields and imposed deformation (Oguro et al., 1992; Shahinpoor et al., 1998). Compared to other types of electromechanical transducers, such as piezoelectric materials, ionomeric transducers have the advantage of high-strain output ($> 9\%$ is possible), low-voltage operation (typically less than 5 V), and high sensitivity in the charge-sensing mode. The electromechanical coupling in ionomeric polymer transducers is thought to be due to the mobility of cations in the polymer network as shown in Figure 1.1.

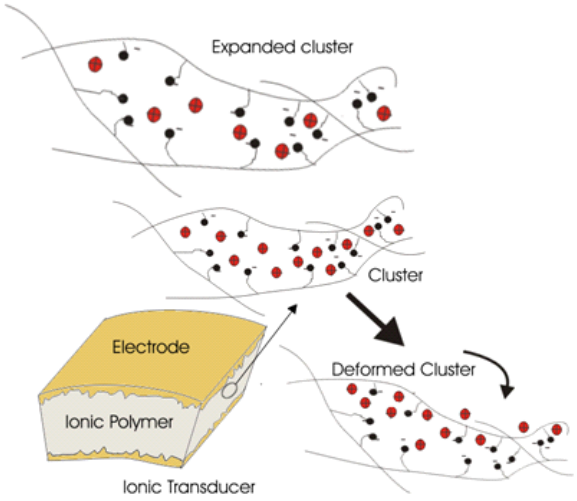

Figure 1.1: Schematic representation of the transduction mechanisms in ionic polymer transducers, also shown is the cluster of anions (-) and the cations (+) free to move.

In this dissertation we studied and modeled the electrode area in ionic polymer transducers and more specifically the conductor-ionomer interface. A new fabrication process was developed which provided good control on the architecture of the electrode. The new process was optimized to enhance the performance of ionic polymer transducers by increasing the generated strain and strain rate. A model that assumes the electrode as the active area is presented in this thesis. Finally, we report and characterize extensional actuation, which is according to our knowledge the first account reported for such transduction mechanism in ionomeric polymer transducers.

1.2 Smart Materials: The Big Picture

Smart materials are defined as materials that adapt to a change in the physical environment, such as electrical, thermal, magnetic, chemical, pH, or light environment. They can be used in the form of sensors, actuators, active dampers, and energy generators (Leo, 2001). In the area of control engineering we are interested mostly in electromechanical transducers. Materials known to demonstrate electromechanical coupling properties include piezo-ceramics, piezo-polymers, electrostrictive polymers,

ionic polymers, conducting polymers, liquid crystal elastomers, carbon nanotubes, and ionic gels. Other thermomechanically coupled smart materials which are actuated electrically using the resistive properties of the material are shape memory polymers and shape memory alloys. AOne noted that those electroactive materials exist in the liquid, gel, polymer, ceramic, or metal form. Observing Figure 1.2 one

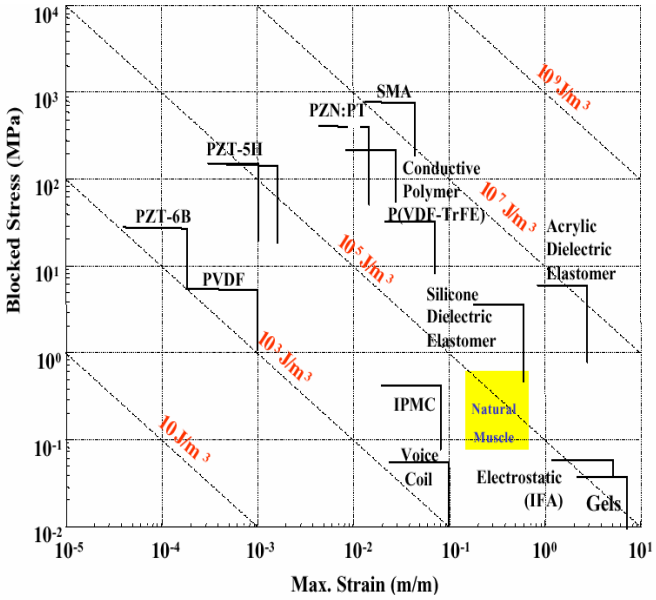

Figure 1.2: Energy density plot of several electroactive polymers.

would conclude that shape memory alloys (SMA) or the dielectric elastomers are better transducers. However, energy density plots do not present the full characteristics of the actuators. Other figures of merit should be considered in assessing the usability of a certain smart material in potential applications. Figures of merit includes generated strain and stress that are represented in the energy density plot in Figure 1.2. In order to amplify the strain of some of the transducer materials, uniform and bimorph configurations are used as shown in Figure 1.3 (Leo et al., 2003). These configuration are widely used in piezoelectric polymer benders and piezoceramics thunder benders (Zhang, 1998) such as bimorph and unimorph respectively. Strain is defined as the deformation per unit length of the material, sometimes in literature strain is confused by defining it as "the displacement normalized by the original material length in the direction of actuation" (Madden et al., 2004). For a bimorph and unimorph

the strain is computed using continuum mechanics as elaborated in Leo et al. (2003). Other important transducer properties are the strain rate, work and power densities, reliability, efficiency and operating voltage.

SMAs are thermocoupled materials that deform due to phase transition upon the change in temperature. SMAs exhibit a shape memory effect in which the material remembers a previous shape and can be transitioned between shapes by heating and cooling the material (Liang and Rogers, 1992). Nickel Titanium (NiTi) alloys (better known as Nitinol) are the most extensively studied SMA materials (Funakubo, 1987). The actuation mechanism is due to the rearrangement of the molecular structure between a martensitic phase and an austenitic phase. SMAs have a very slow response (seconds to minutes) and are highly dependent on the temperature and thermal conductivity of the surrounding environment. The strain this material can provide is in the order of 5 to 8%, while the stress is as large as 200 MPa (Madden et al., 2004).

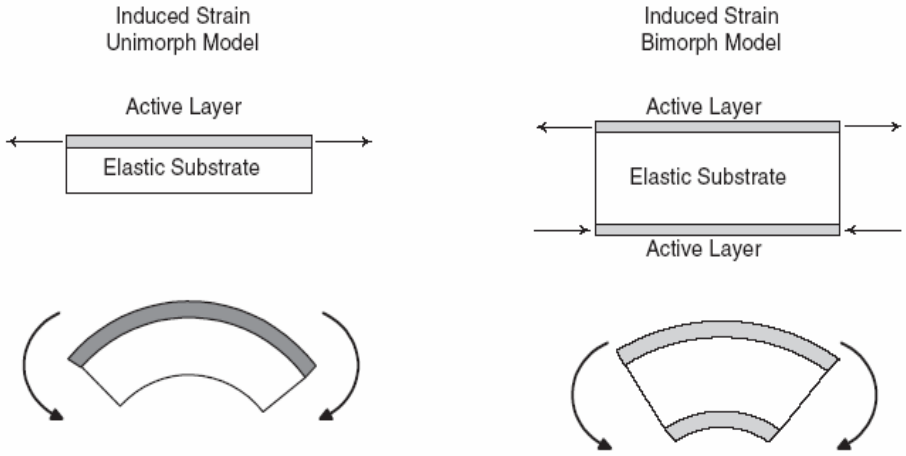

Figure 1.3: Unimorph and bimorph induced strain actuation.

Shape memory polymers are a novel class of smart polymeric material that undergo large thermally induced deformations ($>$ 100 % strain) that are analogous to heat shrink tubing (Lendlein and Langer, 2002). These transducers are limited to one cycle life time.

Piezoelectric materials also known as ferroelectric materials exists in the ceramic or polymeric structure. Examples of ceramic piezoelectric material is the PZT

(Lead Zirconate Titanate), while the commonly used copolymer is poly(vinylidene fluoride trifluoroethylene), abbreviated as P(VDF-TrFE) (Madden et al., 2004). The actuation mechanism occurs due to the rotation of the dipoles upon the application of an electric field (Cross and Rossetti, 1991). Dipoles in PVDF are due the large electronegativity of the fluorine in the polymer backbone (Bar-Cohen, 2001). In order to prepare an actuator, PVDF is poled at temperatures larger than the Curie point and quenched down while the electric field is still applied (Cheng et al., 2001). Piezo-materials operates at high frequencies, and piezoceramics provide large forces. The main disadvantage is the high operating voltage (in the order of 1kV) and small displacement which is amplified using bimorph or unimorph configuration as shown in Figure 1.3 (Madden et al., 2004).

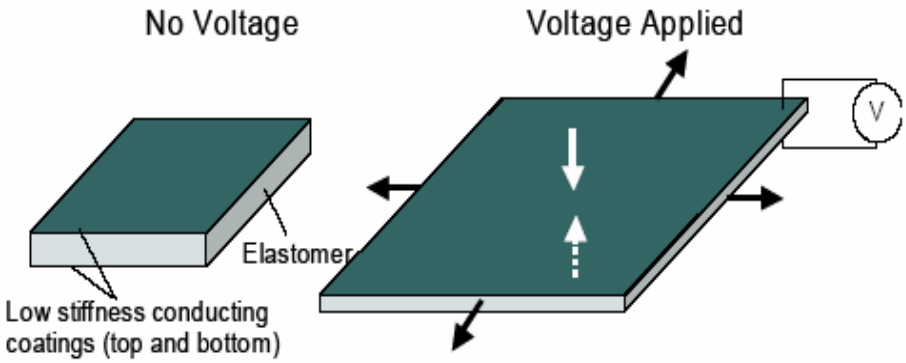

Figure 1.4: Actuation of a dielectric elastomer under the application of large electric potential

Dielectric elastomer actuators are made of a compliant polymer membrane sandwiched between two conductive electrodes(Bar-Cohen, 2001). The electrostatic attraction between the electrodes due to the application of a potential (150 MV/m) generates a pressure on the compliant polymer and cause the deformation as shown in Figure 1.4 (Kornbluh et al., 1999). Electrostrictive transducers have large displacement in the order of 380% for 3M VHB 4910 acrylic elastomer (Pelrine et al., 2000). Other advantages of this actuator is the easy manufacturing process and the large stresses depending on the stiffness of the elastomer used (Bar-Cohen, 2001). The main disadvantage of these actuators are the large operating voltages, the low

reliability and the fact that they also bend in one direction in cantilever form.

Liquid crystalline elastomers actuate upon inducing phase changes in liquid crystalline polymers that changes of order and alignment of liquid crystalline side chains, leading to a generated stresses in the polymer backbone(de Gennes and Seances, 1975). Those materials are still in their early stage of development, but the main disadvantage would reside in relatively high operating voltage (1.5 MV/m) and low stiffness.

Conducting polymers are electronically conducting organic materials having conjugated structures in their molecular backbone. Applying an electric potential will change the oxidation state leading to the addition or removal of charge from the polymer backbone and a flux of ions to balance the charge. Insertion of ions between polymer chains is the primary reason for actuation of the material (Madden et al., 2004). Conducting polymers are attractive transducers due to the large deformations under relatively small voltages. The main disadvantages of conducting polymers is their slow response time, and low electro-mechanical efficiency, and they also require an electrolyte to operate.

Ionic gels are very similar to ionic polymers previously introduced, except they have a gel polymer backbone. They produce larger strains compared to ionic polymers, but exhibit much slower response time. The disadvantages of this smart material is that it suffers from low mechanical strength and consequent structural failure under large deformations and therefore have a short lifetime (Osada et al., 1992).

Carbon nanotubes (CNT) are hollow cylinders consisting solely of carbon. These tubes are either conductive or semi-conductive. CNTs could be used as actuators when a voltage is applied to them against an electrode soaked in an electrolyte. The actuation mechanism is due to the motion of ions that are attracted to the nanotubes, leading to the accumulation of ionic charge at their surfaces, which is balanced by an electronic charge within the tubes (Baughman et al., 1999). The charging leads to a rearrangement of the electronic structure of the nanotubes, and to Coulombic forces, both of which result in dimensional changes. This is considered

to be a quantum mechanic actuation process (Baughman et al., 1999).

Electro-rheological fluids change their viscous properties upon the application of an electric field. This material is not as an actuator but rather as a fluid for active damping. The actuation mechanism is due to alignment of some particles in the fluid leading to a change in the shear rates (Lindler and Wereley, 1999).

Finally Polyethyleneoxide and Polyethyleneglycol (PEO-PEG) based ion conducting polymers are also used as actuators (Shahinpoor and Kim, 2002c). Those solid polymer electrolytes have been made of high molecular weight PEO mixed with some low molecular weight PEG (Gray, 1987). PEO-PEG actuators are large displacement (10% strain) low voltage (1 to 3V) diluent free actuators, with the disadvantage of low operating frequencies (10Hz) (Shahinpoor and Kim, 2002c). Moreover Watanabe et al. (2001) reported the use of Polyurethane-Polyethyleneglycol (PU-PEG) polymers as actuators. PU-PEG transducers shows electrostriction properties under large voltage (2MV/m). The bending direction of these actuators could be controlled by the species of the doped ions (Watanabe et al., 2001).

1.3 Ionic Polymer Transducers

In this section ionic polymer transducers will be thoroughly described, with a historical background, fabrication techniques, actuation mechanisms and models, current characterization methods, and finally potential applications.

1.3.1 Background

Polymer-metal composites were developed as early as the 1930's as precipitated of colloidal silver on prepared substrates (Bar-Cohen, 2001). In the early 1990's Sadeghipour, et al., reported that they could act as vibration sensors. Ionic polymers were developed as "solid polymer electrolyte fuel cell membranes" (Bar-Cohen, 2001). Later in 1992 while Sadeghipour and coworkers were getting close to discovering their actuation capabilities, Oguro's group in Japan described the bending of the ionic polymers under the application of a potential across its thickness. Since that

time, several groups in the USA and across the world are working on improving the manufacturing process, characterizing and modeling the performance, and searching for applications for these new intelligent materials.

1.3.2 Actuation Mechanisms and Models

To date the physical mechanisms that produce actuation are still uncertain. Several researchers are suggesting different actuation models. One of the salient features of ion-exchange membranes is selective ion conduction. Ion-exchange membranes are polyelectrolytes which contain charged sidegroups covalently bound to the polymer chain. This property leads to charge aggregation within the material and phase separation between hydrophilic regions containing the charged sidegroups and the hydrophobic backbone. The charge aggregation also leads to an ionic selectivity in which only certain charged groups, either cations or anions, can be transported through the material.

Ion conduction is known to play an important role in the electromechanical transduction of ionomeric polymers. The conduction of ions was identified by Shahinpoor et al. (1998) as the reason for bending upon application of an electric field, and de Gennes et al. (2000) proposed a model that related pressure and velocity within the material to electric field and charge flux. This model is similar to form as one developed and experimentally verified by Newbury and Leo (Newbury and Leo, 2002, 2003a,b), although Newbury and Leo used force, displacement, charge, and voltage as the state variables for the model. The steady-state distribution of charge due to ionic conduction was determined by Nemat-Nasser and Li (2000), where they showed that application of an electric field produces an accumulation of positive charge at one surface and a depletion of cations at the opposite surface. A similar model was recently proposed by Farinholt and Leo (2002) to model charge sensing in ionomeric materials. Recently, Nemat-Nasser (2002a) combined his model of charge redistribution within the material with a model that coupled the charge state within the polymer to the mechanical deformation.

There is increasing evidence in the literature for a link between charge accumu-

lation and mechanical deformation in ionomeric materials. The deflection response of ionomeric transducers of various compositions and cation forms was recently studied by Nemat-Nasser and Wu (2003a). Their results highlighted the relationship between the total charge flow in the polymer to the motion generated at the tip of the transducer. For transducers that utilized the fluoropolymer Flemion (a commercial polymer from Asahi Glass) instead of Nafion as the ionomer , Nemat-Nasser and Wu (2003a) demonstrated a linear relationship between normalized deflection (tip deflection relative to length) versus normalized charge (charge transported versus total fixed charge). Nafion-based transducers exhibited relaxation when subjected to a DC voltage, thus complicating the analysis of the deflection-to-charge analysis. A thorough study of the electromechanical response of Nafion and Flemion in various cation forms was also performed by Asaka et al. (2001a). They reported that the 'charge-specific displacement', defined as the ratio of tip deformation to induced charge, varied as a function of cation form for both ionomers. The charge-specific displacement was then related to the conductivity and freezable water content of the polymer.

The common idea between all suggested actuation models is that anions in the clusters are attached to the polymer backbone, while the free cations will move within the diluent medium under the application of an electric field, causing them to migrate towards the cathode in the hydrophilic polymer chancels (Bar-Cohen, 2001). This redistribution will cause some changes in the properties of the polymer membrane at the anode and cathode sides.

Several parameters control the amount and speed of diffusion of ions into the electrode. As mentioned earlier actuation mechanisms can be correlated with the motion of cations in the transducer. Therefore maximum strain and strain rate are correlated with the amount and speed of diffusion of the ions respectively. Two main properties determine the speed of response, first is the electrode architecture and second is the diluent content in the ionomer. Electrode architecture also determine the amount of strain in an ionic polymer actuator. The viscosity and polarity of the diluent has a major effect on the conductivity of the ionomer electrolyte. Using a less viscous diluent allow ions to move faster while a more polar diluent may induce

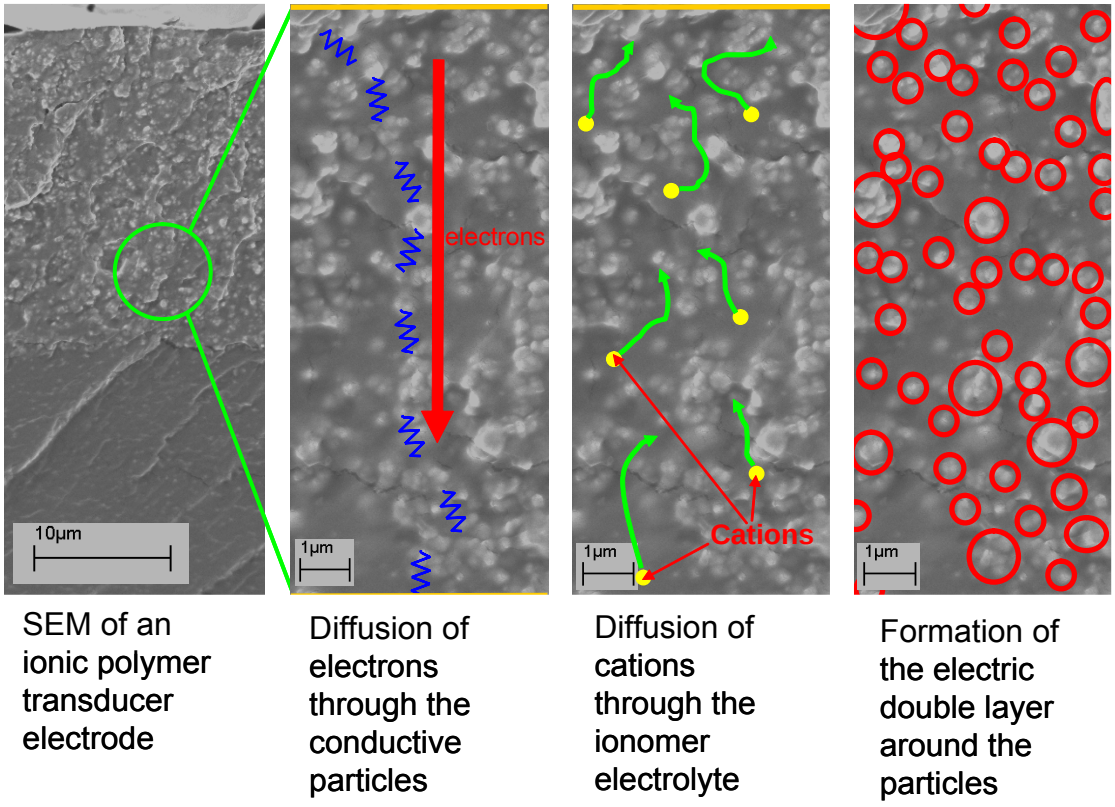

Figure 1.5: Ionomer-Conductor interface, (a) SEM of an ionic polymer transducer electrode, (b)Diffusion of electrons through the conductive particles, (c)Diffusion of cations through the ionomer electrolyte, and (d)Formation of the electric double layer around the particles.

charge seperation between the cation from the anion.

Electrode architecture had three main effects as shown in Figure 1.5. The electrode consists of a well dispersed conducting particles in an ionomer matrix as shown in the SEM picture in Figure 1.5 (a). According to Ohms law, the diffusion rate of the electrons into the electrode is proportional to the conductivity through thickness of the electrode:

$$\frac{dq}{dt} = \frac{V}{R} \tag{1.1}$$

The resistivity of a conductive phase dispersed in an insulator matrix is studied using the percolation theory (see Figure 1.5 (b)). Percolation theory will be discussed later in the chapter. After the charging of the metal particles in the electrode, mobile

ions will move to form the electric double layer as shown in Figure 1.5 (c). These cations are mobile only in an electrolyte medium, which is the ionomer in ionomeric transducers. In brief the electrons require more conductor particles while ions require more polymer for fast diffusion. Therefore an optimal concentration of conductor to ionomer ratio is expected. Finally the cations forms an electric double layer and accumulate around the conductive particles (see Figure 1.5 (d)). The electric double layer theory which is detailed in a later section demonstrates that the amount of charge accumulated per unit volt is proportional to the interfacial area between the conductor and the electrolyte. In this dissertation, the electric double layer and percolation theory are analyzed qualitatively to interpret the behavior of ionic polymer transducer due to variation in electrode architecture.

1.4 Electroactive Polymers and the Need for Large Displacement Actuators

Electroactive polymer (EAP) transducers are usually large displacement low force actuators. Compared to brittle ceramics EAPs are soft and compliant structures. Piezoceramics provide micron scale displacements with a large forcing output. Several applications requires large displacement, therefore piezoceramics are often manufactured in stacks that amplify the motion. Moreover stacks might not provide sufficiently large displacement, then mechanical amplification is used. Using the stacking and mechanical amplification techniques defies one major advantage of smart materials that they are parts free with large energy density. Therefore the need for large displacement actuators. Applications that would benefit from such transducers includes flapping mechanisms for a Micro Air Vehicle(Akle and Leo, 2003), and artificial muscles especially for EAPs that operates under low voltage. Moreover several polymers such as Nafion, the widely used ionomer for ionic polymer transducers, are biocompatible making them potential muscle implants.

1.5 Potential Applications of Ionic Polymer Transducers

All the interesting properties mentioned in the previous section gives ionic polymers a number of potential applications. Those applications can range from using them as sensors or as actuators. They could be used in water submerged applications, or in other environments either as packaged polymers or ionic liquid diluent based polymers (Bennett and Leo, 2004). Ionic polymers are usually made in the form of thin plates (50 to 200 micrometer) enabling them to be use in MEMS (Micro Electro-Mechanical System) application. They might be used as sensors to create micro-accelerometers, or as actuators to create micro swimming robots. Another interesting property of ionic polymers is that they are not toxic for human cells since they are made of Nafion^{TM}, noble metals (Platinum, and Gold for the coating), and Li or Na ions. This makes it possible for them to be implemented inside the body. Application can range from health monitoring as pressure and pulse sensors, or vein replacement as actuators. A current application under research by our group, is using those transducers to detect acoustic signals generated by the turbulence induced by a stenosis. Detecting and characterizing this turbulence enables us to measure the severity of the closure. The end product of this research is a non-invasive ionic transducer device capable of detecting early stenosis. Also in collaboration with our group Etebari et al. (2004) showed that ionic polymers could be used as wall shear sensors in submerged applications, and they managed to correlate the skin friction coefficient to the signal from the sensor. As actuators our team is collaborating with other companies in fabricating an adaptive mirror for outer space applications (Buechler and Leo, 2004). The polymers will be plated with a reflective material, and the potential applied across the transducers will deform the shape of the mirror increasing or decreasing the convexity. Akle and Leo (2003) proved the feasibility of using those transducers as flapping mechanisms for a Micro Air Vehicles. Furthermore, ionic polymer mechanical properties are quite similar to the human muscle, which raise there potential of replacing Human muscle (Shahinpoor, 1994). Their high dexterity makes them

perfect for robotics applications, they can be used to build end-effectors as dexterous as the human hand or as soft malleable end-effectors

1.6 Motivation

As mentioned earlier, transducers that operate at lower voltages are highly desired. Such actuators will have better biological compatibility, higher safety standards, and they will be easier to incorporate in systems especially for space applications. Figures of merit of an actuator include the maximum achievable strain, strain rate and energy density. Increasing these actuation characteristics broadens the applicability of ionic polymer transducers. During the early stages of this dissertation a linear relationship between capacitance and bending performance in ionic polymer actuators is established. This relationship between normalized deflection versus capacitance indicates that a fundamental relationship between charge motion and actuation mechanism in ionic polymer transducers. Capacitance in ionomeric actuators is mainly due to an electric double layer, which forms at the interface between the ionomer and the conducting electrode (Sadeghipour et al., 1992). Moreover diluents have a limited electrochemical stability window. For example water hydrated ionic polymer transducers are limited to an operating voltage of 1.23V . Above this voltage water molecules starts to break down into hydrogen and oxygen gases, leading to the loss of the diluent and degradation in performance (Bar-Cohen, 2001). This process is known as the electrolysis of water. For most ionic liquids and organic liquids this voltage is limited to approximately 3V. The linear relationship indicates that increasing the capacitance of an actuator increases its displacement per unit volt. Thus increasing the capacitance of the transducer will enhance the maximum achievable strain. Apart from electrical and environmental stability the viscosity of the diluents critical to speed of ions in the transducer. The diluent in ionic polymer transducer effects the strain rate. As mentioned in the previous section, increasing the conductivity of the electrode also enhances the strain rate. This is achieved by exploring the percolation theory and its effects on the electrode. As mentioned in the introduction a novel

fabrication technique called the Direct Assembly Process is developed during this research in collaboration with Dr. Kenton Wiles and Dr. James McGrath at Virginia Tech. The Direct Assembly Process provides us the ability of varying the electrode conducting powder and therefore control on the electric double layer and pseudocapacitance properties of the transducer. Finally the extensional experimental results made it possible to model the effect of varying the thickness of the electrode. This work lead to the active area bimorph model. The next sections presents a literature review of the percolation process and electric double layer theory.

1.7 Percolation Process

Percolation process describes the behavior of a flow in a random medium. These flows include but not restricted to fluids, ions, electrons, magnetic flux, heat, or even viruses (Zallen, 1983). The random medium is composed of a blocking phase and a flow permitting phase (Domb, 1983). The study of percolation first arose by Broadbent in 1954 (Broadbent, 1954), later introduced mathematically by Broadbent and Hammersley in 1957 (Broadbent and Hammersley, 1957). Percolation theory is applied to a diversity of phenomena that ranges from epidemic spread in a population to the study of quarks in nuclear matter (Zallen, 1983). The percolation theory states that there is a certain threshold level denoted p_c at which the medium transitions from a generally flow blocking medium to a flow permitting medium.

In the case of ionic polymer transducers the percolation theory is used to study the transition of a conductor-insulator medium from an insulator to an electron conducting material. There are two types of percolation processes on a lattice: the bond percolation and site percolation (Zallen, 1983). The bond percolation considers connected or disconnected paths, while the site percolation considers sites that are clustering together. The conductor-insulator matrix is a site percolation problem. A continuous conducting network is formed by the coalescence of the grains in the insulator medium. Percolation theory predicts that there is a critical percolation threshold at which a conductive path is formed causing the material to convert from

a insulator to a conductor (Park et al., 2002a). The mathematical development of the percolation theory is a stochastic-geometry process (Zallen, 1983). Classical percolation theory is typically modeled using a power law which is a function of the volume percent of the conducting phase:

$$\sigma = k_p(p - p_c)^{\beta_p} \tag{1.2}$$

where β_p is an exponent with a theoretical value of 2, and k_p is a scaling constant depends on the conductivity of the materials involved (Stauffer and Aharony, 1992). Equation 1.2 indicates that increasing the conductor phase decreases exponentially the resistivity of the electrode. The shape and more importantly the aspect ratio of the cites is critical on the value of p_c (Park et al., 2002a).

1.8 Electric Double Layer

Capacitance in ionic polymer transducers is mainly due to an electric double layer, which forms at the interface between Nafion and platinum (Sadeghipour et al., 1992). Moreover, other slow Faradaic charges are mobilized due to processes that occur on the metal-ionomer interface. Those reactions and processes are known as pseudocapacitance.

During the search on methods to increase capacitance we came across highly capacitive devices known as supercapacitors or electrochemical capacitors. Those devices have large capacitance per unit weight or unit volume and used mainly as an intermediate solution between a capacitor and a battery. Their design is similar to ionic polymer transducers, they consist of two high surface area electrodes in a bath of electrolyte with a separator in between. They take the advantage of high capacitance of the electric double layer, and also the slow and large pseudocapacitance of some electrode materials. The goals of this well-established field of supercapacitors are similar to the ones for ionic polymer transducers. They need large capacitances, fast response, and environmental stability. Several of the ideas and models that will be discussed hereafter are obtained from supercapacitor literature.

The electric double layer (EDL) is defined as an electrically neutral system that occurs at an interface or surface, in which a layer of positive charges opposes a layer of negative charges, surrounded by oriented polar molecules (Sparnaay, 1972). In electrolytic solutions the charge accumulates at the interface between the surface of the conductor and an electrolytic solution and hence forms a double layer, the separation of each layer being of the order of a few angstroms (Endo et al., 2001). The models of the EDL will be presented in the historical progressive development of its structure. The electric double layer was first defined by von Helmholtz (1853) as the accumulation of charges on the interface of two dissimilar metals. Gouy (1910) and Chapman (1913) developed a model independently which accounted for the thermal motion of the ions and described the diffuse layer. Stern (1924) presented a new model that combined the Helmholtz and Gouy-Chapman models. His model treated the overestimation of the electric double layer capacitance. Conway (1999) and Grahame (1947) added the specific adsorption of ions to the Stern model. Graham's model constituted by three regions of inner Helmholtz plane (IHP), outer Helmholtz plane (OHP) and the diffuse region (Endo et al., 2001). Several other chemical concepts and mechanisms were added to the modeling of the electric double layer. The Bockris, Devanathan and Muller model (Bockris et al., 1963), which adds the predominance of diluent molecules near the interface to the Graham model, is considered an acceptable model for most current applications (Endo et al., 2001).

1.8.1 The Helmholtz model

Helmholtz suggested the double layer in 1853 for a metal-metal interface, but it was not until 1879 that he developed it for the metal-electrolyte interface (Sparnaay, 1972). This model, is also known as the Helmholtz molecular condenser (Kitahara and Watanabe, 1984), assumes an interface that consist of a layer of electrons at the surface of the electrode, and an array of ions in the electrolyte (Conway, 1999) as shown in Figure 1.6(a) . The specific capacitance of the Helmholtz double-layer is

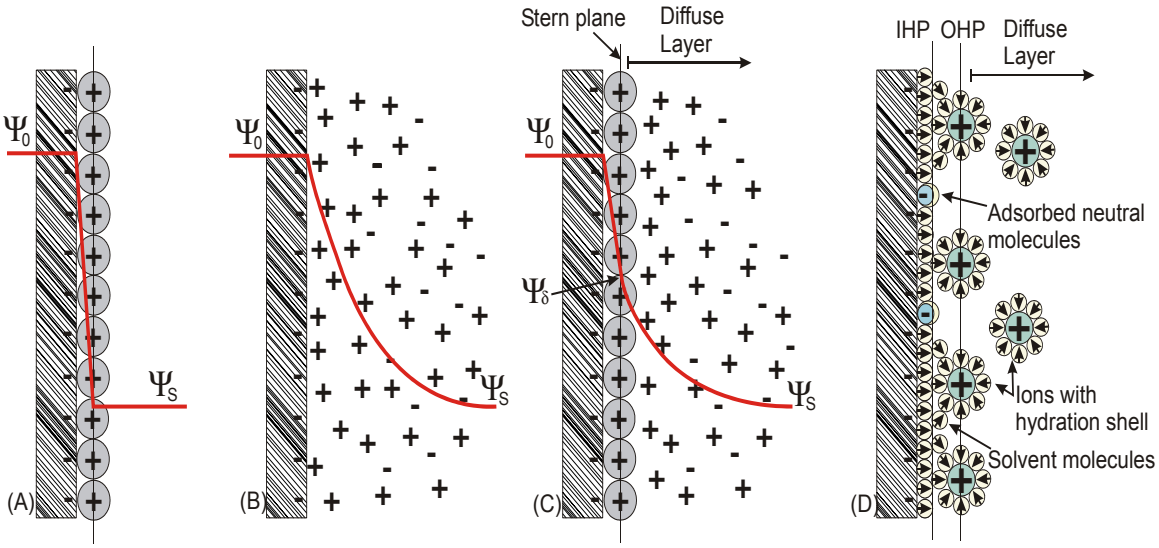

Figure 1.6: Electric double layer models (a)Helmholtz model, (b)Gouy-Chapman, (c)Stern, and (d)Bockris, Devanathan, and Muller (BDM) model

given by the following equation (Endo et al., 2001),

$$C = \frac{\varepsilon A}{4\pi\delta}, \tag{1.3}$$

where ε is the dielectric constant of the electrolyte, δ is the distance from the electrode interface to the center of the ion, and A the effective surface area of the electrode interface. This model failed to account for the electrolyte concentration and it neglects interactions occurring further from the electrode than the first layer of adsorbed species (Endo et al., 2001). Equation 1.3 indicates that the capacitance increases linearly with the Area (A), and C/A is defined as the specific capacitance, which is a constant for a conductor in a given electrolyte.

1.8.2 The Gouy-Chapman model

Gouy and Chapman independently developed a double layer model which is also known as the diffuse double layer (Endo et al., 2001). This model considered the thermal motion of the ions and accounted for the applied potential and considered the electrolyte concentration, both influencing the value of the double layer capacity (Kitahara and Watanabe, 1984). The double layer would not be as compact as in the

Helmholtz description, but of variable thickness and the ions being free to move as shown in Figure1.6(b).

This model is analyzed in terms of the two basic equations, first the Poisson equation,

$$\frac{d^2\psi}{dx^2} = -\frac{4\pi\rho}{\varepsilon}, \tag{1.4}$$

where ρ is the volume charge density at a point where the electric potential is ψ and ε is the dielectric constant (Kitahara and Watanabe, 1984). The other is the Boltzmann equation at the two electrodes:

$$n_+ = n_{+0}e^{-\frac{v_+ e\psi}{kT}} \tag{1.5}$$

$$n_- = n_{-0}e^{\frac{v_- e\psi}{kT}} \tag{1.6}$$

where $n_{+(-)}$ is the number concentration of ions in the diffuse layer, $n_{+(-)0}$ that of the bulk solution, $v_{+(-)}$ the valence of the ions, e the elementary charge (1.602 176 53 10^{-19} C), k the Boltzmann constant (1.38 10^{-23} J/K), and T the absolute temperature (Kitahara and Watanabe, 1984). As mentioned earlier the Gouy-Chapman model typically predicts larger capacities compared to experimental results due to the assumption that ions are point charges.

1.8.3 Stern and Grahame models

Stern (1924) considered that ions have a finite size and that the charge is located in the center. He divided the double layer into two parts, a compact layer of ions next to the electrode followed by a diffuse layer extending into bulk solution as shown in Figure 1.6(c) (Endo et al., 2001).

Grahame divided the Stern layer into two regions. He denoted the closest approach of the diffuse ions to the electrode surface as the outer Helmholtz plane. The layer of specifically adsorbed ions at the electrode surface was designated as being the inner Helmholtz plane (Endo et al., 2001).

The Stern and Graham models are analyzed using the Langmuir theory. The capacitance is computed by combining the capacities of the different layers in series. The capacitance of the Stern plane C_s which is computed according to Equation 1.3, and the capacitance of the Gouy-Chapman diffuse layer C_d. While the specific adsorption capacitance is computed according to the following,

$$C_a = C_d \frac{\partial \sigma}{\partial \sigma_A}, \tag{1.7}$$

where σ is charge density on the electrode, and σ_A is the surface charge of the specifically adsorbed ions(Sparnaay, 1972).

1.8.4 Bockris, Devanathan, and Muller (BDM) models

In 1963 Bockris, Devanathan and Muller proposed a model that included the influence of the diluent near the interface. They suggested that a layer of water was present within the inner Helmholtz plane at the surface of the electrode (Bockris et al., 1963). The dipoles of these molecules would have a fixed alignment because of the charge in the electrode. Some of the water molecules would be displaced by specifically adsorbed ions as shown in Figure 1.6(d). Other layers of water would follow the first, but the dipoles in these layers would not be as fixed as those in the first layer. A summary of the advantages and disadvantages of the each model with the formula used to compute the capacitance is presented in Table 1.1.

1.9 Pseudocapacitance

In addition to the electrostatic capacitance that arises from the separation of charge in the electric double layer, a contribution to capacitance can be made from reversible Faradaic reactions that can occur on the surface of the electrode. The charge required to facilitate these reactions is for thermodynamic reasons dependent on the potential, resulting in a Faradaic pseudocapacitance (Kotz and Carlen, 2000). Those type of reactions are slow in nature, and are similar to store electrochemical energy in

	Pros	Cons	Capacitance
Helmholtz	Works in high concentration electrolytes	Failed to account for electrolyte concentration and potential dependence of the capacitance	$C_H = \frac{\varepsilon A}{4\pi\delta}$
Gouy-Chapman	Accounted for the thermodynamic diffuse layer	Assumes ions as point charges	$C_G = \sqrt{\frac{v^2e^2n\varepsilon}{2\pi kT}} \cosh \frac{ve\psi_0}{2kT}$
Stern	Combined Helmholtz and Gouy-Chapman and works well for pure electrostatic double layer	NA	$C_S = \frac{C_H C_G}{C_H + C_G}$
Graham	Added adsorption to the Stern model	NA	$C_G = \frac{C_a C_S}{C_a + C_S}$
BDM	Accounted for the dipoles of the diluent molecules	NA	NA

Table 1.1: Summary of the advantages and disadvantages of each model with the corresponding capacitance.

batteries. Pseudocapacitance could occur due to two types of processes, the first is adsorption and the second the redox process.

1.9.1 Adsorption

It is also known as the underpotential deposition, and consist of two dimensional depositions of adatom arrays on the electrode surface (Conway et al., 1997). Adsorption capacitance could be 10-100 times larger than that of the double layer (Conway et al., 1997). Examples of adsorption includes the deposition of H or Cu on Pt, Pb or Bi on Au, Bi on Ag, H on Rh or Pt (Conway et al., 1997). A typical underpotential deposition reaction is as follows,

$$M + H_3O^+ + \overline{e} \rightleftharpoons M - H + H_2O, \tag{1.8}$$

Compared to the electrostatic double layer, pseudocapacitance is a slow process (Grzeszczuk and Poks, 1995). The current of the underpotential deposition process as a function of time(Equation 1.8) is written as (Conway, 1999),

$$i = \frac{FQ_1}{RT} \frac{K_1 C_{H_3O^+} \exp -\frac{F(V \pm st)}{RT}}{\left(K_1 C_{H_3O^+} + \exp -\frac{F(V \pm st)}{RT}\right)^2} s, \tag{1.9}$$

where s is the sweep rate.

In some situations adsorption could be so large that the potential will flip polarity in some regions of the double layer (Kitahara and Watanabe, 1984).

1.9.2 Redox pseudocapacitance

Redox pseudocapacitance is 10x larger than the adsorption and 100x the double layer capacitances (Frackowiak and Beguin, 2001). Redox stands for Reduction-Oxidation, and it is a chemical process involving electron transfer between an oxidized species Ox and a reduced species Red according to the following (Conway, 1999),

$$\mathrm{Ox} + \mathrm{z}\overline{\mathrm{e}} \rightleftharpoons \mathrm{Red}, \tag{1.10}$$

Other types of pseudocapacitance which include the 3-dimensional sorption process (electrochemical intercalation) with charge transfer. This process occurs in lithium ion batteries, where the Li^+ ion is adsorbed into a layer-latice host materials on the cathode, while the anode is a lithium metal (Conway, 1999). The last pseudocapacitive process is the phenomenon of partial charge transfer which usually occurs on the anode with the anion. This occurs in the electrostatically adsorbed ions in the electric double layer, when some specific electronic interaction between the ion's valence electrons the electrode's surface orbitals occur. The chemical reaction involving an ion is as follows,

$$\mathrm{M} + \mathrm{A}^- \rightleftharpoons \mathrm{M/A}^{(1-\delta)-} + \delta\overline{\mathrm{e}}, \tag{1.11}$$

where δ is a fraction of an electron charge Conway (1999).

1.10 Electromechanical Coupling Models

Physics-based modeling efforts by Nemat-Nasser (2002b) and Leo et al. (2005) highlighted the role charge distribution at the boundary layer that forms at the interface of the electrode and the polymer. Although the understanding of fundamental actuation mechanisms in ionic polymer transducers is still under debate, our results and several other models relates such mechanisms to ion conduction across the membrane. Leo et al. (2005) modeled the electromechanical coupling by the expansion form

$$\sigma(x,t) = \alpha\rho(x,t) + \beta\rho^2(x,t), \tag{1.12}$$

where α and β are coefficients that define the linear and quadratic terms of the transduction model, while σ represent the stress and ρ is the space-temporal charge density. In this dissertation a similar approach is adopted and the electromechanical coupling model is assumed to be in the form of:

$$\epsilon = \alpha Q + \beta Q^2 \tag{1.13}$$

where ϵ represents the strain and Q is defined as the charge per unit area. The quadratic term in this model produces a 1^{st} harmonic response for a sine wave voltage input. For ionic polymer transducers with symmetric electrodes this term generates a zero net bending moment, due to the expansion of both active areas. If the actuation response is measured in the thickness direction the total strain in the transducer is the addition of strains in both electrodes. Hence, the positive βQ^2 term is cumulative in extensional actuation. Moreover, the linear term is canceled in extensional actuation of transducers with symmetric electrodes. Non-linear behavior in the bending actuation is reported in literature (Kothera and Leo, 2005). The quadratic term generates small 1^{st} harmonic response in slightly assymetric electrodes.

1.11 Objectives

The objectives of this dissertation are classified in three categories. The first is the development of experimental and fabrication tools that enable the variation and characterization of desired parameters. The DAP provided the fabrication tool which can

precisely vary most parameters in the transducer including the polymer, diluent, electrode species and architecture. Bending and extensional characterization setups are build to characterize the mechanical, electrical and electromechanical properties of the transducer. The second category is transduction properties enhancement. The properties that are targeted in this dissertation are the maximum strain and the strain rate. The last category is the modeling and the understanding of actuation mechanisms of the transducers. These models will serve as transducer design tools, and toward the understanding of the basic physics of the electromechanical coupling.

1.12 Contributions

This dissertation has three major contributions to the field of ionic polymer transducers. These contributions enhance the performance of ionic polymer transducers, provide tools to the fabrication and characterization of the actuators, and finally highlights some physic based actuation concepts through models and correlations. The following is a list of these contributions:

- The first major contribution is the determination of a correlation between capacitance and mechanical strain. This correlation indicates that the actuation response in ionic polymers is directly related to the charge displacement in the material. This result has a major impact on the modeling and on the understanding of the actuation mechanisms.

- The second major contribution is the development of a fabrication process which allows good control on the composition of ionic polymer transducers. This process, called the Direct Assembly Process, facilitates the study of different diluents in ionomeric actuators. This resulted in a dry actuator with EmI-Tf ionic liquid diluents that can operate in air for over 250000 cycles. The DAP allows the variation in the electrode architecture which enabled us to fabricate dry transducers with 50x better performance compared to transducers made using the impregnation-reduction technique. DAP fabricated transducers

achieved a strain of 9.38% at a strain rate of 1%/s. This DAP allows variation of several other transducer parameters including the ionomer used leading to more performance.

- Finally, an extensional actuation mechanism in ionomeric polymer transducers is reported for the first time in this dissertation. This actuation mechanism enables a new class of ionic polymer transducers with large force and small displacement. Furthermore this actuation mechanism leads to the development of an active areas model that emphasizes the importance of the boundary layer on the conductor-ionomer interfacial area.

1.13 Document Organization

This document is organized in six chapters. In this chapter an introduction and literature survey are presented; the next chapter will cover the experimental methodology. Chapter two begins with a description of the electromechanical characterization procedures and setups. A fixture is built to characterize the polymers in bending, while another fixture provide the extensional electromechnical properties of a transducer. The second part of the chapter presents a novel fabrication technique for ionic polymer transducers which is developed in this dissertation. Typically, platinum and gold electrodes are plated on an ionic polymer membrane using an electroless chemical deposition process known as the impregnation-reduction. The impregnation reduction method provides indirect and limited control on the morphology of the electrodes. Moreover this impregnation-reduction method is a function of polymer morphology and ionic content. In this work several process parameters need to be manipulated and optimized for different ionomers. A novel method named as the Direct Assembly Process (DAP) is developed, which enables more precise control on electrode morphology. This process is developed in collaboration with Dr. Kenton Wiles and Dr. James McGrath at Virginia Tech. The method consists of mixing an ionic polymer dispersion or solution with a fine conducting powder and attaching it to the membrane as an electrode. Direct Assembly Process allows the use of any type of ionomer, diluent,

conducting powder, and counter ion in the transducer. The novel plating method permits the exploration of any novel polymeric design. Several conducting powders are incorporated in the electrode including single-walled carbon nanotubes (SWNT), polyaniline (PANI) powders, high surface area RuO_2, and carbon black electrodes. The DAP provided the tool which enabled us to study the effect of electrode architecture on performance of ionic polymer transducers.

The third chapter covers the correlation between capacitance and actuation performance of those transducers, while the fourth discuss the experimental results that optimized the direct assembly process. Charge motion in ionomeric actuators is mainly due to an electric double layer, which forms at the interface between the ionomer and the conducting electrode (Sadeghipour et al., 1992). As mentioned earlier the adsorbed positive ions are critical to the generation of electromechanical strain. The electric double layer capacitance increases linearly with the interfacial area Endo et al. (2001), and therefore increasing the interfacial area between the metal and the ionomer mobilize more ions and increases the performance of the actuator. Ohms law states that charge injection rate is proportional to the conductivity of the electrode. Therefore the conductivity through the electrode is critical to the speed of the actuation mechanism in ionic polymer transducers. In this chapter the effect of manipulating the metal powder content in the electrode on the actuation of ionic polymer transducers is explored. The trends in speed and maximum performance are explained in terms of the electric double layer theory and percolation behavior of the metal-polymer matrix in the electrode.

In order for ion conduction to occur in Nafion membranes, the cations within the membrane must be dissociated by saturation with an appropriate diluent. Typically, the diluent used has been water. Water is a volatile diluent, leading to dehydration and the corresponding loss in performance of ionic polymer transducers when operated in air. Bennett and Leo have shown that the hydration problem can be overcome by using ionic liquids as the diluent in these transducers Bennett and Leo (2004). Ionic liquids offer increased environmental stability and a larger electrical operation window compared to water but suffer from high viscosity. Transducers

solvated with 1-ethyl-3-methylimidazolium trifluoromethanesulfonate (EmI-Tf) ionic liquids have slower strain rates compared to water hydrated samples. Five organic diluents are also considered in this study, PolyEthylene Glycols (PEG) with four molecular weights (MW) and Formamide. Viscosity and polarity of such diluents are correlated with the strain rate response in actuators. These organic diluents operates in air for 3 to 5 hours before dehydration. Chapter 4 will present a detailed study of transducers with these diluents.

In Chapter 5 the active areas model is mathematically derived and experimentally verified. Extensional actuation in ionic polymer transducers is first reported and characterized in this dissertation. An electromechanical coupling model presented by Leo et al. (2005) determined the strain in the active areas as a function of the charge. This model is presented with a linear and a quadratic term that produces a 1^{st} harmonic response for a sine wave actuation input. The quadratic term in the strain generates a zero net bending moment for ionic polymer transducers with symmetric electrodes. The linear term is also canceled in extensional actuation for symmetric electrodes. Moreover, in Chapter 5 the extensional and bending actuation in ionic polymer transducers are explained using a bimorph active area model. Several experiments are performed to compare the bending actuation with the extensional actuation capability. The active area in the model is assumed to be high surface area electrode in the transducer. The electric double layer theory states that ions accumulate in a thin boundary layer close to the metal-polymer interface. Since the metal powders are evenly dispersed in the electrode area of the transducer, this area is expected to actuate evenly in the actuator. Finally the last chapter provides a summary and conclusions of this work.

Chapter 2

Experimental Methodologies

In this chapter a description of the ionic polymer testing experiments with fixtures and electrical circuits is presented. Electromechanical characterization of the samples is accomplished with two experimental test apparatus. One setup characterizes the bending response of the transducers, while a second apparatus measures the extensional response. A novel fabrication technique for ionic polymer transducers is developed for this dissertation. The impregnation reduction method commonly used in plating the ionomer provides indirect and limited control on the morphology of the electrodes. Moreover this impregnation-reduction method is a function of polymer morphology and ionic content. In this work several process parameters need to be manipulated and optimized for different ionomers. A novel method named as the Direct Assembly Process (DAP) is developed, which enables more precise control on electrode morphology. The method consists of mixing an ionic polymer dispersion or solution with a fine conducting powder and attaching it to the membrane as an electrode. Direct Assembly Process allows the use of any type of ionomer, diluent, conducting powder, and counter ion in the transducer. Several fabrication schemes could be followed for the DAP. Optimal fabrication parameters are usually determined by a critically controlled parameter such as the diluent species in the transducer, the morphology of the electrode, etc. This chapter starts with a detailed description of the direct assembly process while highlighting all the parameters that can be explored. Next, the conducting powders studied in this work are presented with their distinct

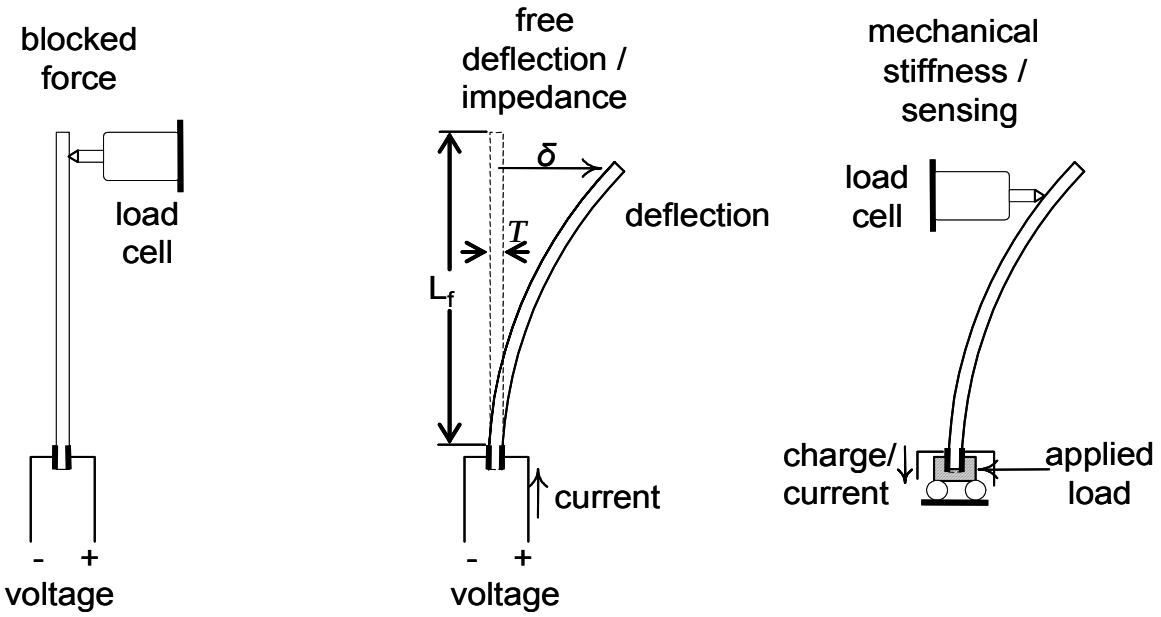

Figure 2.1: The experimental setup used to for the electromechanical measurements.

properties. Third we present the diluent used and finally the method is characterized in term of reliability, repeatability and some performance matrix.

2.1 Electromechanical Characterization: Bending

The electromechanical characteristics of ionic polymer transducers in bending are measured from three sets of experiments. These experiments measure five transducer properties: the electrical impedance, mechanical impedance, sensor response, actuation blocked force, and actuation free displacement. Each experiment is performed using a step input or a random input. The five tests are first described and details on the circuitry and equipment is provided.

The samples used for these tests are usually cut in 3 mm x 30 mm rectangles and held in a cantilevered configuration in a clamp with fixed gold electrodes (see Figure 2.1). The free length of the transducer, L_f, is 19 mm. The thickness of the transducer, T, varies between approximately 0.08 mm and 0.26 mm depending on the number of electrode layers and the thickness of the membrane. The first test is a blocked force test which characterizes the maximum force the actuator generates

due to an applied voltage. In this experiment the tip of the polymer is blocked by a load cell which measures the force generated due to a random voltage with a RMS magnitude of 1 V is applied on the electrodes using a Fourier analyzer and amplifier. In the second test the load cell is removed and a non-contact laser vibrometer measures the maximum displacement $\delta(t)$ of the transducer in response to an applied voltage. This is the free deflection test. During this test the current $i(t)$ induced in the polymer due to the applied voltage $v(t)$ is also measured allowing the measurement of the electrical impedance of the polymer. The frequency response function between the excitation voltage and the output displacement and between the input voltage and induced current are measured over the frequency range 0.2 Hz to 200 Hz. This setup is also used to measure the time domain response of the transducer to a sine wave or step voltage input. The final test performed on the ionic polymers determines the mechanical impedance. In this test one end of the transducer is mechanically displaced by an external shaker, while the other end is blocked with a load cell. Referencing the measured force to the displacement results in a measurement of the stiffness of the polymer.

The measured data is then post-processed to compute the material parameters of the samples. The free deflection $\delta(t)$ (in the time domain) or the free deflection frequency response ($\delta(\omega)/v(\omega)$) are used with equations (2.1) and (2.2), respectively, to compute the bending strain as a function of time or frequency. Equations (2.1) and (2.2) assume that the transducer bends with a constant curvature; experimental results demonstrate that this is an appropriate assumption for the experiments performed in this dissertation (Akle et al., 2004a). Furthermore those equations are only valid below the first reasonance frequency, where the mode shape of the beam has a constant curvature.

$$\epsilon(t) = \frac{\delta(t)T}{L_f^2} \tag{2.1}$$

$$\frac{\epsilon(\omega)}{v(\omega)} = \frac{\frac{\delta(\omega)}{v(\omega)}T}{L_f^2} \tag{2.2}$$

where ϵ is strain in the outer fibers of the transducer.

The impedance $Z(\omega)$ of the samples is computed using equation (2.3), and the capacitance C is computed using equation (2.4) by assuming the polymer is a network of capacitors and a resistor in series (Akle et al., 2005).

$$Z(\omega) = \frac{v(\omega)}{i(\omega)} \tag{2.3}$$

$$C = \frac{1}{Im(Z(\omega))\omega A} \tag{2.4}$$

where A is the area of the transducer and $Im(Z(\omega))$ is the imaginary component of the impedance. In some cases the modulus of elasticity is computed from the natural frequency of the system using equation (2.5) and the measured geometry. Assuming that the ionomeric transducer is a cantilever beam, the modulus of elasticity E is

$$E = \frac{\omega_n^2 \lambda}{k_n^4 I}, \tag{2.5}$$

where ω_n is the measured natural frequency determined from the reasonance peaks in the displacement frequency response function. The variable λ is the linear mass density of the beam, I is the moment of inertia around the axis of bending, and k_n is computed for the first frequency according to (Inman, 2000)

$$k_n = \frac{1.875104}{L_f}. \tag{2.6}$$

Damping properties of the transducer are also obtained from the experimental data. Therefore strain per charge frequency response functions provide a better estimate of the damping ratios. The half power method, also known as the 3dB method is used to compute the damping ratio. The damping ratio is estimated according to

$$\xi = \frac{|\omega_a - \omega_b|}{2\omega_n}, \tag{2.7}$$

where ω_a and ω_b are the frequencies corresponding to the intersection between the 3dB line below the maximum of the peak with the frequency response function (Ewins, 2000). The damping properties are also approximated by assuming the beam to be a single degree of freedom damped system and the frequency response function is fitted to the transfer function

$$H(s) = \frac{\omega_n^2}{s^2 + 2\xi\omega_n S + \omega_n^2} \tag{2.8}$$

where s is the Laplace variable (Ewins, 2000).

A direct measurement of the stiffness is obtained from the third set of experiments. Assuming that the polymer is a sliding-pinned beam, the Young's modulus of elasticity is approximated to the first mode using the following equation (Wesley, 2003),

$$E = \frac{kL^3}{\left(\frac{\pi}{2}\right)^3 \left(\frac{WT^3}{12}\right)}, \tag{2.9}$$

where k is the measured stiffness, L is the free length, W is the width, and T is the thickness. Wesley (2003) showed that the experimental apparatus used in this study is only valid at low frequencies (usually lower than 30Hz). Above this frequency some fixture dynamic effects will deteriorate the accuracy of the frequency response function.

A single sensing test is also performed on the ionic polymers. In this test one end of the polymer is mechanically displaced by an external shaker while the other end is blocked with the load cell (see Figure 2.1). The charge generated across the thickness is sensed either by a charge sensor or a short circuit current sensor. The sensor sensitivity is defined as the measured charge or current per unit induced velocity.

Each of the tests could be run in two forms. The first is the step response. A step input in applied to the system, and the corresponding response is measured. This test is essential to determine the relaxation of the polymers. It is also used to determine the static values of the electrical and mechanical impedances. The main disadvantage of the step response analysis is repeatability. The back relaxation in ionic polymer transducers varies in speed and magnitude from test to test. The second is analyzed in the frequency domain. This analysis proved to be more robust and repeatable for ionic polymer transducers. The input for this test is a random white noise signal of a frequency range from 0Hz to 256Hz. An anti-aliasing filter is used to filter the response above 200Hz. Data in the frequency range of 200Hz - 256Hz is considered distorted by the anti-aliasing filter and consequently it is removed from the analysis. The response is then transformed to the frequency domain using

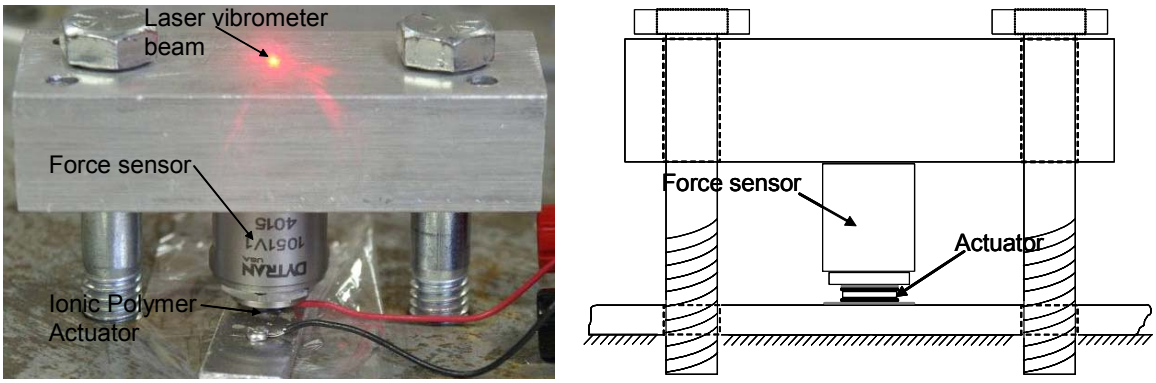

Figure 2.2: Experimental setup used for the extensional electromechanical measurements.

the Fourier transform to yield the frequency response function between the relevant input-output pair.

2.2 Electromechanical Characterization: Extensional

The extensional electromechanical properties are computed from force measurements. A force measuring setup is built and calibrated (see Figure 2.2). The load cell is a 10 lb piezoelectric Dytran 1051v1 force sensor. This load cell is pressed against the actuator film via a stiff structure shown in Figure 2.2. A laser vibrometer measures the displacement on the top of the support structure. The samples are prepared in a square shape of 3mm x 3mm dimension. In some experiments the ionomeric actuator is sandwiched between two metal plates and displacement is directly measured with the laser vibrometer. Data from direct displacement measurement is generally noisy. Transducers in the thickness direction are relatively stiff (around 10MN/m) and thickness is in the order of 100 to 200 μm. For a 300μstrain that a typical actuator generates it is difficult to measure the 60 nm of deformation. This justifies measuring the force compared to direct displacement measurements.

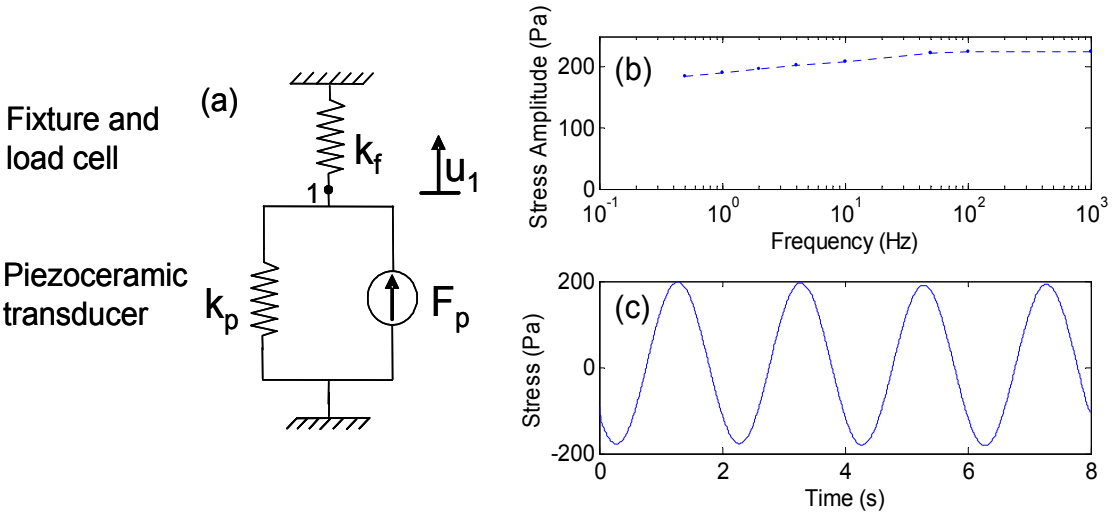

Figure 2.3: (a) Stress amplitude generated by the piezoceramic transducer under 75kV/m **electric field. time response of the piezoceramic under** 75kV/m **sine wave of** 0.5Hz **frequency.**

2.2.1 Extensional Test Fixture Calibration

The fixture is calibrated using a T110-A4E-602 piezoceramic transducer. The piezoelectric wafer is placed in the fixture instead of the ionic polymer transducer and actuated with a 20 to 40 V signal (75 to 150 kV/m). The d_{33} coefficient is 390x10^{-12}m/V and the elastic modulus E_p is 5.2x10^{10}Pa. The corresponding strain due to an electric field Φ of 75kV/m is computed to be $\epsilon = 2.9x10^{-5}$ and the stress generated is around $\sigma = 1.5$MPa according to the following

$$\epsilon = d_{33}\Phi, \tag{2.10}$$

$$\sigma = \epsilon E_p. \tag{2.11}$$

Figure 2.3(a) shows the mechanical model of a the fixture and the load cell in series with the piezoceramic spring and force generator. The following equation compute fixture stiffness K_f

$$K_f = \frac{\frac{F_m}{F_p}K_p}{1 - \frac{F_m}{F_p}}, \tag{2.12}$$

where F_m is the load cell measured force, F_p is the computed piezoceramic generated force, and K_p is the stiffness of the piezoceramic wafer. The measured stress under

75kV/m is 225Pa as shown in Figure 2.3(b). Replacing the numbers in equation 2.12 K_f is computed to be $2.4N/\mu m$. Most importantly, the shape of the signal is undistorted (see Figure 2.3) and the ratio of the first harmonic to the fundamental frequency response is computed to be smaller than 10^{-3}. This verfies that any measured nonlinearity will be due to transduction in the ionic polymer transducer and not a fixture effect.

2.3 Ionic and Electric Conductivity Measurements

The electric conductivity is of particular interest to measure the percolation properties of the conductive powders incorporated in an electrode of a transducer. The ionic conductivity of the membrane is an important property that is measured using the conductivity measurements and complex plane frequency analysis. Conductivity is measured with an HP 4192 low frequency impedance analyzer.

2.3.1 Complex Plane Frequency Response

This test is experimentally similar to the frequency response electrical impedance test elaborated in the previous section. The difference is the frequency range and the way the data is interpreted. Usually the frequency range of this test is in the order of 5Hz to 1MHz. The data is plotted in the complex as shown in Figures 2.4 and 2.5. Also shown in Figures 2.4 and 2.5 is the ability this tool provides to analyze the data by distinguishing the electrostatic double layer effect from the pseudocapacitance and providing better insight on the type pseudocapacitance and the resistances. These figures present the complex plane response for the ideal circuits shown next to each plot.

2.4 Ionomers

Several ionomers are studied and characterized. Three different ion selective ionomers are studied in this research, and the molecular structure is shown in Figure 2.6.

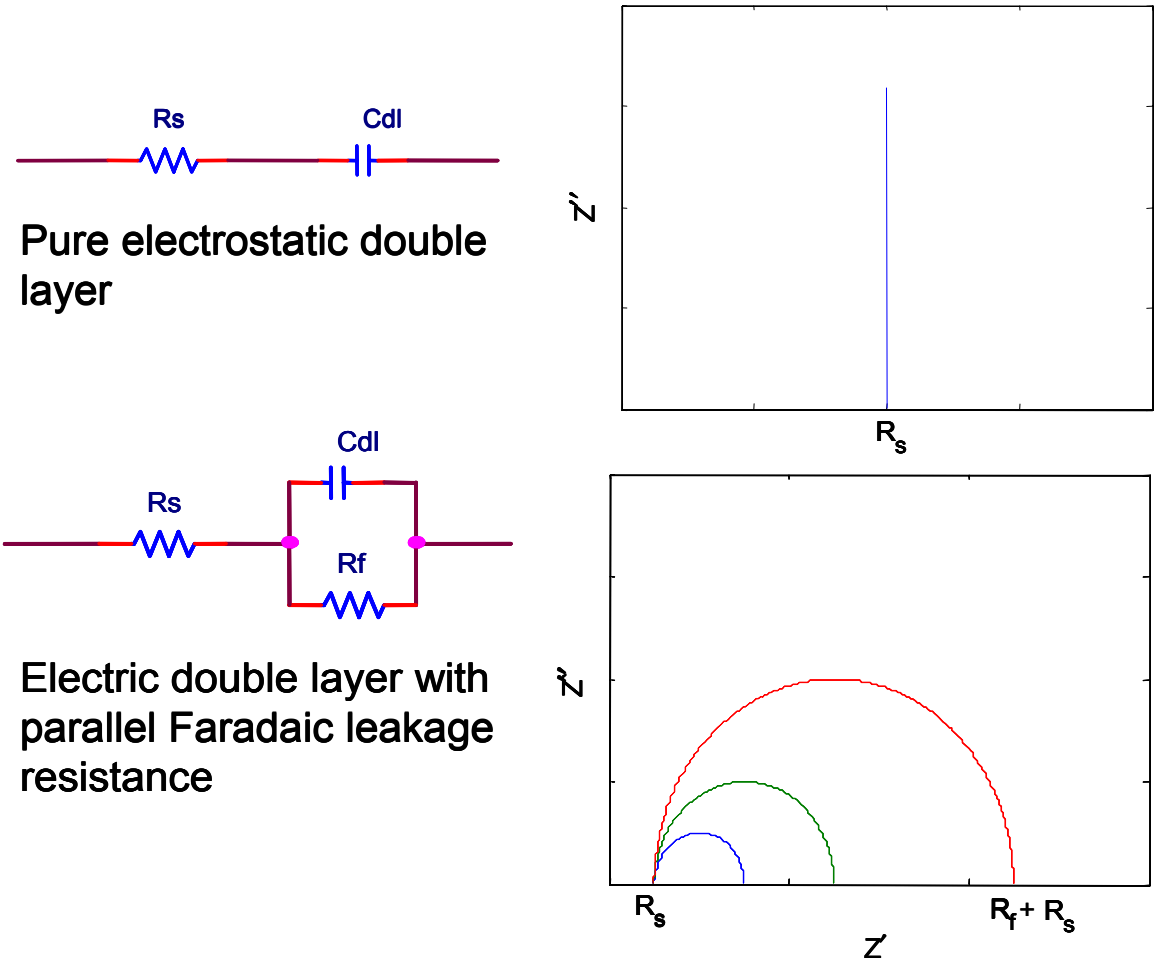

Figure 2.4: The complex plane representation of a simple electrostatic double layer, and a double layer with leakage resistance.

The materials studied consist of Nafion, a product of DuPont and one of the most widely studied materials associated with ionomeric transducers, and two alternative ionomers, BPS (sulfonated poly(arylene ether sulfone)) (Wang et al., 2002) and PATS (poly(arylene thioether sulfone))(Wiles et al., 2002), that are synthesized by the McGrath group using direct polymerization of sulfonated monomers. This synthetic scheme affords precise control of the amount and the location of ionic groups along the polymer backbone. These polymers differ from Nafion in two major aspects. First, the concentration of ionic groups on a mass basis is almost double that of standard Nafion, 1.70 meq/g for BPS-40 versus 0.91 meq/g for Nafion 1100. Also, the backbone of the BPS and PATS copolymers are much stiffer than Nafion, which produces a higher modulus material. Moreover Polyurethane-Polyurea with PEG seg-

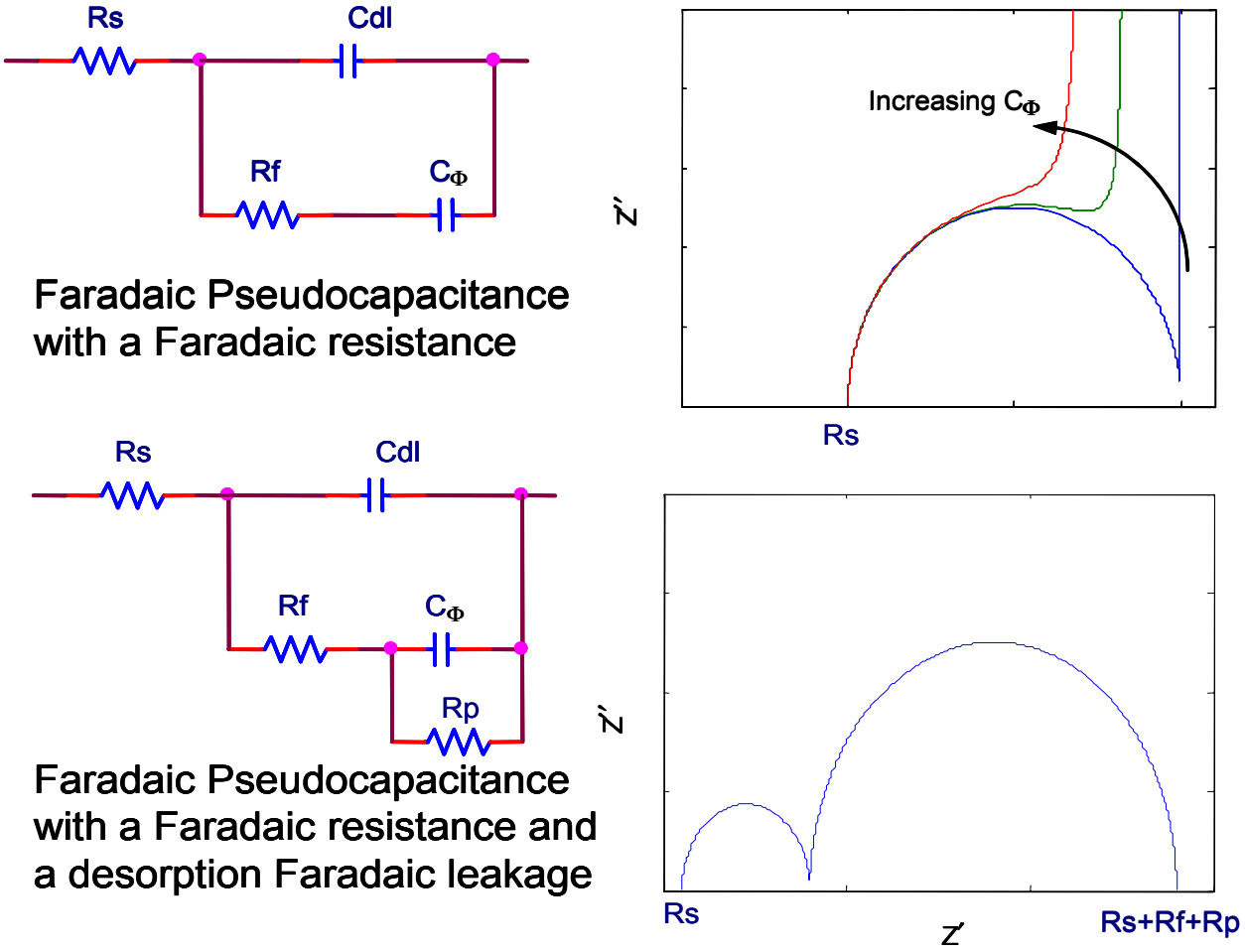

Figure 2.5: The complex plane representation of a simple electrostatic double layer, and a double layer with leakage resistance.

ments and crosslinked PEG/PEO ion conducting polymers are studied as potential transducers. These PEG/PEO polymers are dry solid electrolytes leading to diluent free transducers.

2.5 Traditional Fabrication Methods of Ionic Polymer Transducers

This section will describe the impregnation-reduction process traditionally used to fabricate ionic polymer transducers. Variations to that process are also presented.

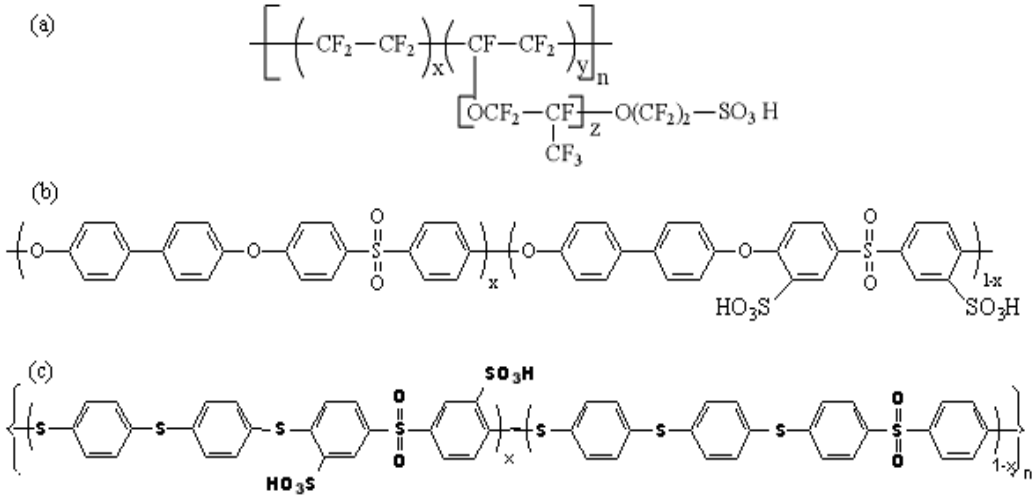

Figure 2.6: (a)Chemical Structure of Nafion, (b)Chemical Structure of BPS, (c)Chemical Structure of PATS.

2.5.1 Impregnation-Reduction Process

The impregnation-reduction method is applicable to a wide range of ionomers. Theocratically this electroless chemical plating method is implementable to any ion selective ionomer membrane. The impregnation-reduction consists of three main steps. The first step is to soak the polymer in a metal salt solution such as $PtNH_3Cl_2$ to populate it with a reducible metal (Kim and Shahinpoor, 2003). The next step is to reduce the metal salt on the surface of the membrane by soaking it for 4 to 6 hours in $NaBH_4$ or $LiBH_4$. The reduction occurs according to the following reactions,

$$NaBH_4 + 4[Pt(NH_3)_4]^{2+} + 8OH^- \longrightarrow 4Pt^0(s) + 16NH_3(g) + NaBO_2(sd) + 6H_2O \tag{2.13}$$

and

$$NaBH_4 + 4H_2O \longrightarrow 4H_2(g) + NaOH(Na^+ + OH^-) + B(OH)_{3(sd)} \tag{2.14}$$

A schematic representation of the reduction process is shown in Figure 2.7

The initial concentration of reducing agent used for Nafion is 0.05% w/w, and then another 0.05%w/w $NaBH_4$ salt is added every 30 minutes (Kim and Shahinpoor, 2003). Varying the concentration of the reducing agent controls the penetration depth

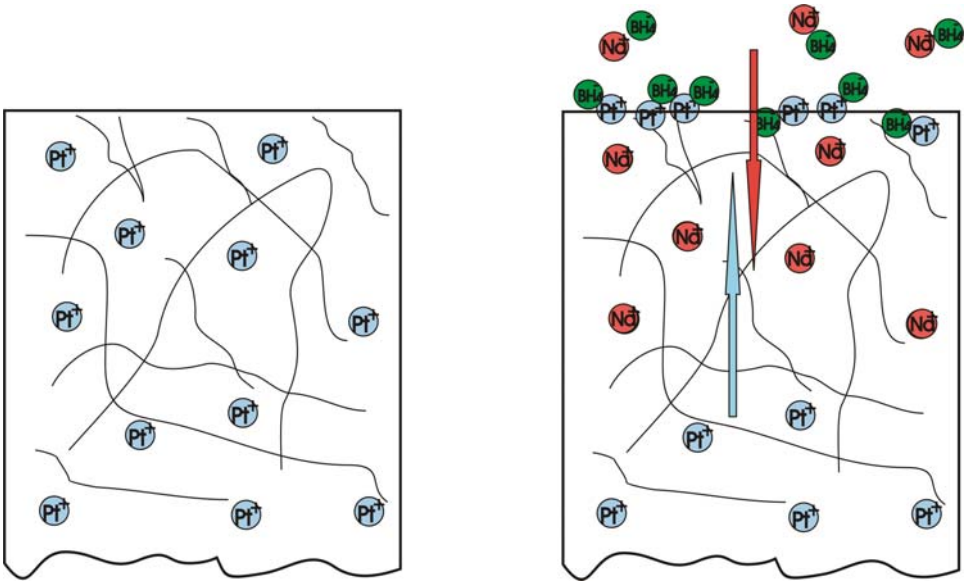

Figure 2.7: Schematic showing the reduction of platinum on the surface forming the electrode of the ionic polymer transducer

of the electrodes inside the polymer. The depth and the uniformity of the electrodes has been shown to increase the performance of the transducer (Nemat-Nasser, 2002b). The last parameter optimized for impregnation-reduction is the number of plating layers. As discussed in Oguro et al. (1999), increasing strain per unit voltage is observed with increasing number of platinum layers until the mechanical stiffness of the electrode reduces the deflection. This increasing trend suggests better performance with increasing the number of plating layers. Although Oguro et al. (1999) indicated that five layers provided the optimal bending performance, the optimal number of plating layers need to be verified for different ionomers, metal cation, and reducing agent. This attribute of the transducer fabrication will be investigated in this work.

The third step is to electroplate the polymer composite with a thin (50 nm to 100 nm) of gold to increase the surface conductivity of the transducer. A fourth optional step is to perform ion exchange, such as exchanging Na^+ for the Li^+ ion. This is done by soaking the polymer in an NaOH or LiOH solution.

2.5.2 Variations to the Impregnation-Reduction Method

Impregnation reduction reactions requires several chemical compounds and diluents. These methods are expensive and are not environmentally friendly. Shahinpoor and Kim (2002a) incorporated silver, graphite and palladium particles in the membrane using a physically loading method. The metal powder is hot-pressed on membrane surfaces and impregnation-reduction is later performed. Physically loading the membrane reduces the number of impregnation-layers from an average of 5 to 1. Less expensive powders such as graphite are possible to incorporate using this method. Shahinpoor and Kim (2002b) also reported a fabrication path to make three-dimensionally shaped transducers. Nafion solution is casted in molds with the desired shape, and later an electrode is plated using any of the previously mentioned methods. The 3D technique is implemented to create thick transducers. In this same article Shahinpoor and Kim (2002b) suggests but does not implement, casting two conductor-ionomer mixed electrodes around the main casted membrane. The suggested path starts with casting a layer of the electrode mix, followed by a layer of pure ionomer and finally a layer of the mix is casted on the top to form the second electrode. Taegeun et al. (2001) developed a replication method to manufacture a large surface-area ionic polymer actuator. High surface area etched aluminum foil was used as a template for replication using liquid Nafion solution, and finally Pt was plated on this high surface are surface to form an transducer with superior actuation properties, such as large strains and strain rate.

2.6 Direct Assembly Process (DAP)

As mentioned in Chapter 1, a novel fabrication process of ionic polymer transducers is developed in this dissertation. The Direct Assembly Process is inspired by fabrication techniques used in preparing supercapacitors and hydrogen fuel cells. The DAP was developed in collaboration with Dr. Kenton B. Wiles in Dr. James E. McGrath group. Their expertise in fuel cell fabrication and polymer synthesis was instrumental for the development of this process. The Direct Assembly Process can be implemented in

two main schemes. The first is to apply the electrode on a dry membrane and a second method is to solvate the membrane and then apply the electrode. Moreover, in both methods the electrode can be either painted directly on the membrane or painted separately on a decal and later hot press it on the membrane.

2.6.1 Direct Assembly Process with Dry Membranes

The Direct Assembly Process consists of first dissolving the polymer into an alcohol solution. In this study Nafion 1100 5% weight polymer solution is used. Solutions of BPS and PATS ionomers are also attempted but the resulting electrodes are very stiff and exhibit low ion conduction, therefore Nafion 1100 5% solution is used for all samples discussed in this work. The Nafion dispersion is obtained from fuelcellstore.com and used without further modification. The next step in the process consists of mixing a metal powder with the polymer solution. For some metal particulates such as carbon nanotubes and large conductor loading, additional solvents are added to the mixture enhancing dispersion. Isopropyl alcohol (IPA) is an inexpensive and easy to evaporate solvent, while glycerol is added to increase viscosity. The mix is sonicated and stirred for 1 to 4 hours to ensure homogeneity and dispersion of the metal grains. The duration of mixing and sonication depends on the type of conducting powder and concentration of polymer solution and metal volume percent. The conductor-polymer is applied to the polymer in one of two ways. The first method consist of directly painting several layers of the mix on each side of the membrane using a brush. The sample is placed in an oven at 130 C for 15 min between each layer. The resulting composite is then hot pressed at 210 C and a pressure of 20 MPa. This step adheres the electrode to the membrane surface and decrease the interface resistance between the electrode and the membrane.

The second DAP method is to paint several layers of the polymer-metal mix on a Teflon reinforced glass fabric named Furon, and then hot press these decals on the polymer using same pressure and temperature as in previous method. Once cooled down the membranes are hydrated, and the Teflon mesh is detached from the polymer. For dry actuators, the decal method controls better the loading and

uniformity of the electrode. Loading is controlled by weighing the decals before and after painting the electrodes. Painting the electrode directly on the membrane causes the polymer to swell due to solvents from the electrode mix leading to wrinkles in the membrane. A vacuum plate is placed under the membrane during painting to decrease wrinkling. The conductivity of the conductor-ionomer electrodes is usually around 1 to 20 S/cm compared to 94000 S/cm for Pt. Therefore a conducive layer is required to increase the surface conductivity of the transducer.

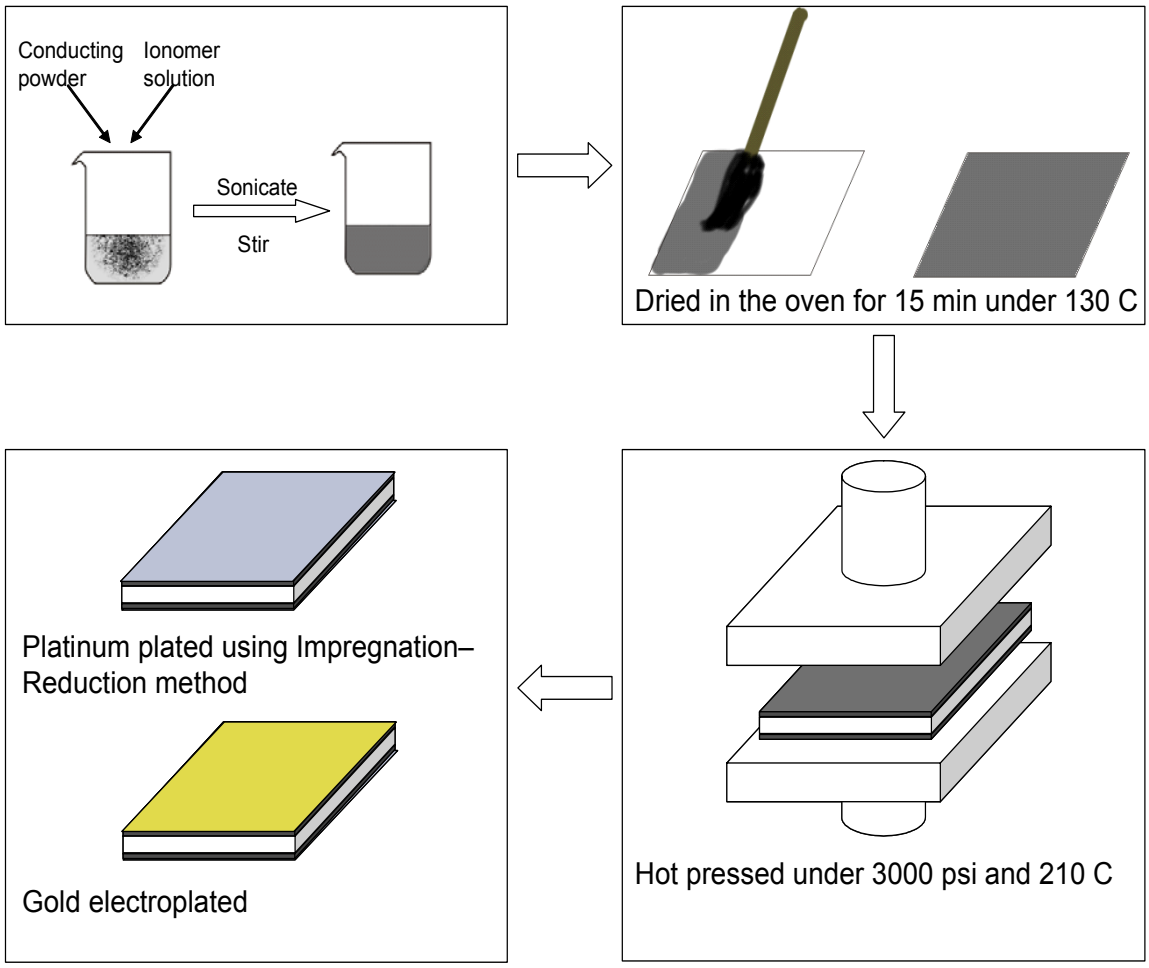

Figure 2.8: Schematic showing the four steps Direct Assembly Process (DAP) for building dry transducers.

In this dissertation two methods are developed to increase surface conductivity of water hydrated ionic polymer transducers. The first method, an additional platinum layer is applied to the surface using the impregnation-reduction method

previously described. A gold overlayer is then electroplated on the outer surface of the platinum. The alternative method is composed of depositing of a Au layer by self assembled monolayers. Supriya et al. (2005) demonstrated that solution-based assembly of Au on Nafion suffered from poor adhesion of the electrodes to the substrate and after a few cycles of actuation the electrode debonded from the surface. A thin layer of a linear amine-terminated poly(urethane urea) (PUU) elastomer was used as a linking or adhesive agent to enhance the adhesion properties of the electrode. A thin layer of 1%(w/w) solution of PUU is painted on the outer surface of the membrane. Au particles can attach to the amine and amide groups in the PUU. A monolayer of Au thus formed can serve as the starting layer for the seeding process (Supriya et al., 2005) to form electrodes. Transducers with Pt/Au electrodes deposited according to the first method perform better compared to actuators with Au solution-based assembly. Degradation in performance is due to the low conductivity of PUU, and therefore the adhesive layer has to be very thin ($< 1\mu$m). The advantage of using the second method is the patternability of the solution-based assembly of Au. A photoresist material is applied on the PUU and a light etching lithography technique is applied pattern the surface. This method enables distributed actuation/sensing on the submicron level. As in the impregnation-reduction an optional ion exchange step could be made by boiling the membrane for 2 hours in a 1 M chloride solution such as LiCL or NaCl. A schematic of this process is shown in Figure 2.8.

diluents other than water could also be incorporated into the resulting dry membrane by following any of the previously discussed methods. In this study four diluents are incorporated in the membrane: water, formamide, DiEthylene-Glycol (DEG), and 1-ethyl-3-methyimidazolium trifluoromethanesulfonate (EmI-Tf) ionic liquid. Several methods of adsorbing the diluent to the membranes are developed. Some diluents such as formamide require approximately 24 hours to saturate the membrane at room temperature. This duration is decreased to 3 hours if the membrane is sonicated inside the solution. This duration is shortened to less than 1 hour by heating the membrane inside the solution at 100 C. The diffusion of EmI-Tf ionic liquid in Nafion is slower compared to formamide. To date, our group achieved a

maximum absorbtion of 58% w/w (weight of EmI-Tf to dry polymer weight). This uptake is achieved by heating the membrane at 150 C for 4.5 hours in the presence of EmI-Tf. A temperature of 150 C degrades EmI-Tf after several heating cycles. Using a co-diluent such as ethanol or N-methylformamide proved to increase diluent uptake. The co-diluent is later evaporated by baking the sample at an elevated temperature under vacuum. Table 2.1 shows that an optimal composition of 40 vol% (volume of N-methylformmaide to volume of EmI-Tf) and temperature of 130 C for 4 hours had an uptake of 58.2%w/w. This is a more stable method due to a 20 C decrease in temperature. Table 2.1 presents absorbtion of EmI-Tf corresponding to several temperatures, compositions, and durations.

Table 2.1: Diluent uptake as a function of diluent composition, temperature, and duration. The composition present the volume of N-methylformmaide to the total volume of EmI-Tf and N-methylformamide. The last column presents the formamide vol% of the mixture in the membrane before evaporating the co-diluent.

Percent N-methylformamide	Temp (C)	Time (hrs)	Total uptake (%w/w)	EmI-TF uptake (%w/w)	Formamide uptake (%w/w)	Vol% Formamide
20%	70	3:30	36.7	30.2	6.6	23.2
20%	130	4:30	70.4	56.1	14.2	26.0
40%	130	4:30	83.5	41.7	41.8	58.2
40%	130	1:30	91.3	51.2	40.1	52.1

Apart from water all these diluents excessively swell the membrane. For example formamide swells the membrane over 100% of its original volume, leading to cracks in the conductive surface electrode. Therefore the last step of increasing the surface conductivity is postponed until after the diluent is incorporated. The Pt/Au chemical deposition or solution-based assembly of Au previously described are implemented in aqueous environment and therfore limited to water swollen transducers. A third method of increasing surface conductivity is developed for non-hydrated transducers. The transducer is sandwiched between two 100 nm-thick conductive gold foils and the entire composite is intimately bound together by a hot-pressing process. For

dry membranes this hot-pressing is carried out at 20 MPa and 210 C for two minutes. However, the non-aqueous solvated ionomers will flow under this high pressure and long duration leading to the deformation of the transducer. In order to maintain the dimensional stability of the membrane during the hot-pressing process while still binding the three layers together, the pressure and pressing time are reduced. It is found for EmI-Tf ionic liquid that good results are obtained for hot-pressing carried out at 4 MPa and 160 C for around 10 to 20 seconds depending on the metal loading and thickness of the electrode. As for volatile diluents such as formamide 140 C and less than 5 to 10 seconds are sufficient and preserves the dimensional stability of the transducer better. The gold foils used are Falcon-Brand 24 carats gold leafs; they helped decreasing the surface resistance from greater than 100 kΩ/cm for the painted metal layers to less than 1 Ω/cm. Transducers with high metal loading in the electrode ($>$ 25 vol%) a thin layer of diluted ionomer solution (50% w/w IPA/Nafion 5%) is painted over the high surface area electrodes. This step enhances the adhesion of the gold foils to the electrode.

2.6.2 Direct Assembly Process with Solvated Membranes

The Direct Assembly Process is implemented in the solvated polymer state. Dry assembly of the electrode might be inadequate for some diluents. As mentioned earlier, some diluents excessively swell the membrane leading to delamination of not only the gold overlayer but even the high surface area electrode. Moreover some diluents might desolve the ionomer in the high surface area electrode. Nafion ionomer solution requires a complicated processes to cast into the semicrystalline structure of the membrane. In amorphous state Nafion in the high surface area electrode is unstable under high temperature required for some diluents to be absorbed into the transducer. In this DAP scheme, the membrane is solvated with the proper liquid after being exchanged with the desired cation. A proportional amount of diluent is added to the mix. Usually this amount corresponds to the weight of diluent absorbed in the membrane. The electrode is painted on the both surfaces of the membranes, then sandwiched between two gold leaves and melt pressed together under the appropriate

temperature, pressure, and duration. These parameters are usually similar to the ones mentioned in the previous section, but the duration is shortened by 20% to 30%. Challenges of this scheme are diluent loss and dimensional stability. Organic diluents evaporate at the elevated melt-press temperature though it is below their boiling point. A significant amount of diluent evaporates out of the membrane. This amount is around 30% depending on the boiling point of the diluent, melt press temperature, and diluent uptake. Some highly volatile diluents are impossible to incorporate using this method. The diluents with boiling point less than 10 C smaller than the flow temperature of the solvated ionomer (T_g) are hard to incorporate using this scheme of DAP. The only possible path for such diluents is to build dry transducers and then incorporate the diluent. The platinum and electroplated gold layers are plated in solutions with the final diluent if possible. Otherwise, the impregnation-reduction reaction and the electroplating are done in a diluent (or a mixture of diluents) that have similar swelling properties to the low boiling point diluent to be incorporated. A schematic of the direct assembly process with solvated membranes is shown in Figure 2.9.

2.7 Electrode Materials

Platinum and gold are traditionally used as electrode materials for ionic polymer transducers (Kim and Shahinpoor, 2003), although Bennett and Leo (2003) have used low cost non-precious metals such as copper as electrode material. Tamagawa et al. (2003) plated Nafion with combinations of silver, copper and nickel metals using impregnation-reduction. Shahinpoor and Kim (2002a) reported loading the polymer membranes with metal particulates such as palladium. The metal powder is hot-pressed on membrane surfaces and palladium or platinum impregnation-reduction is later performed.

The ability to incorporate different electrode materials is enabled by our development of the direct assembly process for fabricating the ionic polymer transducers. Hybrid ionomeric transducers consisting of several conducting powders are also man-

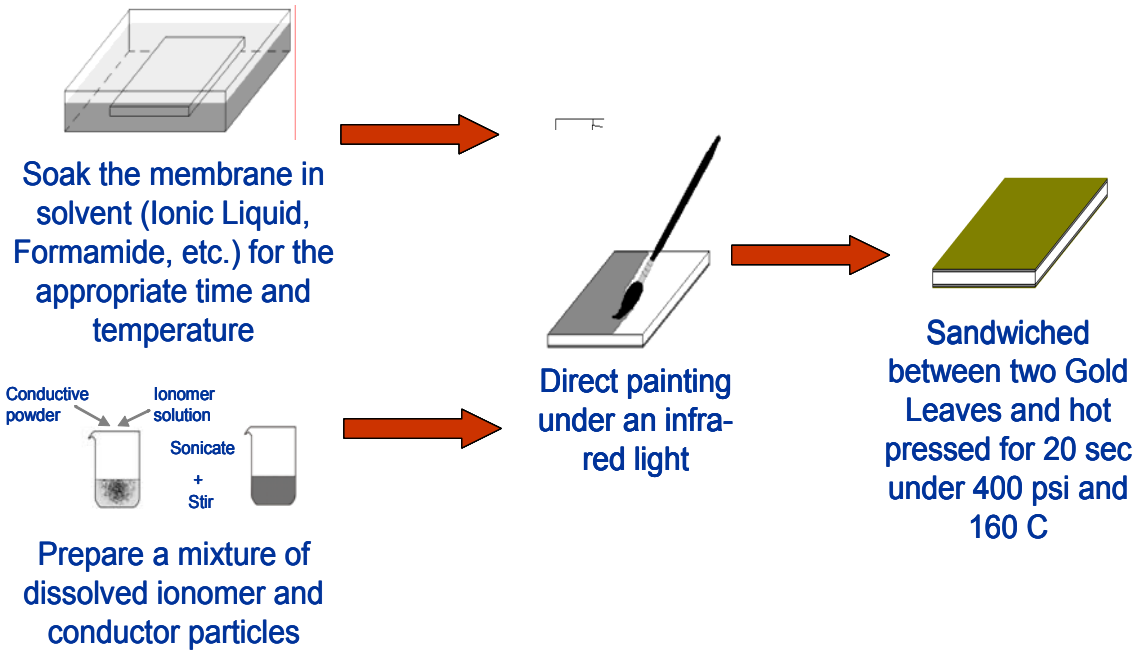

Figure 2.9: Schematic showing the four steps Direct Assembly Process (DAP) for building solvated transducers.

ufactured.

Several interesting materials will be explored in the following chapters with the focus on their electrical and electrochemical properties. In this dissertation we will consider high surface area platinum, gold flakes, hydrous and anhydrous RuO_2, single walled carbon nanotubes (SWNT), carbon black, and polyaniline (PANI) conducting polymers. The following sections will discuss the properties and activities of each of these materials. A summary of the properties will be presented in Table 4.2 in a later chapter.

2.7.1 Carbon black

Carbon is widely used as a high surface area electrode material for several systems including electrochemical capacitor devices(Frackowiak and Beguin, 2001). Advantages of this material includes the low price and availability. Although less conductive than graphite, carbon black is a good electrical conductor. It has a well established fabrication processes resulting in large specific surface area materials (up to 2500 m^2/g)in

the form of powders, woven cloths, felts, or fibers (Frackowiak and Beguin, 2001). The specific capacitance of carbon black is around $10\mu F/cm^2$ and this value is mostly due to the electric double layer (only around 1 to 5% pseudocapacitance)(Frackowiak and Beguin, 2001). Carbon is one of the rare materials that could approximate a pure electrostatic double layer (Also Hg between +0.23 to -1V RHE in acid solutions and Au from -0.1 to +1.33V RHE in alkaline solutions show pure electrostatic double layer capacitance)Conway et al. (1997). The small pseudocapacitance in this material is due to the impurities on the surface of the carbon particles. This could be controlled by special treatment for increasing the surface functionality using one of the following methods:

- Chemical treatment (by hot nitric acid treatment).
- Electrochemical polarization (these changes are reversible and they disappear with capacitor cycling).
- Cold plasma treatment (enhance the pore radius distribution and surface atom concentration.

According to our knowledge carbon black was never reported as a electrode material in ionic polymer transducers. Carbon black used in this dissertation is purchased from Alfa Aesar with a surface area of around $80m^2/g$ and used without further purification.

2.7.2 Single-Walled Carbon Nanotubes

Carbon nanotubes (CNT) were discovered in 1991 by Iijima are formed by rolled graphite sheets, with an inner diameter starting from 1 nm up to several nm and a length of ten to one hundred μm. Tubes formed by only one graphite layer are called single wall nanotubes (SWNT). Tubes consisting of multiple concentric graphite layers are called multi-wall nanotubes (MWNT). Depending on the purification and manufacturing process CNTs could be good conductors of electricity. SWNTs have

large effective surface area up to $1000 m^2/g$. Like carbon black, capacitance in CNTs is mostly electrostatic double layer.

CNT actuators are first reported by Baughman et al. (1999). The mechanics of actuation is due to some quantum mechanical effects such as changes in orbital occupation and band structure and electrostatic double-layer charging for high-density charge injection of either sign (Baughman et al., 1999). Due to their large elastic modulus, CNT actuators generates large forces and small strains (0.1 to 1% strain) (Barisci et al., 2003). As actuators they bend toward the anode(+), which is the same direction as ionic polymers. Moreover, at high charge density the electrostatic effect dominates and material expansion occurs regardless of the charge sign. Therefore, such an actuating system, at high charge density, principally cannot work in the bimorph cantilever geometry when asymmetrical electromechanical properties of both sides are required for cantilever bending (Levitsky et al., 2004). Due to the immobility of anions in Nafion, the quantum stretching in SWNT and electrostatic actuation in ionomers are cumulative. Those reasons would make them a good candidate for electrode materials in ionic polymer transducers.

Another attractive property of SWNT is the low percolation level they exhibit in polymer matrix composite. Well dispersed SWNT/polymer matrix is proved to percolate at 0.2 volume percent compared to around 30% for spherical particles (Park et al., 2002b). The major disadvantage of SWNT is the high price, and the difficulty in dispersing them in the polymer matrix (Park et al., 2002b).

The SWNTs used in this study are high purity single walled carbon nanotubes obtained from Carbon Nanotechnologies Incorporated and is used without further purification.

2.7.3 Conducting polymers

Polymeric materials, such as p- and n-dopable poly(3-arylthiopene), p-doped poly(pyrrole), poly(3-methylthiophene), poly(1,5-diaminoanthraquinone), or polyaniline (PANI) have been suggested as electrode materials in electrochemical devices such as supercapacitors (Prasad and Munichandraiah, 2002).

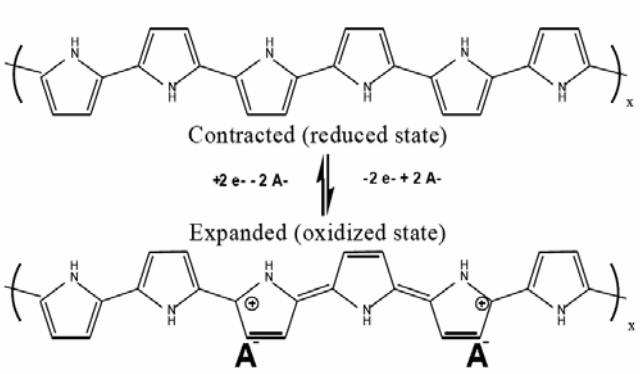

Figure 2.10: Charge and discharge redox mechanism of conducting polymers

The pseudocapacitance arises from slow charge and discharge redox reactions, and the mechanism is shown in Figure 2.10 In terms of actuation they expand when ions enter them, and contract in the reduced state (Madden et al., 2004). PANI powder is purchased from Alfa Aesar doped with HCl and used without further refinement. The typical conductivity of doped conducting polymer is on the order of 100 S/cm compared to 1000 S/cm for carbon and larger for RuO_2 and Pt metals. As an active material conducting polymers provides strains on the order of 2 % (Madden et al., 2002), and maximum strain rates on the order of 12 %/s have been reported (Ding et al., 2003). Rates are limited by internal resistance of the polymers and electrolytes, and by ionic diffusion rates of ions inside the polymer (Madden et al., 2002).

2.7.4 Metal oxides

In electrochemical devices RuO_2 and IrO_2 are the preferred materials due to the large surface area $(50 - 70 m^2/g)$ and good electrical conductivity while TiO_2, Cr_2O_3, MnO_2, and Co_2O_3 used with a carbon support (to increase conductivity)Kotz and Carlen (2000). Metal oxides show significant pseudocapacitance in aqueous acids and the following is an example for RuO_2 (Conway, 1999)(Frackowiak and Beguin, 2001)

$$2RuO_2 + 2H^+ + 2e \rightleftharpoons Ru_2O_3 + H_2O, \tag{2.15}$$

and in the case of hydrous ruthenium oxide,

$$2\mathrm{RuO_x(OH)_y} + \delta\mathrm{H^+} + \delta\mathrm{e} \rightleftharpoons 2\mathrm{RuO_{x-\delta}(OH)_{y+\delta}}. \tag{2.16}$$

RuO_2 has a typical specific capacitance of $80\mu\mathrm{F/cm^2}$, while hydrous $\mathrm{RuO_x(OH)_y}$) can go up to $1000\mu\mathrm{F/cm^2}$ (Sugimoto et al., 2004). Moreover Sugimoto et al. (2004) proved that the redox reactions for the ruthenium dioxide depends greatly on the sweep rates. As for actuation our group is the first to report actuators with ruthenium dioxide electrodes (Akle et al., 2004b).

Anhydrous RuO_2 with a surface area (SA) of 45 to 65 $\mathrm{m^2/g}$ are purchased from Alfa Aesar and used without further refinement. RuO_2 is a less expensive material compared to noble metals such as platinum. The bulk density of RuO_2 solids is 7.05 g/cc leading to a volumetric surface area of 388 $\mathrm{m^2/cc}$. Hydrous RuO_2 are also purchased from Alfa Aesar and used without further refinement.

2.7.5 Platinum

Platinum is the material of choice for ionic polymer actuators with Nafion membranes due to its good electrochemical stability and availability in cationic form for the impregnation-reduction fabrication process. As reported earlier platinum-Nafion actuators show back-relaxation for several cation species including H^+, Li^+, Na^+, and K^+. This same actuator doesn't show any back relaxation when used with large organic ions like TBA^+ (Nemat-Nasser and Wu, 2003b). Platinum is known to have a large adsorbtion pseudocapacitance especially in acidic medium. High surface area platinum powder of 3 to 5 nm sized particles acts as a catalyst in several electrochemical devices especially hydrogen fuel cells. The surface area of such powders are in the order of 24 to 29 $\mathrm{m^2/g}$ and volumetric surface area of 506 to 611 $50 - 70\mathrm{m^2/g}$. The main interest in this material is large electrical conductivity of 94000 S/cm with relatively large volumetric surface area. The disadvantage is that it is very expensive.

2.7.6 Gold Flakes

Fujiwara et al. (2000) recently introduced gold as high surface area electrodes on Flemion membranes. Transducers with gold electrodes don't show any back-relaxation in their response for several cation species including Li^+ and TBA^+Nemat-Nasser and Wu (2003b). Gold powders are available either as spherical or in the shape of flakes. Due to the large aspect of flakes, they tend to have a low percolation level. The conductivity of gold is very large around 454500 S/cm. The major disadvantage of gold particles is the low surface area in the order of 0.4 to 0.75 m^2/g, and being a very expensive material. As mentioned earlier the charging mechanism is mostly an electrostatic double layer type. In this study the gold powder is purchased from Alfa Aesar in the form of flakes of $\tilde{3}$ microns in length and has a specific surface area lower than 0.5 m^2/g. It is used without further purification.

2.8 Electrode Morphology

Scanning electron microscopy was performed on selective polymer samples. The resulting electrode morphology is studied for various plating methods. Samples with Impregnation-reduction plated platinum electrodes are compared to samples built using the direct assembly process. SEM images for samples varying electrode thickness and metal to polymer ratio in the electrode are also presented.

Impregnation-reduction fabricated electrodes demonstrates a gradient metallic profile and dendritic morphology as shown in Figure 2.11(a). A transducer fabricated using DAP is shown in Figure 2.11(b). This transducer is designed with water as the diluent, and hence an impregnation-reduction platinum layer was plated with a gold electroplated on top. The 10 μm layer is the large surface area electrode made of RuO_2 / Nafion mix.

Shown in Figure 2.12 are two SEM images of a DAP built transducer. The SEM in Figure 2.12 (a) represents 9.5μm thick RuO_2 / Nafion electrode painted on a Nafion 117 membrane. Figure 2.12 (a) represents 38μm thick RuO_2 / Nafion electrode painted on a Nafion 117 membrane. Those transducers are solvated with EmI-Tf ionic

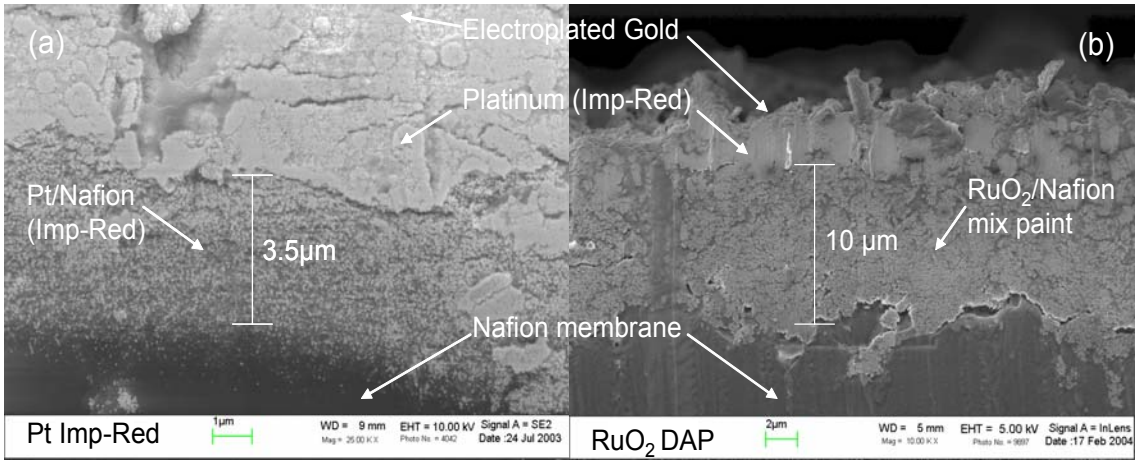

Figure 2.11: Scanning electron microscopy (SEM) showing (a) the top cross-section of a Nafion 117 plated with platinum following 6 layers of impregnation-reduction, and (b) the top cross-section of a Nafion 117 ionomer painted with 6 layers of RuO_2 and Nafion mix . Also shown in (b) is the platinum interface between the painted layer and the electroplated gold overlayer.

liquid.

The concentration of the metal to ionomer is also varied and SEM images of the electrodes in these transducers are shown in Figure 2.13. The electrodes are composed of RuO_2 / Nafion mixture, and Formamide solvated the polymer. Figures 2.13 a,b,c,and d, represents the high surface area RuO_2 electrode with 22, 30, 36, and 66 Vol % metal respectively.

Varying the thickness of the electrode controls the amount of metal particles and this also referred to as the metal loading. The amount of well dispersed metal particles is proportional to the metal-ionomer interfacial area. The electric double layer capacitance increases with this interfacial area. This is one parameter to be studied in later parts of this dissertation. The concentration of the conductor particles to the Nafion ionomer in the electrode is a control of the conductivity through the electrode. This percolation follows the percolation theory model presented in Chapter 1. This is also optimized later in this dissertation. Finally these SEM images shown in Figures 2.11, 2.12, and 2.13 demonstrates the ability of the direct assembly method to control the morphology of the electrodes in ionic polymer transducers.

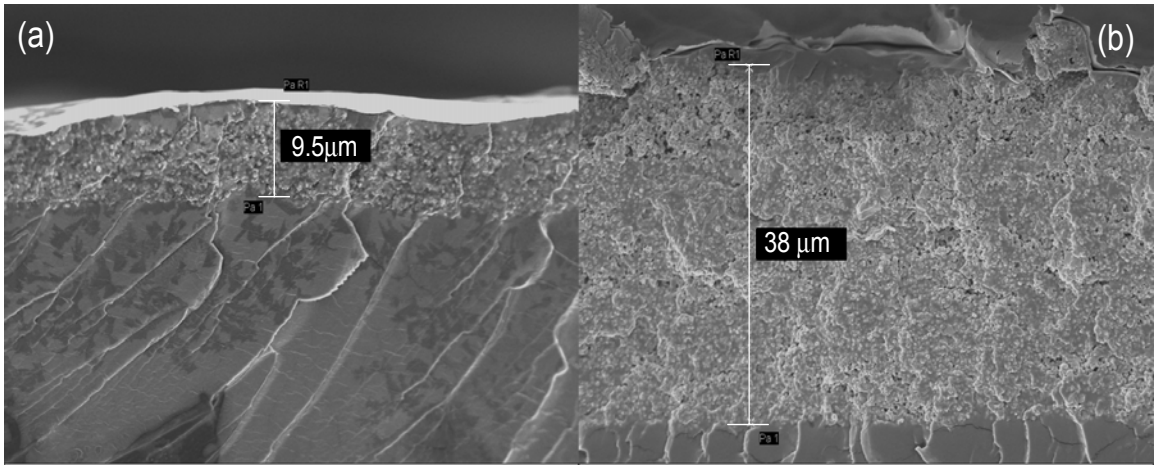

Figure 2.12: Scanning electron microscopy (SEM) showing (a) the top cross-section of a Nafion 117 ionomer painted with a 9.5 μm RuO_2 / Nafion electrode. (b) shows the top cross-section of a Nafion 117 ionomer painted with a 38 μm RuO_2 / Nafion electrode.

2.9 Conclusion

Testing procedures for the characterization of ionic polymer transducers in bending and extensional directions are presented. Equations for computing mechanical, electrical, and electromechanical properties from experimental results are provided. A new fabrication method for ionic polymer transducers is developed and characterized. The method named the direct assembly process allows greater control of the electrode morphology through precise control of the fabrication parameters. Transduction and electrochemical properties of several conducting powders including high surface area platinum, gold flakes, hydrous and anhydrous RuO_2, single walled carbon nanotubes (SWNT), carbon black, and polyaniline (PANI) conducting polymers are introduced in this chapter. These materials will be studied in later chapters of this dissertation as electrode materials. This is made possible due to the introduction of this novel fabrication method. The detailed presentation of the steps in the direct assembly process is given for different types of diluents.

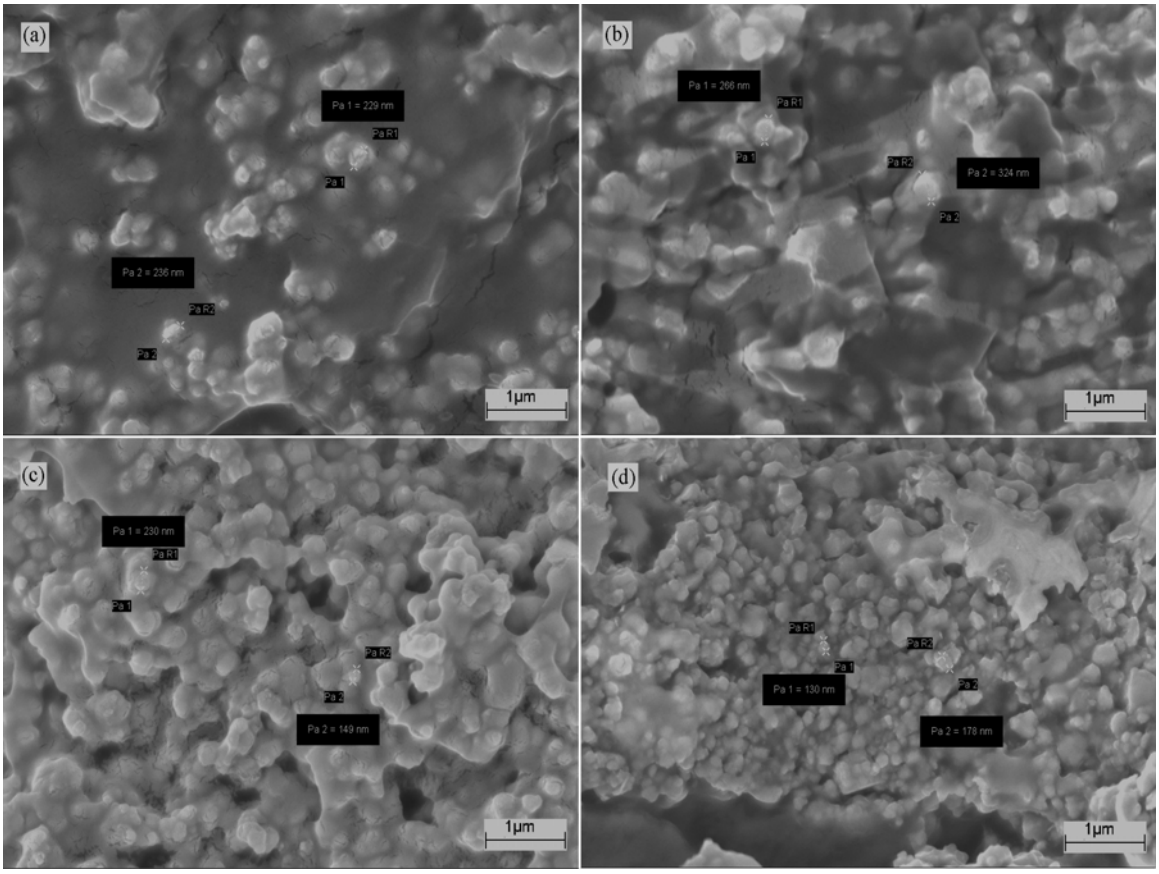

Figure 2.13: Scanning electron microscopy (SEM) SEM images of the high surface area RuO_2 electrode with (a) 22, (b) 30, (c) 36, and (d) 66 Vol % metal.

Chapter 3

Correlation of Capacitance and Actuation in Ionic Polymer Transducers

In this chapter, we discuss a series of experiments that characterize the electromechanical actuation response of three families of ionomers: Nafion (a product of DuPont), BPS (sulfonated poly(arylene ether sulfone)) and PATS (poly(arylene thioether sulfone)). The first polymer is commercially-available while the second and third polymers are synthesized by the direct polymerization of sulfonated monomers in Dr. McGrath's Lab at Virginia Tech ((Wang et al., 2002) and Wiles et al. (2002)). The mechanical properties and actuation response of Nafion-117, BPS, and PATS of varying ionic content are studied in the Lithium cation form. Transducers are built from membranes of 100 to 180μm thick. Platinum layers are deposited using the impregnation reduction method. The strain response of the materials varies from 50 μstrain/V to 750 μstrain/V at 1Hz. A linear correlation was found between the strain response and the capacitance of the material. This correlation is independent of the polymer composition and the plating parameters. All of the ionomers analyzed in this work exhibited a strain-to-charge response between 9 $\frac{\mu strain}{\frac{C}{m^2}}$ and 15 $\frac{\mu strain}{\frac{C}{m^2}}$. Due to the fact that the low-frequency capacitance of an ionomer is strongly related to charge accumulation at the blocking electrodes, this correlation suggests a strong relation-

ship between surface charge accumulation and mechanical deformation in ionomeric actuators. This correlation of capacitance and actuation performance motivated most of the work in this dissertation.

3.1 Surface Charge Accumulation in Ionomeric Materials

Ion conduction is measured by applying a voltage to the polymer and measuring the resulting current flow according to Equation 2.3. The experimental procedures for measuring the impedance are detailed in Chapter 2.

The dielectric properties of the material can be studied by transforming the impedance into a relationship between charge, Q, and voltage V,

$$\frac{Q(j\omega)}{V(j\omega)} = \frac{1}{j\omega Z(j\omega)} = C(j\omega), \tag{3.1}$$

The variable $C(j\omega)$ represents the measured complex capacitance of the polymer. The complex capacitance can be separated into real and imaginary components

$$C(j\omega) = C'(\omega) - jC''(\omega), \tag{3.2}$$

where the real part represents capacitive storage and the imaginary component represents loss. The measured complex capacitance is related to the complex permittivity through the expression (Daniel, 1967)

$$\varepsilon(j\omega) = \frac{C(j\omega)T}{\varepsilon_o A} = \varepsilon'(\omega) - j\varepsilon''(\omega), \tag{3.3}$$

where T is the sample thickness, A is the surface area of the electrode, and ε_o is the vacuum permittivity.

The dielectric properties are used to characterize the ionic conduction properties of the polymer. For pure insulators, the complex permittivity yields information about the dielectric relaxations of the polymer (Daniel, 1967). Dielectric relaxation measurements in ion-exchange membranes have been performed by a number of researchers. Mauritz and co-workers presented a thorough study of dielectric relaxations in ion-exchange membranes (Mauritz and Yun, 1988; Mauritz and Fu, 1988).

They noted a power-law dependence of the complex permittivity as a function of frequency (Mauritz, 1989) and related this characteristic to long range ion transport within the material. Impedance measurements performed by Cahan and Wainwright (1993) indicated that this power-law dependence was really an artifact of 'blocking electrode', or, 'space charge' effects at the polymer-electrode interface. The relationship between electrode effects and dielectric measurements was also studied by Fontanella et al. (1993) and their results independently confirmed the analysis of Cahan and Wainwright (1993). Further studies by Wintersgill and Fontanella (1997) demonstrated that the ionic conduction mechanism was strongly affected by water content and that the low-frequency (less than 100 Hz) power law dielectric behavior was strongly affected by blocking electrode and space charge effects.

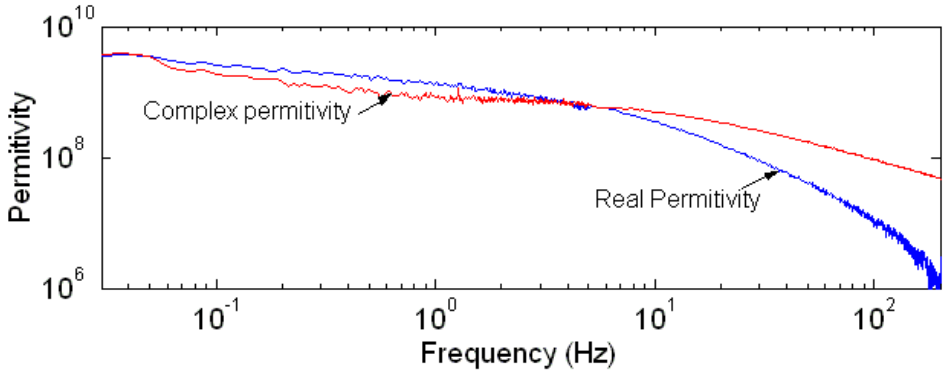

Figure 3.1: Real and complex permitivities of a typical Nafion-based ionic polymer transducer.

Shown in Figure 3.1 is the real and complex permitivities of a typical Nafion-based ionic polymer transducer fabricated by our research group. These measurements are consistent with those published by Mauritz, et al., for hydrated Nafion in various cation forms. The significant feature of the data is the large low-frequency permittivity exhibited by the polymer; relative permittivity values on the order of 10^9 to 10^{10} are not uncommon for ionomeric polymers.

The large low-frequency permittivity is attributed to charge accumulation at the electrodes due to ionic conduction. This was discussed clearly in Wintersgill and Fontanella (1997) through examination of the dielectric response of 'dry' and

'wet' Nafion samples. Wintersgill and Fontanella (1997) performed several tests and demonstrated that the apparent ionic conductivity changed dramatically depending on sample size. They attributed this size-dependent variation to the existence of charge accumulation and 'blocking electrode' effects at the interface between the polymer and the electrode.

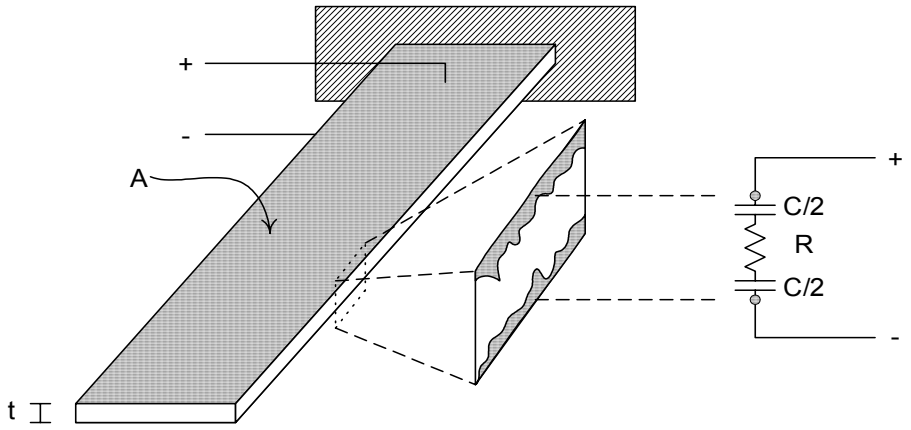

Figure 3.2: Blocking electrode model using a resistor and two capacitors in series.

A common model of ion conduction that incorporates blocking electrode effects is shown in Figure 3.2. The polymer is modeled as a pure resistance with capacitors placed in series to account for charge accumulation at the surface. Assuming this model for ion conduction results in the impedance function,

$$Z(j\omega) = R + \frac{1}{j\omega C}, \tag{3.4}$$

where the imaginary part of the impedance is related to the capacitance of the blocking electrode. Assumptions in this model are similar to the assumptions made in Chapter 2, Section 2.1. during the derivation of Equation 2.4. This conduction model leads to the relationship

$$\frac{C(\omega)}{A} = \frac{\varepsilon'(\omega)}{T} \tag{3.5}$$

for the areal capacitance. The frequency-dependence of the capacitance has been added to the function due to the measured variation in the dielectric behavior as a function of frequency.

3.1.1 Transducer Preparation

Nafion 117 (1100 equivalent weight, 7 mils (178 μm) thick) membranes are used as the control material for this study. Nafion membranes are commercially available from DuPont and the chemical structure of Nafion is shown in Figure 2.6 (a).

Two other ion exchange polymers are also investigated in this study. The two polymers are sulfonated poly(arylene ether sulfone) or BPS (Wang et al., 2002), and sulfonated poly(arylene thioether sulfone) or PATS (Wiles et al., 2002). The chemical structures of BPS and PATS are shown in Figures 2.6(b) and (c), respectively. The number following BPS or PATS represents the number of sulfonic acid groups attached to the polymer backbone (IEC). Both BPS and PATS membranes were solvent cast from N,N-dimethylacetamide. Details on membrane preparation are found in Kim et al. (2003). The advantages of BPS and PATS copolymers include larger modulus than Nafion when hydrated and an ion content that can be precisely controlled during the copolymer synthesis. A comparison of the general physical properties of Nafion, BPS, and PATS copolymers is given in Table 3.1.

Table 3.1: Properties of Nafion, BPS, and PATS Copolymers.

	EW (g/eq)	IEC (meq/g)	Water Uptake [1] (% weight)	Protonic Conductivity[2] (S/cm)	Hydrated Modulus[2] (MPa)
Nafion 117	1100	0.91	22	0.11	120
BPS 30	1110	1.3	29	0.06	920
BPS 35	770	1.53	40	0.08	640
BPS 40	650	1.7	56	0.10	400
PATS 30	860	1.17	20	0.06	1040
PATS 40	660	1.51	86	0.11	400

EW = Equivalent Weight

IEC = Ion Exchange Capacity

Water Uptake, Protonic Conductivity, and Hydrated Modulus determined in liquid water at 30°C - see indicated references for experimental methods.

1-Wang et al. (2002)

2-Hickner et al. (2001)

Table 3.2: Fully hydrated transducer thickness, optimal reducing agent concentration, and platinum layers surface conductivity before and after electroplating for each ionomer.

Ionomer	Transducer thickness (μm)	Optimal reducing agent concentration %(w/w)	Surface resistivity before electroplating (Ω/sq)	Surface resistivity after electroplating (Ω/sq)
Nafion 117	200	0.05	<1	< 0.5
BPS 30	170	0.01	2.2	< 0.5
BPS 35	190	0.01	0.6	< 0.5
BPS 40	195	0.005	0.9	< 0.5
PATS 30	180	0.003	0.9	< 0.5
PATS 40	140	0.002	>8	< 0.5

The electrodes are fabricated on the polymers using an impregnation-reduction method illustrated in Chapter 2, Section 2.6. The main parameters optimized in the impregnation-reduction process for the novel ionomers, are the concentration of the reducing agent, the time delay between the increase of reducing agent concentrations, and the number of plating layers. The resulting optimal designs are illustrated in Table 3.2. The number of Pt layers from impregnation-reduction is fixed to four, and is not optimized for each polymer.

The surface resistivity results are reported in Table 3.2. Surface resistivity is measured using the Guardian Manufacturing four point probe surface resistivity meter (SRM-232). Apart from the BPS 30 and PATS 40, all the surface conductivity measurements fall bellow 1 Ω/sq after the addition of the platinum layers. A gold overlayer is than electroplated on the platinum surface. This gold layer reduces the surface conductivities of all the ionomers below 0.5 Ω/sq.

The samples are cut into rectangles 30 mm in length and 5 mm in width. The transducers are clamped between the fixture electrodes for all the tests, which results in a free length is 20mm throughout the experiments. The thickness of the unplated polymer films varied form 0.13 mm to 0.19 mm, and the thickness of the plated transducers varied from 0.14 mm to 0.20mm. Controlling the thickness of the membranes is difficult to achieve due to the nature of the solvent casting procedure.

3.2 Experimental Results

The experimental methods described in Chapter 2, Section 2.1 are used to characterize in bending a series of ionomeric polymer transducers fabricated from Nafion, BPS, and PATS. Figure 3.3 shows the amplitude of the free deflection frequency response function (FRF) of five transducers fabricated from BPS and PATS and compared to a Nafion-based ionic polymer transducer. This FRF represents the μstrain per unit volt as a function of frequency in the range of 1 Hz to 200Hz. In the frequency range below 10 Hz, the strain per unit volt is approximately constant and the values range from 80 microstrain/volt to approximately 300 microstrain/volt for BPS 35. The free deflection FRF exhibits a strong frequency dependence near the resonance of the transducer. Resonance frequencies for the six transducers are in the range of 20 Hz to 60 Hz. All the polymers apart from PATS 40 had higher resonance frequencies compared to that of the Nafion transducer. The higher resonance is due to the increased stiffness of the polymer and less water uptake (less mass).

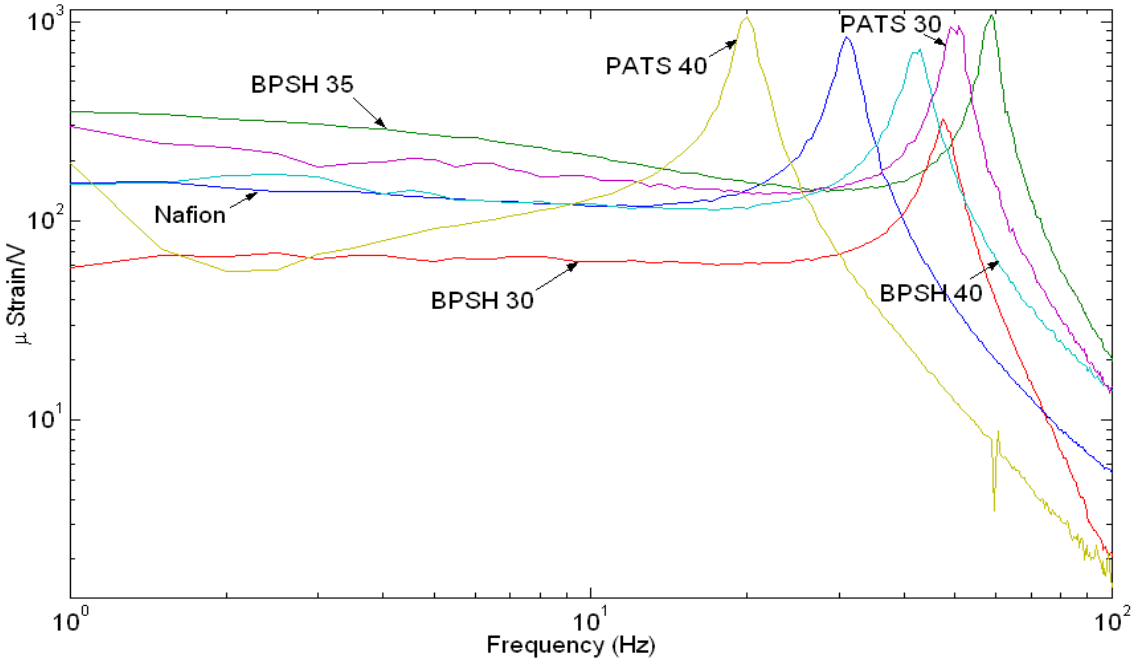

Figure 3.3: Stain per unit volt of the BPS and PATS transducers compared to Nafion.

The stiffness of the polymer is measured and the modulus is computed using equation 2.9. The results are summarized in Table 3.3 for each of the transducers. The results demonstrate that the modulus of the BPS materials is approximately twice that of Nafion.

Polymer	Stiffness (N/m)	Modulus (MPa)
BPS 30	1.29	1580
BPS 35	1.86	1276
BPS 40	0.98	624
PATS 30	1.40	1211
PATS 40	0.11	115
Nafion	0.74	511

Table 3.3: Values for the stiffness and the Young Modulus estimated using equation 2.9.

The modulus values for the materials are consistent with previously published data (Nemat-Nasser and Thomas, 2001). Note that the modulus results shown in Table 3.3 differ from the ones shown in Table 3.1 since the polymers are in the lithium cation form and they have a platinum electrode on the surface.

The increased modulus of the BPS materials is also reflected in the measured blocked force. The frequency response functions of the blocked force per unit volt for the six transducers are shown in Figure 3.4. The measured blocked force for the transducer sizes studied are in the range of 0.1 mN/V to 1.0 mN/V except for the PATS 40 sample. The BPS 35 transducer produced the largest blocked force of slightly greater than 1.0 mN/V at frequencies below 10 Hz. The blocked force output of all of the transducers exhibited a slight frequency dependence.

The measured impedance functions of the transducers are shown in Figure 3.5. All of the transducers exhibit capacitive behavior at low frequencies and approximately resistive behavior at higher frequencies. The impedance of the materials is between 5 Ω and 100 Ω for frequencies between 1 Hz and 100 Hz.

3.3 Discussion of Results

Electromechanical measurements on the polymer transducers demonstrate that the BPS materials produce the highest strain and blocked force per unit voltage of any of the materials studied. The BPS 35 material produces approximately 300 microstrain/volt of free deflection and approximately 1 mN/V of blocked force for the sample sizes studied in this work.

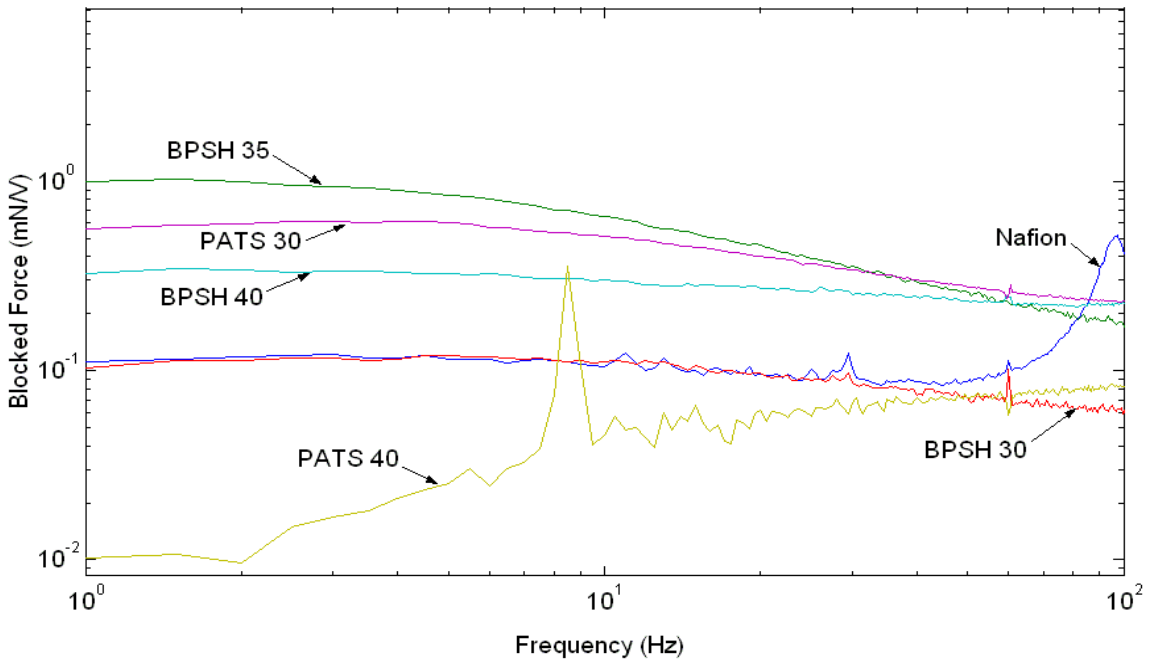

Figure 3.4: Blocked force per unit volt of the BPS and PATS polymers compared to Nafion.

One of the primary objectives of this work is to study the relationship between polymer properties and transducer performance. Originally we had hypothesized that the ion-exchange capacity of the polymer or its conductivity would be strongly correlated to any variations we would see in the transducer performance. Unfortunately these trends did not emerge from the results of our study. For example, BPS 35 is found to have the highest free deflection and blocked force, yet it is a lower conductivity than Nafion 117, BPS 40, and PATS 40, and its ion-exchange capacity is smaller than BPS 40. This is believed to be due to the variations in the electrode deposition that occur using the impregnation reduction method. Later results will demonstrate the importance of the electrode architecture on performance.

Very clear trends do emerge when the transducer performance is correlated to the measured capacitance of the material. The frequency-dependent capacitance of the material is computed using equation 2.4 from the measured impedance of the sample and is displayed in Figure 3.6. As discussed earlier in the paper, the capacitance of the material varies as a function of frequency. At low frequencies the values are on the order of 1 to 10 mF/cm^2 and become smaller at higher frequencies.

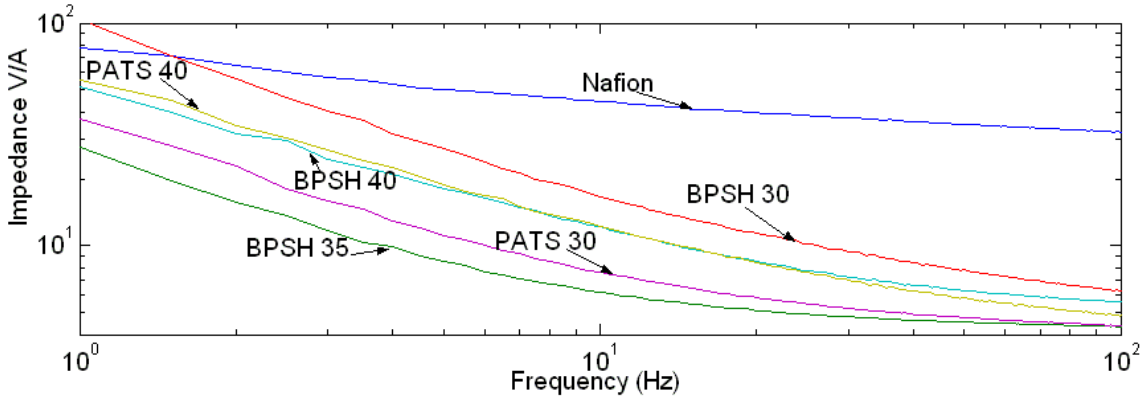

Figure 3.5: Impedance of the novel polymers compared to Nafion.

Figure 3.3 illustrates that the strain produced per unit voltage varies substantially as a function of the base polymer below approximately 10 Hz. If we transform these measurements into strain per unit charge using the expression

$$\frac{\epsilon(j\omega)}{Q(j\omega)} = j\omega \frac{\epsilon(j\omega)}{V(j\omega)} Z(j\omega) \tag{3.6}$$

where $\epsilon(j\omega)/V(j\omega)$ is the measured strain per unit volt and $Z(j\omega)$ is the measured impedance, we see that the variation in the strain response between the different polymers tested is reduced substantially. Figure 3.7 is a plot of the strain per volt and strain per charge response over the frequency range 1 to 12 Hz for all of the polymers tested except for PATS 40, which suffered problems in the plating process. Each of the plots is normalized by the maximum value of the response for any polymer at any frequency, thus, all of the values lie between 0 and 1 over the frequency range. We see in the bottom plot in Figure 3.7 that at each frequency, there is between a five-fold (5X) and ten-fold (10X) variation in the strain per volt between the different transducers tested. Normalizing the strain to the charge induced in the polymer as shown in the top plot, we see that the variation at any frequency is reduced to approximately 1.5X at any frequency.

This analysis demonstrates that the large variation in strain output as a function of voltage is primarily due to the large variation in the voltage-to-current relationships for the polymers tested. Once the results are normalized with respect to charge instead of voltage, then the performance variation in the polymers decreases substantially at the low-frequency range of the tests.

Clear trends also emerge when the strain per unit voltage is compared to the mea-

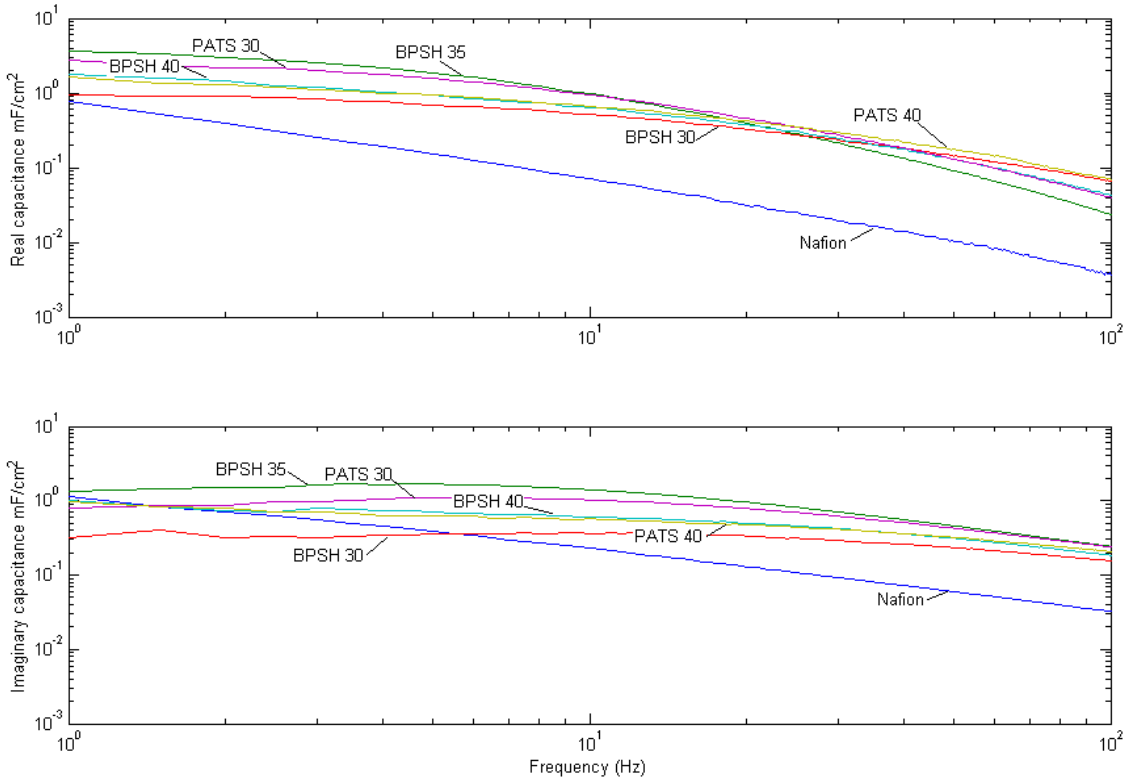

Figure 3.6: Real and imaginary FRF of the capacitance per cm^2 of the different BPS and PATS actuators to Nafion.

sured capacitance of the material. Figure 3.8 is a plot of the measured strain per unit voltage as a function of the measured capacitance for four different frequencies. Each data point represents a particular polymer sample tested during the optimization of the plating process as discussed earlier in the paper. The figure demonstrates that, at each frequency, there is a linear relationship between the capacitance and the strain output.

The slope of the linear fit to the data shown in Figure 3.8 has important physical significance. The units of the slope are microstrain/charge/area, which is equivalent to the average strain produced in the polymer normalized with respect to the electrical displacement induced by the voltage. This parameter can also be computed from the measured data for the polymers tested in this work. Table 3.4 summarizes these results and shows that the strain per unit electric displacement is between 9 $\frac{\mu strain}{\frac{C}{m^2}}$ and 15 $\frac{\mu strain}{\frac{C}{m^2}}$ for all of the polymers tested. Once again, we see that normalizing the strain response as a function of charge tends to demonstrate consistent performance between the polymers tested.

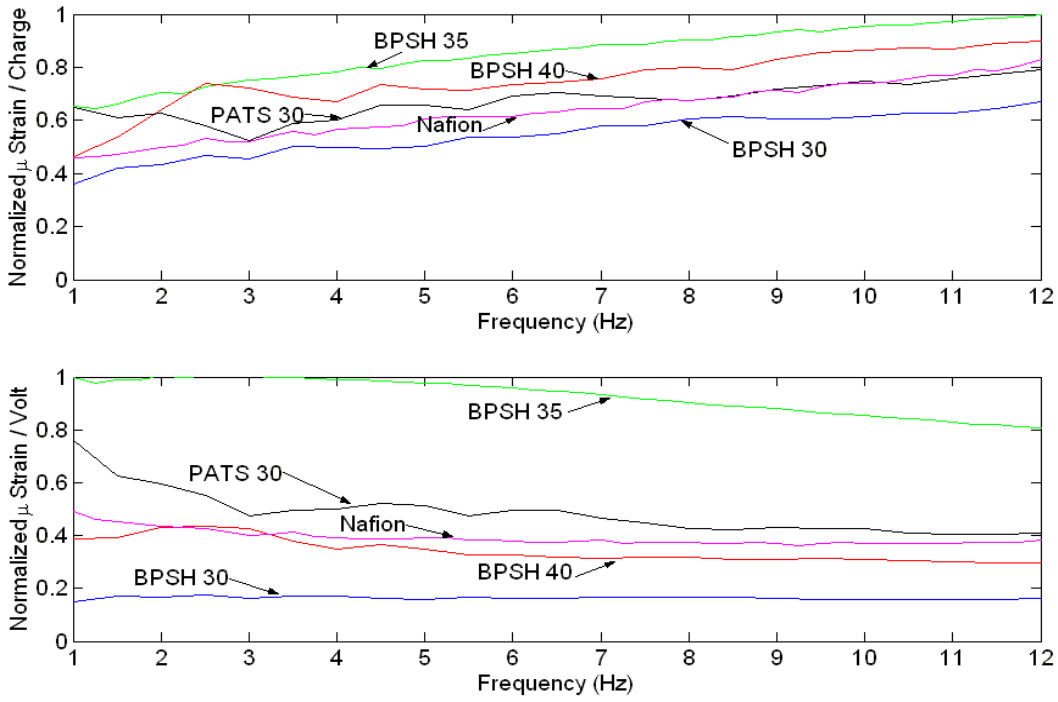

Figure 3.7: Normalized microstrain per unit charge and normalized microstrain per unit volt for several ionomer transducers.

It is interesting to compare the results obtained in this work to experimental investigations previously published in the literature. Recently, Asaka et al. (2001b) investigated the performance of Nafion-based and Flemion-based ionomeric transducers as mechanical actuators. In their work they computed the charge-specific displacement, defined as the displacement of the actuator tip to the charge induced by the voltage (in units of mm/C), for Nafion and Flemion actuators with different cations. For lithium as the cation (which is used in this work), their data can be analyzed to compute the strain produced as a function of the electric displacement.

The results of this comparison are shown in Table 3.4 in addition to the data from this work. The results illustrate that Asaka's result is consistent with the data obtained in our analysis. It is important to note that the results summarized in Table 3.4 are listed for four different ionomer materials, with widely different polymer properties, yet the strain per unit electric displacement is between approximately 10 and 15 $\frac{\mu Strain}{\frac{C}{m^2}}$ for all polymers studied.

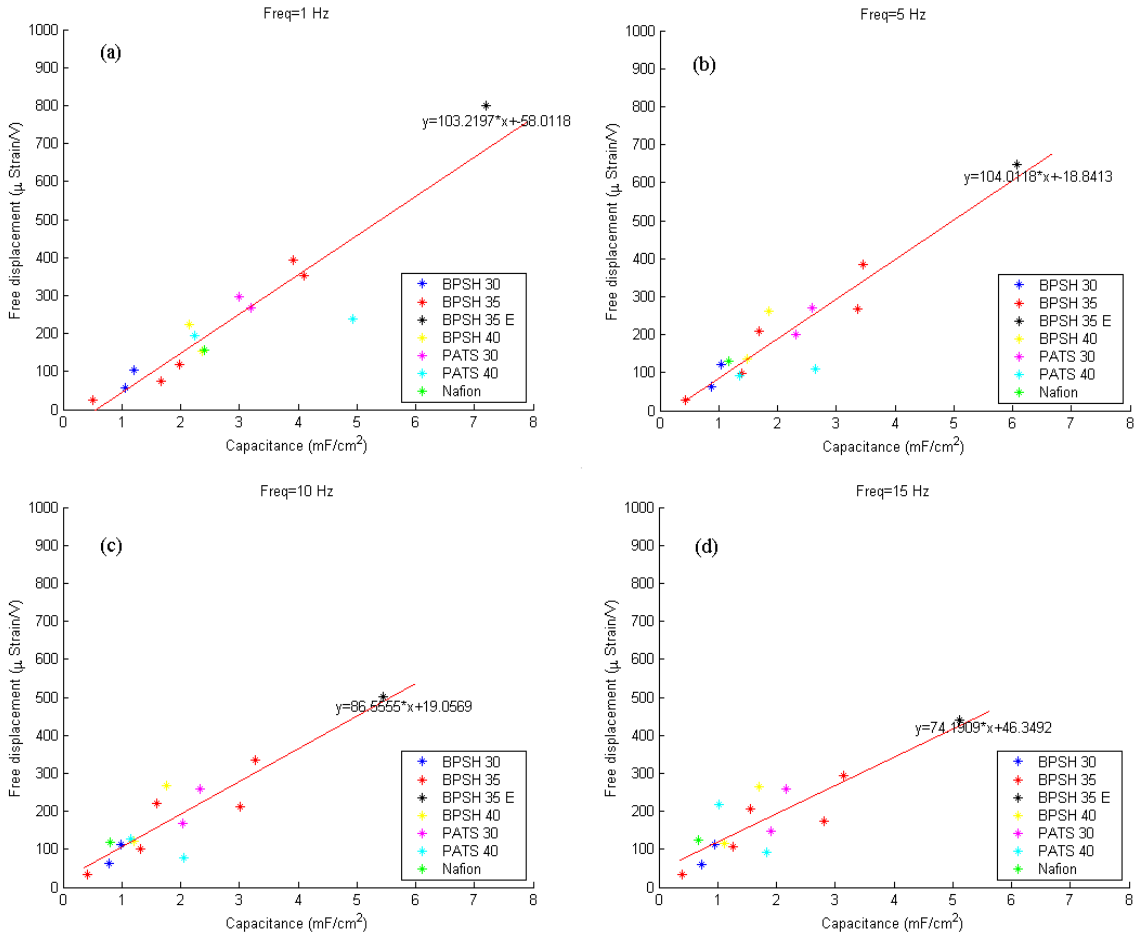

Figure 3.8: MicroStrain vs. capacitance/cm^2 of each polymer a) at 1Hz, b) at 5Hz, c) at 10 Hz, and d) at 15Hz.

3.4 Conclusions

The strain response of an ionomeric transducer is strongly correlated with the capacitance of the plated material. In this chapter, we studied the transducer performance of several different ionomers from three ionomer families. Results demonstrate that there is an approximately linear relationship between strain response per unit voltage and the capacitance of the transducer. This relationship indicates that the strain output per unit electric displacement is approximately constant for all of the polymers tested. Our experiments indicate that this value ranged between 9.8 $\frac{\mu strain}{\frac{C}{m^2}}$ and 15 $\frac{\mu strain}{\frac{C}{m^2}}$ for the polymers tested in this work, and that this value was consistent with data presented previously by other researchers.

These results suggest a strong relationship between charge accumulation at the

Table 3.4: Microstrain per normalized charge for various ionomer actuators.

Polymer	μstrain / electric displacement $\frac{\mu Strain}{\frac{C}{m^2}}$
BPS 35	15.21
BPS 30	9.83
BPS 40	13.76
PATS 30	11.90
Nafion	11.83
Nafion (Asaka)	14.58
Flemion (Asaka)	15.48

polymer-metal interface and transducer performance. It is known that the low-frequency capacitance of an ionomeric material is due to blocking electrode effects, therefore a strong correlation between capacitance and strain indicates that charge accumulation at the interface between the electrode and the polymer is responsible for mechanical deformation. Although this has been suggested in the literature before, our results demonstrate that the amount of strain produced by this charge accumulation is approximately the same for a wide range of ionomer materials that have substantially different properties. This result motivates the optimization of the electrode properties for the purpose of improving the performance of ionic polymer transducers.

Chapter 4

Optimization of the Direct Assembly Process

The Direct Assembly Process (DAP) of ionic polymer transducers was developed in this dissertation. As mentioned in Chapter 2 the DAP provided control on several variables in the transducer fabrication process. Some of these variables are explored and optimized in this chapter. The variables studied are the diluent content of the transducer membrane, electrode thickness, electrode composition and conducting powder species. Lithium cation is used in the ionomer membranes studied in this dissertation. Results are obtained for five sets of experiments. In the experiments the diluent or the electrode architecture are varied and the time response and frequency response of the transducer is measured. The goal of the experiments is to correlate the electrode architecture and diluent content with the maximum strain output and speed of response of the transducer. In the first experiment the type of diluent in the polymer is varied. Thickness of the electrode is varied in the second experiment. Conductivity of the electrode is increased in this experiment by adding conductive gold flakes. Conducting powder in the electrode is varied for the fourth experiment. Transducers made with each material type are optimized and characterized for electromechanical transduction. The fifth experiment combines the three conducting materials in hybrid electrodes and explores the potential of increasing transducer performance through electrode optimization. Finally the repeatability and reliability of the DAP are characterized in the last section.

4.1 Ionic liquids and Organic diluents

In this study, the ionic liquid EmI-Tf and organic diluents are used to solvate the transducers. EmI-Tf is a nonvolatile molten salt which allows the transducer to operate in air without any significant loss of performance (Bonhote et al. (1996)). Earlier work by the authors (Akle et al., 2004a) indicated that 250,000 cycles are attained at +/-2V and 1Hz without any degradation. The viscosity of EmI-Tf is 45 cP, and the electric stability window is 4.1V (Bonhote et al. (1996)). Five organic diluents are considered, PolyEthylene Glycols (PEG) with four different molecular weights (MW) and Formamide. PEGs are polar alcohols with relatively high boiling point. Ethylene Glycol (EG) is the basic unit, diethylene glycol (DEG) is a two repeating units, triethylene glycol (TEG) is three , and PEG 200 is an average of 4.2 repeating units. These diluents are linear polymers, and therefore increasing the molecular weight increases the boiling point and viscosity of the diluent.

In this experiment six samples are built using the direct assembly process and characterized in bending according to procedures described in Chapter 2. Each of the samples utilizes a Nafion 117 membrane exchanged with Li^+ cation and solvated with one of the diluents. The diluent uptake is the maximum that can be achieved with current methods and are close to 100% of dry polymer weight for organic diluents and approximately 58% for Emi-Tf. Electrodes are composed of 45 vol% high surface area RuO_2 metal powder.

The transducers are characterized using time domain 2V step response shown in Figure 4.1. The high viscosity of the diluent compared to water leads to a slow response in the actuators (see Figure 4.1 and Table 4.1). EG and DEG are relatively faster than the higher molecular weights. EG with a boiling point around 195 C offers limited environmental stability, while DEG provided sufficient stability to run long time experiments. Moreover DEG transducers produced much larger strains in the order of 2% for a +2V step input, therefore more than 4% strain could be achieved in the -2V, +2V window. Formamide is also a relatively stable diluent that has a boiling point of approximately 211 C and a low viscosity of 3.3 cP. Transducers solvated with organic diluents can operate in air only for few hours without a degradation in performance due to diluent evaporation.

Transducers with Emi-Tf diluents are bending slower than actuators with formamide as shown in Figure 4.1. The average strain rate during the first 2 seconds of the step is 430 μstrain/s and 2310 μstrain/s for EmI-Tf and formamide respectively. Diluent uptake

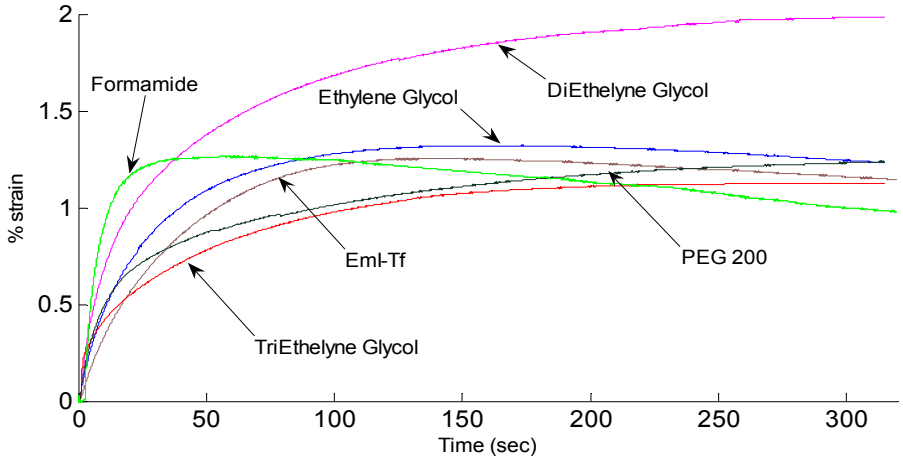

Figure 4.1: (a) Measured response due to a 2V step change in potential for actuators with RuO_2 electrodes and Formamide or EmI-Tf diluents. (b) Strain rate as a function volume uptake ionic liquid.

varied from 58% (weight percent of dry polymer) for EmI-Tf to 100% for the formamide. Diluent uptake of organic diluents could not be accurately controlled due to evaporation during the fabrication process which is done under an infra-red light.

The strain rate response of the transducer with organic diluent is a function of the viscosity and dielectric constant of the fluid. Diluents with a large dielectric constant are more polar and dissociate better the ions in the actuator. Mobility of the ions increases by decreasing viscosity. Table 4.1 shows that formamide solvated transducers are the fastest, while the viscosity of formamide is lowest and has the highest dielectric constant. Comparing the performance of TEG to PEG 200 solvated transducers, it could be noticed that the former is 38% faster than the latter. The viscosity of PEG 200 is approximately 10% larger than that of TEG, while the dielectric constant of TEG is much larger by 51%. Ethylene Glycol is an outlier to the trend, and this is believed to be due to the low boiling point which leads to larger diluent evaporation during transducer fabrication. In this dissertation we studied a single ionic liquid (EmI-Tf) with an uptake of 58% by weight of dry ionomer. It has been also found that the content of ionic liquid within the membrane has an influence on the speed of response (Bennett and Leo, 2005). Finally, ionic liquids offer a superior environmental stability, but due to their fast response formamide is used in the some parts of this study.

Table 4.1: Strain rate of ionic polymer transducers with different diluents. Physical properties of the diluents are provided.

	Strain rate (%/s)	Viscosity (10^{-3} Pa s or cP)	Dielectric Constant	Normal Boiling Point (°C)
Ethylene glycol (Mozga (2005))	0.073	16.1	37.7	197.3
Diethylene glycol (MeGlobal (2005))	0.1331	35.7	31.7	245.3
Triethylene glycol (Dow (2005b))	0.124	49.0	23.69	288.0
PEG 200 (Dow (2005a))	0.090	53.8	15.7	329.7*
Formamide (Mozga (2005))	0.231	3.3	109.5	210.5
EmI-Tf (Bonhote et al. (1996))	0.043	45.0	NA	NA

* Decompose

4.2 Effect of Electrode Thickness on Actuation Response

In this experiment the thickness of the electrode is increased while keeping the composition of the electrode constant. Samples in this experiment are solvated with TriEthylene Glycol. The amount of particles and the interfacial area increase proportional to the thickness of the electrode. Four samples are fabricated with 12, 24, 36 and 48 layers electrode ink painted on each side. Scanning electron microscopy (SEM) images indicates that each 12 layers corresponds to an electrode approximately 9.4 μm thickness.

This experiment explores the electric double layer in ionic polymer transducers. As a whole the electric double layer (EDL) is an electrically neutral system that occurs at an interface or surface, in which a layer of positive charges opposes a layer of negative charges, surrounded by oriented polar molecules (Endo et al., 2001). As mentioned earlier, a larger conductor-polymer interface area increases the capacitance of an electric double layer. Therefore adding more particles in the electrode increases the capacitance of the transducers (see Figure 4.2).

The peak response of these samples is found to increase with the thickness of the electrode (see Figures 4.3(a), and 4.3(b)). This result further supports the fact that actu-

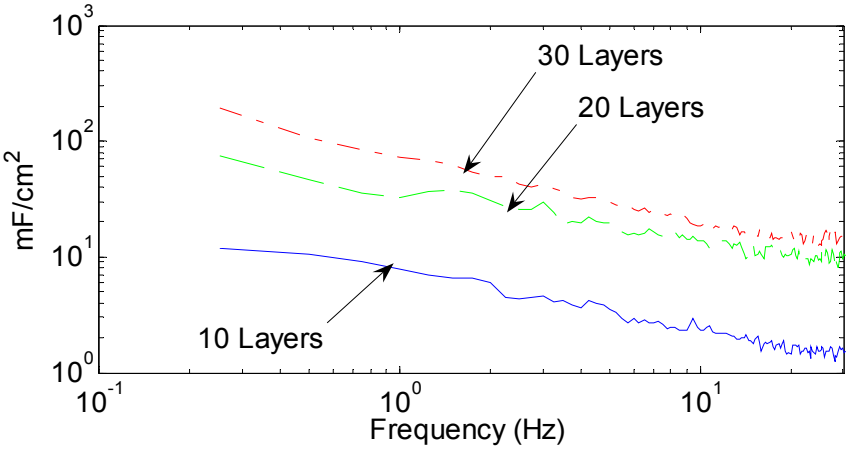

Figure 4.2: Capacitance per area FRF of 3 transducers with 10, 20, and 30 layers of 2.5:1 RuO_2 electrode.

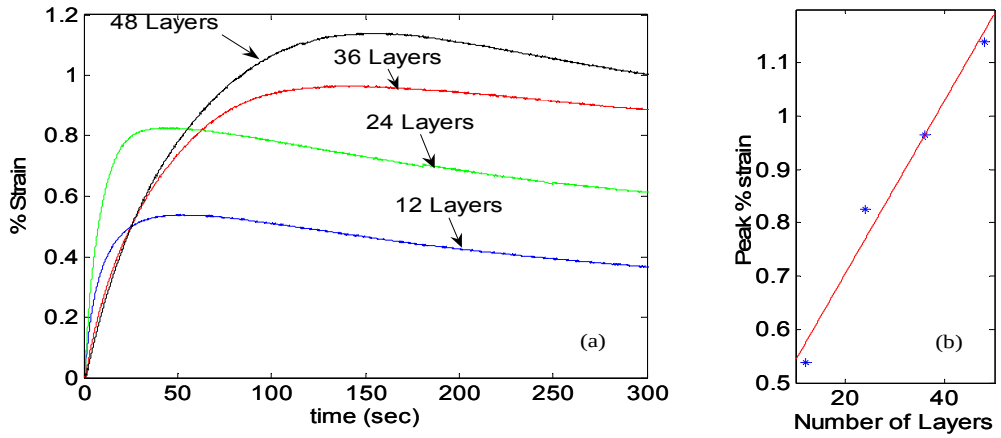

Figure 4.3: (a) Strain response of four samples with different electrode thickness due to a 2V step input. (b) Peak strain as a function of electrode thickness.

ation performance in ionic polymer transducers is proportional to capacitance. Observing the shape of step response indicates that the speed is different from transducer to the other. Ions diffuse from the bulk polymer towards the electrode to form an electric double layer. Figure 4.3 (a) demonstrates that transducers with thicker electrodes tend to strain slower. This is justified by considering ions have to cross a thicker electrode to form the electric double layer, and the resistivity of the electrode increase with thickness. Since both ionic liquids and organic alcohol are viscous diluents, the speed of diffusion could be limited.

4.3 Conducting Electrode Material

In the remaining sections of this chapter several conducting powders are studied. Detailed information on these particles could be found in Section 2.7. A summary of the physical and electrochemical properties of the powders are presented in Table 4.2.

Table 4.2: Physical and electrochemical properties of electrode conducting materials

	σ (S/cm)	Density (g/cc)	Surface Area (m^2/g)	Volumetric Surface Area (m^2/cc)	Actuation mechanism in electrolytes	Price ($/gr)
Carbon Black	1000	2.267	300 to 3000	680 to 6800	EDL	< 10
SWNT	30000	1.33	1000	1330	EDL / Quantum	500
PANI	500	1.329	NA	NA	Redox	10
Hydrous RuO_2	NA	NA	NA	NA	Redox	50
Anhydrous RuO_2	3500	7.05	45 to 65	317 to 458	EDL/ Redox	50
Platinum	94000	21.09	24 to 29	506 to 611	EDL/ Adsorption	120
Gold Flakes	454500	19.3	0.4 to 0.8	7.7 to 14.5	EDL	80

EDL = Electrostatic double layer

SWNT = Single Walled Carbon Nanotubes

PANI = Polyaniline

4.4 Ruthenium dioxide - Gold hybrids

Conductive gold flakes are added to the large surface area RuO_2 powder in order to increase the overall conductivity of the electrode. Experimental results are obtained for three sets of experiments. In each experiment the electrode composition is varied and the time response and frequency response of a transducer is measured. The goal of the experiments

is to correlate the conductivity and capacitance of the electrode with the electromechanical performance of the transducer.

4.4.1 Variation of Metal Content by Weight

In the first experiment the electrode composition is varied according to the weight of RuO_2 or Au contained within the electrode. The samples are solvated with approximately 58% EmI-Tf ionic liquids. The weight percentage of metal in the electrode is varied from 0% Au to 100% Au, with the remaining percentage of the electrode metal being RuO_2. Figure 4.4 (a) is a plot of the frequency response magnitude for the 5 cases studied. The results clearly demonstrate that the RuO_2 electrode is superior to Au in producing strain for an equivalent applied voltage. The strain-per-voltage response of the polymer at frequencies less than 10 Hz is maximized by the pure RuO_2 electrode and is minimized for the pure Au electrode. Using 1 Hz as a reference point, we see that the strain response drops from 273 $\mu\varepsilon$/V to 6 $\mu\varepsilon$/V when the electrode composition is changed from 100% RuO_2 to 100% Au. At intermediate values there is a clear trend of decreasing strain response for increasing Au loading.

The trends in the electrical impedance clearly indicate the tradeoff in capacitance and resistance associated with the addition of gold or ruthenium oxide. A pure RuO_2 electrode produces a higher capacitance electrode due to its larger specific surface area. This results in a lower impedance at low frequencies (electrical impedance is inversely proportional to capacitance). However, the transducer with the pure RuO_2 electrode has a larger impedance at frequencies above approximately 10 Hz because of the higher resistivity of RuO_2 as compared to Au (see Figure 4.4(b)). The addition of small amounts of Au to the electrode decreases the high frequency resistance but also decreases the low frequency capacitance because of the lower specific area of the gold powder as compared to the RuO_2 powder. Capacitance at 0.5Hz for samples with 0%, 25%, 50%, 75%, and 100% gold is 3.9, 3.7, 3.5, 1.6, and 1.0 mF/cm^2 respectively. Therefore, the pure Au electrode has the lowest capacitance but also has lower high-frequency resistance.

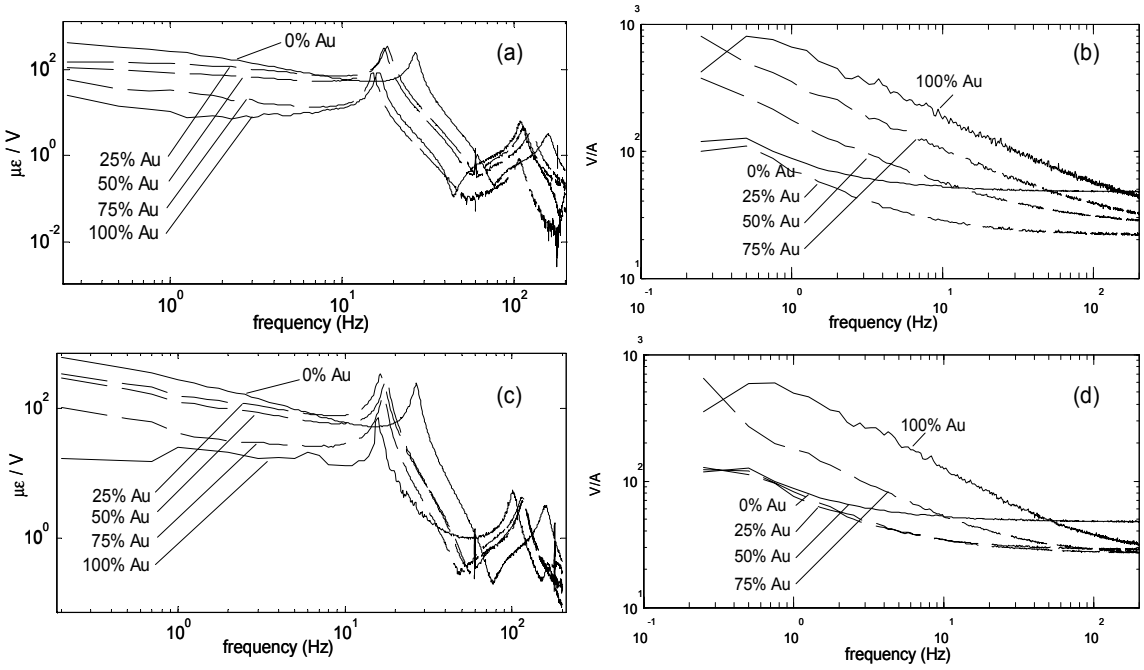

Figure 4.4: (a) Strain response as a function of electrode composition by weight, (b) Electrical impedance as a function of electrode composition by weight, (c) Strain response as a function of electrode composition by volume, and (d) Electrical impedance as a function of electrode composition by volume.

4.4.2 Variation of Metal Content by Volume

The second experiment consists of varying the electrode composition while maintaining a consistent volume of metal in the electrode. In this set of experiments the relative percentage of RuO_2 and Au is varied while the total volume of metal in the electrode layers is held constant at approximately 40%. Table 4.2 summarizes the compositions studied for this set of experiments.

The strain response of the transducers as a function of volume percent of metal exhibited the same trend as the trend obtained when varying the weight percentage (see Figure 4.4 (c)). The electrode fabricated with pure RuO_2 exhibits the largest strain per unit voltage at frequencies below approximately 8 Hz. Increasing the percentage of Au in the electrode reduces the strain output. At 1 Hz the strain output is 272 $\mu\varepsilon$/V for an electrode with 100% RuO_2 while it is 24 $\mu\varepsilon$/V for an electrode with 100% Au.

A clear relationship between the slope of the strain-to-voltage frequency response at frequencies below the first mechanical resonance and electrode composition also emerges in this study. The negative slope of the strain-to-voltage frequency response indicates limited

charge mobility. This is at least partially due to the high resistivity of the RuO_2 particles, as increasing the percentage of gold in the electrode decreases the slope of the frequency response. The decrease in slope is correlated with the variation in the electrical impedance as the electrode composition varies (see Figure 4.4 (d)). The device with a 100% RuO_2 electrode has the highest low-frequency capacitance but exhibits a high-frequency impedance of approximately 5Ω. The addition of small amounts of gold maintains the low-frequency capacitance but decreases the high-frequency impedance to approximately 30Ω. Further increase in the gold content reduces the capacitance and causes a corresponding decrease in the strain generation. Differences in the strain response due to variations in the electrical impedance are reduced by normalizing the strain response to the charge induced in the polymer by the applied potential. The strain per unit electric displacement is illustrated in

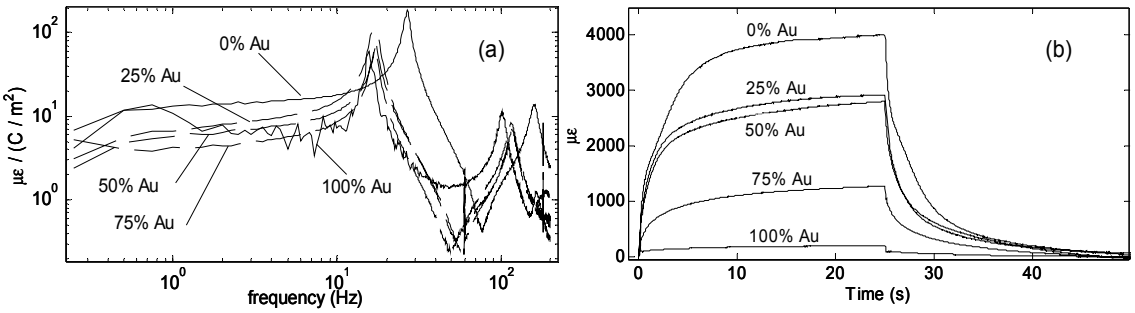

Figure 4.5: (a) Strain per unit charge/area for the samples produced by variation in the metal content with consistent volume, (b) Strain output to the application of square wave potentials of +/- 2 V.

Figure 4.5(a) for the variation in electrode composition by volume. The results demonstrate that low-frequency slope of the strain-to-voltage response is eliminated and the strain per unit charge is approximately flat as a function of frequency. Furthermore, the strain per unit electric displacement is between 5 and 15 $\mu\varepsilon/(\mathrm{C/m^2})$ for all samples considered.

The time response of the transducer displacement to square wave potential waveforms are also measured and the strain is computed using equation 2.1. Results for square wave amplitudes of +/- 2 V demonstrate that strain output of approximately 4000μstrain (0.4%) is achievable with the pure RuO_2 electrode (see Figure 4.5 (b)).

The steady-state value of the strain decreases as the gold loading of the electrode is increased. This is because the capacitance of the transducers decreases as the content of ruthenium oxide is decreased. However, the conductivity of the electrode increases as

Table 4.3: Weights of Au and RuO_2 mixed with 0.5 g of 5% Nafion solution and 0.5g Glycerol. It also presents the durations of sample hot-pressing. The densities of Au and RuO_2 are assumed to be 19300 Kg/m^3 and 7050Kg/m^3 respectively.

Sample	Au (g)	RuO_2 (g)	Thickness (μm)
0% Au 100% RuO_2 (2.5:1)	0	0.0625	205
25% Au 75% RuO_2 (2.5:1)	0.0428	0.0469	180
50% Au 50% RuO_2 (2.5:1)	0.0855	0.0313	180
75% Au 25% RuO_2 (2.5:1)	0.1283	0.0156	180
100% Au 0% RuO_2 (2.5:1)	0.1711	0	180

the loading of gold is increased, leading to a faster response. Although the speed of the response increases notably from the 100% RuO_2 electrode to the 100% Au electrode, this trend is not as evident for the intermediate electrode compositions. This is illustrated by comparing the normalized initial slope of the two samples, which is the initial slope of the step divided by the maximum strain attained. The sample electroded with 100% RuO_2 had a normalized initial slope of 1 s^{-1} as compared to 6.7 s^{-1} for the 100% Au electroded sample. This result is consistent with the frequency-domain analysis, as the pure ruthenium oxide sample exhibits a strong roll-off in the strain-to-voltage response whereas the pure gold sample exhibits a relatively flat response.

4.4.3 RuO_2 - Gold Electrode Optimization

The results of the electrode analysis demonstrate that a metal particulate with high surface area-to-volume ratio (RuO_2) will produce a superior electrode due to the increase in capacitance at low-frequencies. Increasing the content of the high-conductivity particulate (Au) decreases the impedance at frequencies above approximately 10 Hz but does not produce an increase in the strain response because of the corresponding drop in capacitance associated with replacing the RuO_2 particles with the low specific area gold particles.

Three samples were prepared for the optimization and verification study; the first sample had the same metal to polymer ratio in the electrode as in the weight and volume experiments (2.5:1). However, the thickness of the electrode for this sample was increased by 50% to 6 layers as compared to 4 layers for the previous experiments. For the second sample the RuO_2 to polymer ratio was increased by 50% to 3.75:1 while holding the number

Table 4.4: Weights of Au and RuO_2 mixed with 0.5g of 5% Nafion^{TM} solution and 0.5g Glycerol for electrode optimization.

Sample	Au (g)	RuO_2 (g)	Thickness (μm)
0% Au 100% RuO_2 (2.5:1)	0	0.0625	210
0% Au 100% RuO_2 (3.75:1)	0	0.0938	180
33% Au 66% RuO_2 (3.75:1)	0.0855	0.0625	190

of layers constant at 4. The third sample was prepared by replacing the 50% increase in RuO_2 by the equivalent volume of Au. Table 4.3 summarizes the electrode compositions studied for this set of experiments. Therefore, the three samples maintained the same total metal volume loading. The metal in sample 1 is dispersed compared to the other two samples, while gold accounted for the increase of metal in sample 3. In samples 1 and 2 the surface area of the electrode is theoretically maintained, while sample 3 should have a better conductivity through the electrode. Figure 4.6 shows the frequency response functions of the strain per unit volt for the three samples. The frequency response functions of samples 1 and 2 are nearly parallel with sample 1 providing better performance. This is believed to be due to the lack of control on the amount of electrode ink deposited using the brush painting technique. Theoretically the two samples should provide similar capacitance and therefore similar performance. As for sample 3 it is shown to have the smallest low frequency response while it crossed sample 2 almost at 3 Hz and provided better high frequency response. This is consistent with the expectation of a better high frequency response from a more conductive, gold-containing electrode.

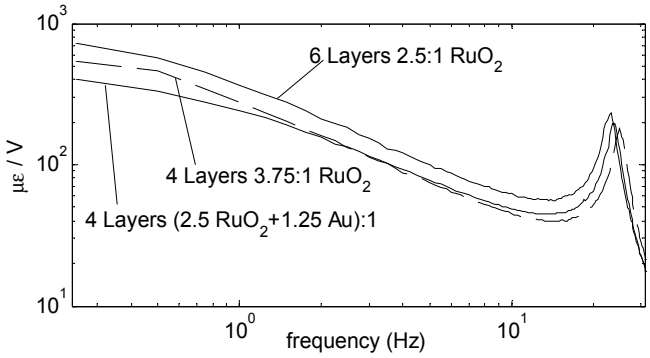

Figure 4.6: Strain per volt frequency response for three RuO_2 samples.

The motion of the transducer to an applied potential is also measured in the time

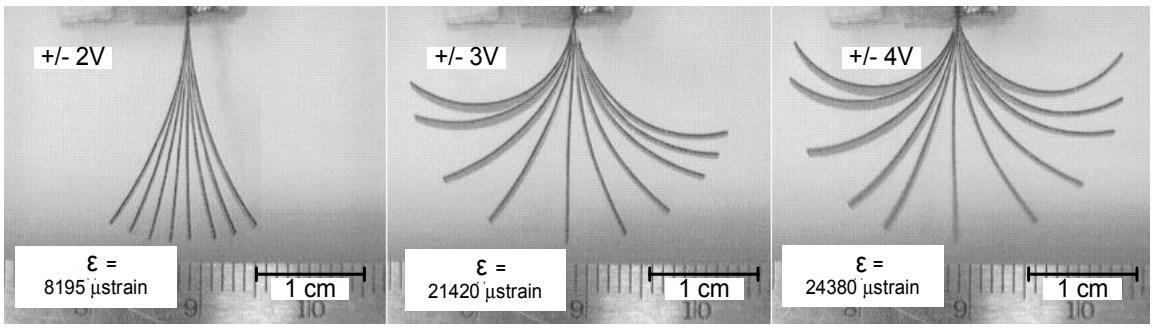

Figure 4.7: Deflected shapes as a function of amplitude for a square wave potential input.

domain. Square wave potentials are applied to the polymer and the resulting displacement is measured using a digital camera due to the fact that the displacements are too large to be measured with the laser vibrometer. The measured deflected shapes are shown in Figure 4.7. The pictures illustrate that the assumption of constant curvature is valid over the range of conditions tested.

The range of motion increases as the amplitude of the square wave input is increased. The peak-to-peak strain in the sample is measured by determining the radius of curvature of the sample at maximum deflection, R_max. The strain at maximum deflection is equal to

$$\varepsilon_{max} = \frac{t}{2R_{max}} \tag{4.1}$$

The radius of curvature was determined on both sides of the neutral position and the peak-to-peak strain is the addition of the two values. The measured strain increases from 8195 (0.82%) at +/- 2V to 24,380 (2.44%) at +/- 4 V. It is interesting to note that the increase in peak-to-peak strain is not linear as a function of input amplitude. We attribute this to nonlinearity in the charge conduction as a function of voltage.

4.5 Optimization of Conductor Powder Concentration in the Electrode

An alternative way of increasing the conductivity of the electrode is by increasing the metal content. The metal composition is modeled and optimized using the percolation theory presented in Chapter 1. Three conducting powders are used separately in this experiment as

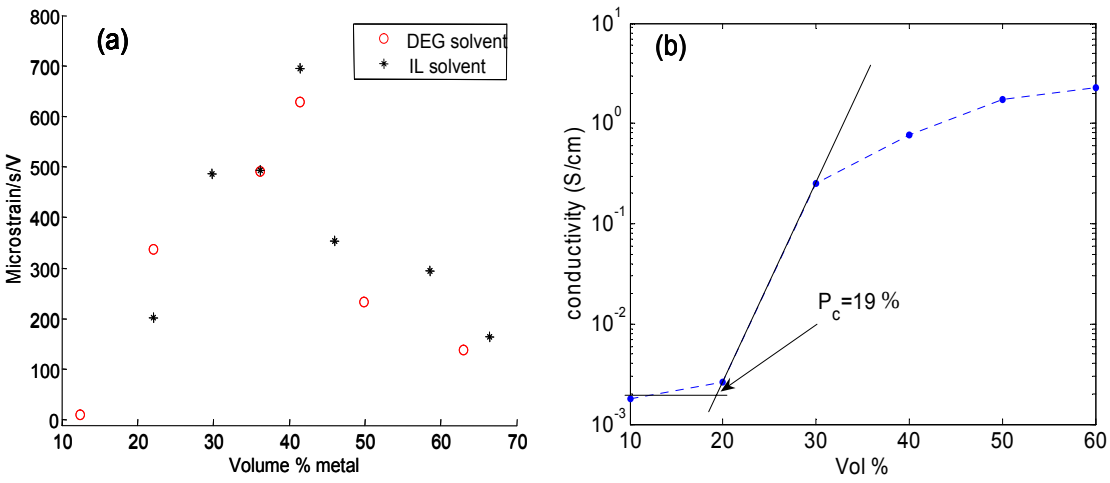

Figure 4.8: (a) Strain rate as a function of RuO_2 volume % in the electrode. Conductivity of the electrode as a function of RuO_2 volume % in the electrode.

electrode materials. The powders are RuO_2, polyaniline (PANI) and Single Walled Carbon Nanotubes (SWNT). These materials are chosen due to the variety in conductivity, surface area, and charging mechanisms. Each material is optimized in terms of speed of response. The properties of these conducting powders are found in Table 4.2. In this experiment the amount of metal was held constant while the concentration of conductor to polymer in the electrode was varied. RuO_2 samples from 12% to 67% (volume % metal particles in the electrode) were tested for ionic liquids and organic diluents.

Two processes are occurring during the charging of the electric double layer. The first is the motion of electrons in the conductor phase, and the other is the diffusion of the ions from the ionomer toward the conductor particles in the electrode. Figures 4.8 (a) and 4.9 are obtained by computing the average slope over the first 2 seconds in the step response. From this result we postulate that two competing actuation mechanisms determine the optimal electrode conductor loading. The first mechanism represents the increasing part of the curve and is explained by the speed of electron injection in and out of the electrode:

$$\frac{dq}{dt} = \frac{V}{R} \tag{4.2}$$

where q is the charge, V the voltage, and R is the resistivity. The electrode consists of conductor and insulator phases, and therefore the motion of electrons could be modeled using conductor-insulator percolation theory. Classical percolation theory states that a

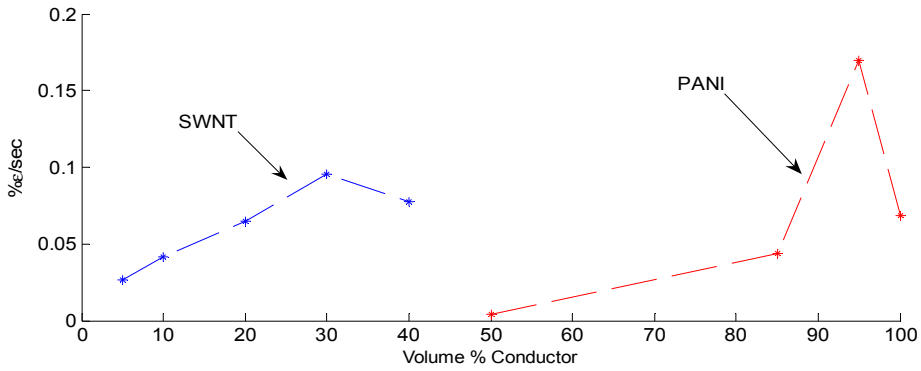

Figure 4.9: Strain rate as a function of carbon nanotube and polyaniline loading (volume %) in the electrode.

continuous conducting network is formed by the coalescence of the grains. The percolation theory is typically modeled using a power law which is a function of the volume percent of the conducting phase

$$\sigma = k_p(p - p_c)^{\beta_p}, \tag{4.3}$$

where p_c is the threshold volume percent, β_p is an exponent with a theoretical value of 2, and k_p is a scaling constant depends on the conductivity of the materials involved. Equation 4.3 indicates that increasing the conductor phase decreases the resistivity of the electrode (Stauffer and Aharony, 1992). The decreasing part of the curve is explained by the decreasing presence of ionomer leading to slow ionic diffusion in/out of the electrode. This fact is reflected in the decrease in the speed of response as shown in Figure 4.8(a). The decrease in the speed of response is postulated to depend on the volume % of the polymer $(1 - p)$. Figure 4.8(b) shows the percolation threshold which was measured to be around 19% for RuO_2 electrodes. Figure 2.13 shows SEM images of a cross-section of electrode with 22, 30, 36 and 66 volume %. It is clear from the micrographs that more connections in the particles are noticed with the increase of metal content. The 22% shows little inter-particle connection while at 36% particles start to develop a conductive network. At 66%, less polymer surround the particle, supporting the conclusion that ion diffusion is limited in such high levels of metal loadings.

SWNT electrode shows optimal performance around 30 vol% as shown in Figure 4.9 (a). PANI actuator have an optimal loading around 95 vol%, but due to the delaminating of the electrode 85 vol% loading was estimated to be the best operating point. As mentioned

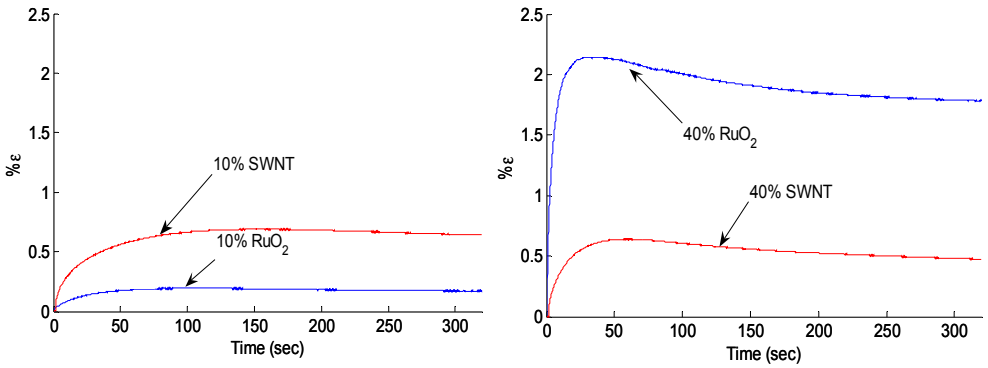

Figure 4.10: (a) Strain response due to a 2V step change in potential for samples with 10% RuO_2 and 10% SWNT. (b) Strain response due to a 2V step change in potential for samples with 40% RuO_2 and 40% SWNT.

Table 4.5: Conductor/ionomer surface area in th electrode, and the corresponding peak strain.

	Surface Area (m_2)	Peak Strain (%)
RuO_2	0.5	2.22
SWNT	1.7	1.64
PANI	NA	0.305

earlier SWNT matrices show low percolation threshold and hence a decrease in the optimal volume %. PANI has a low electric conductivity and it is itself an ionic conducting polymer. This explains the large optimal conductor loading.

Figure 4.10 (a) shows the step responses of a 10 vol% RuO_2 and 10 vol% SWNT samples, while Figure 4.10 (b) shows the step responses of a 40 vol% RuO_2 and 40vol% SWNT samples. The loading of all the SWNT samples in Figures 4.10 (a) and (b) were close to 1 mg/cm^2 and 10 mg/cm^2 for RuO_2 samples. One can notice that the maximum strain for RuO_2 increased from approximately 0.18 % to 2.2 % when increasing the loading from 10 vol% to 40 vol%. As for the SWNT both 10 vol% and 40 vol% samples had almost a constant maximum 0.65 %strain. This could be explained by the fact that 10 vol% loading in a RuO_2 electrode is below the percolation threshold and therefore the electrode is not be fully charged. Three samples with constant electrode thickness of 25 μm (on each side) were fabricated with 45 vol% RuO_2 45 vol% SWNT and 85 vol% PANI. Computed from Figure 4.11, the maximum strains are 2.22 %, 1.64 %, and 0.305 % respectively. The conductor/ionomer interfacial surface area in the active electrode for the RuO_2 and

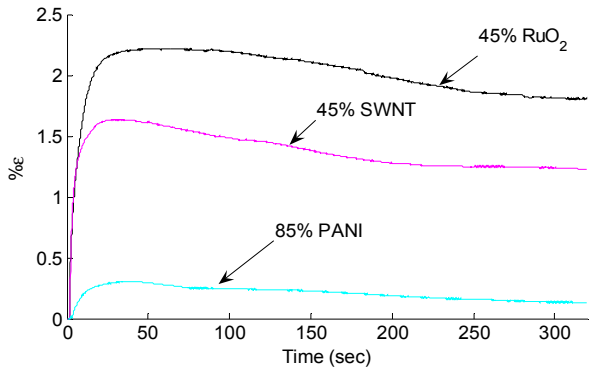

Figure 4.11: Strain response due to a 2V step change in potential for samples with 45% RuO_2, 45% SWNT, and 85% PANI.

SWNT samples is $0.5m^2$ and $1.7m^2$ respectively. Despite the smaller surface area of RuO_2 it outperformed the SWNT actuator, and this is believed to be due to its high pseudocapacitive storage of charges.

4.5.1 Hybrid Conductors/Ionic Polymer Actuators

Each of the conducting materials showed interesting properties as a standalone electrode material. In this experiment the RuO_2, SWNT, and PANI conducting powders are combined in pairs to produce what we denote a hybrid actuator. In order to optimize the composition of the hybrid actuators, the thickness of the electrode is maintained at 25 μm (on each side) for all the samples.

First the SWNT and RuO_2 are combined and five samples are prepared. Samples are prepared with 10 vol% SWNT, 35 vol% RuO_2, and this loading is combined in one actuator of 10 vol% SWNT + 35 vol% RuO_2. Also this actuator is compared to a pure 45 vol% SWNT and another pure 45 vol% RuO_2 actuators. The response to a 2V step change in potential is shown Figure 4.12(a) and the peak strain and strain rate of the transducers are shown in Table 4.6. Noticeably, the hybrid actuator outperformed both 45 vol% RuO_2 and 45 vol% SWNT in both the peak strain produced and the strain rate. The peak strain of the hybrid actuator is much larger than the combined strain of the 10 vol% SWNT and 35 vol% RuO_2 separately (4.69 %strain compared to 1.64 %strain). Moreover, the hybrid actuator bends at a strain rate of 1 %strain/s compared to 0.36 %strain/s for 45% RuO_2 actuator. The transducer fabricated with 45 vol% SWNT electrode is bending faster than

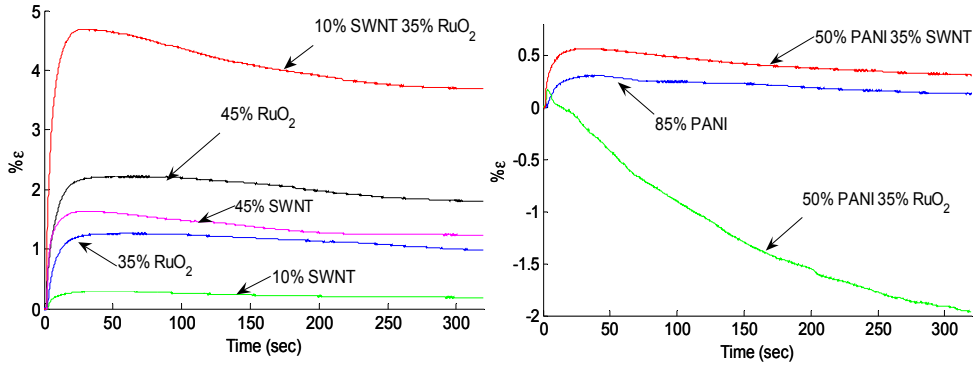

Figure 4.12: (a) Strain response due to a 2V step change in potential for samples with 10% SWNT, 45% SWNT, 35% RuO_2, 45% RuO_2 and a mix of 10% SWNT with 35% RuO_2. (b) Strain response due to a 2V step change in potential for samples with 85% PANI, 50% PANI with 35% RuO_2, and 50% PANI with 35% SWNT.

Table 4.6: Peak strain and strain rate of five actuators built for the SWNT/RuO_2 hybrid experiment.

	% peak strain	% strain/s
10vol% SWNT	0.28	0.05
35vol% RuO_2	1.36	0.17
45vol% SWNT	1.63	0.50
45vol% RuO_2	2.20	0.36
10vol% SWNT + 35vol% RuO_2	4.69	1.00

the transducer with 45vol% RuO_2, while the peak strain is smaller. This indicates that there is more ion build up in the RuO_2 electrode, while the conductivity of the SWNT is larger.

Next PANI was hybridized with SWNT and RuO_2. Three samples were fabricated with 85 vol% PANI, 50 vol% PANI mixed with 35 vol% SWNT, and 50 vol% PANI mixed with 35 vol% RuO_2. Step response measurements of these transducers is shown in Figure 4.12 (b). The results demonstrate that the addition of SWNT to the PANI actuators increases the peak strain from 0.3 %strain to 0.57 %strain and the strain rate from 0.0430 %strain/s to 0.12 %strain/s. RuO_2 had an adverse effect on the performance of the actuator when mixed with the PANI. The initial response increased the strain rate to 0.08 %strain/s, but after 1.5 seconds a strong back relaxation was triggered. This might be contributed to some chemical reaction between RuO_2 and PANI.

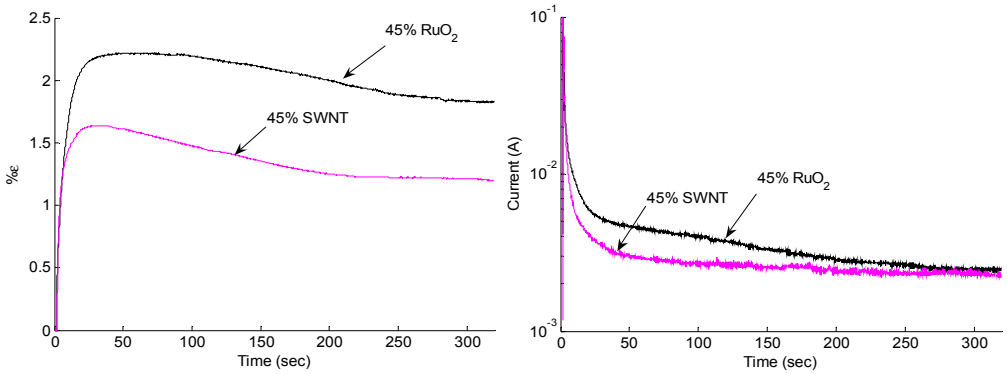

Figure 4.13: (a) Response to a 2V step for transducers with 45vol % RuO_2 and 45vol% SWNT. (b) Corresponding current response.

4.6 Electrical and Mechanical Property Characterization

In this section the electrical and mechanical impedances are analyzed for different transducers. The capacitance, modulus of elasticity and damping ratios are computed from the frequency response functions.

4.6.1 Electrical Properties Characterization

SWNT samples shows faster back-relaxation in the step response strain curve (Figure 4.13(a)) compared to that in the RuO_2 actuators. The shape of the curve between 100 and 200 sec after the step is steeper in the SWNT compared to the RuO_2. This could be also observed in all SWNT and RuO_2 samples (see Figure 4.12(a)). The shape of the current response is also different, and corresponds to the strain curves. This could be interpreted as a slower electrochemical process is occurring in the RuO_2 samples, and it is slowing down the back-relaxation. As mentioned earlier, RuO_2 demonstrates extra redox or pseudocapacitive activities compared to the pure electrostatic behavior for SWNT. The capacitance of the RuO_2 and SWNT samples followed the trend in step response (see figure 4.12(a) and Table 4.6). The hybrid actuator had a capacitance of $50mF/cm^2$ at 0.25Hz (see Figure 4.14(a)). As for the PANI hybrids, addition of the SWNT improved the high frequency capacitance (above 15 Hz) as shown in Figure 4.14(b). SWNT improves the conductivity in the electrode and therefore it is easier to mobilize the electrons at higher frequencies. This

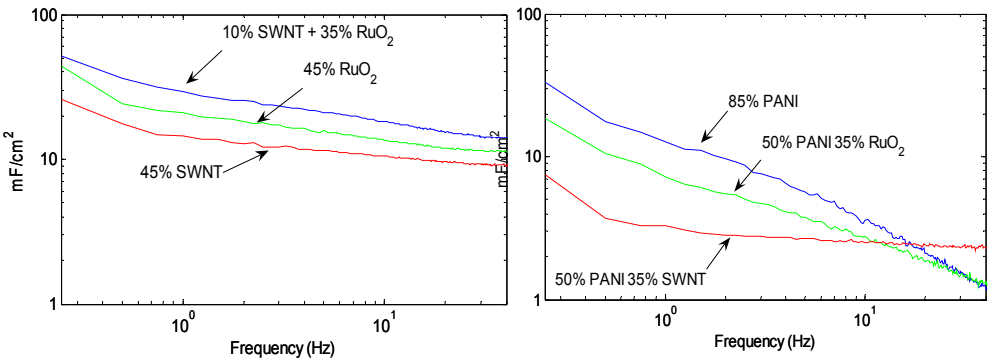

Figure 4.14: (a) Capacitance frequency response functions of transducers with 45vol % RuO_2 and 45vol% SWNT. (b) Capacitance frequency response functions of transducers with 85vol% PANI, 50%vol PANI + 35vol % RuO_2, and 50vol% PANI + 35vol% SWNT.

trend didn't hold in the RuO_2/Nafion composite electrode shown in Figure 4.14(a).

4.6.2 Mechanical Damping

The strain per unit volt and strain per unit charge frequency response functions are used to evaluate the mechanical properties of the transducers. Strain per volt frequency response functions are presented in Figures 4.14(a) and (c). They follow trends observed earlier in Section 4.3 (Figures 4.13(a) and (b) and Table 4.6). The hybrid SWNT/RuO_2 actuator produces large strains of 0.45 % strain/volt at 0.25 Hz compared to 0.27 % strain/volt for RuO_2 and 0.19 % strain/volt for SWNT transducers. All transducers other than the PANI/SWNT exhibit a roll off in the frequency response between 0.1 Hz and 10 Hz. Addition of SWNT to RuO_2 electrodes did not decrease the roll-off and that could be attributed to the increase in damping in SWNT samples compared to RuO_2 (see table 4.7). Decreasing damping widens the effect of the resonance as it could be observed in Figure 4.15(b). As for the PANI a 35vol% addition of SWNT drastically decreased the roll-off. Normalizing the strain per volt frequency response function by charge eliminates the roll-off in the frequency response of the transducer. The difference in the magnitude for strain per volt at 0.25Hz was a factor of 2.4, while in strain per charge the maximum difference varied from 11.9 to 8.4 μstrain/(C/m^2) which is a factor of 1.4 (see Figure 4.15(b)). As for the PANI experiment, this factor has decreased from 6.2 for strain per volt to 2.0 for strain per charge at 0.25Hz. This is a significant results considering the wide range of materials used.

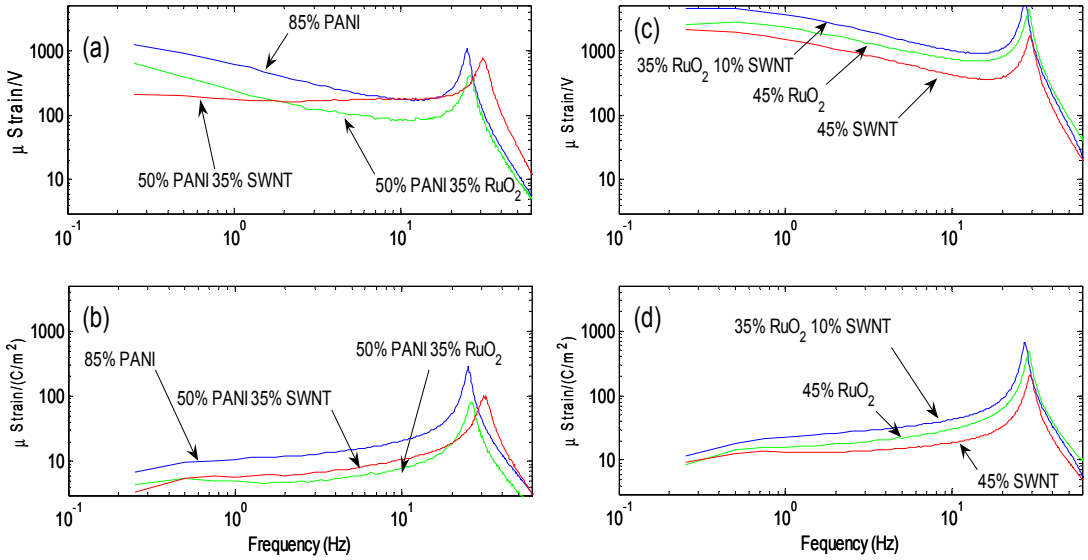

Figure 4.15: (a) Strain per volt frequency response functions of transducers with 45vol % RuO_2 and 45vol% SWNT. (b) Micro-Strain per charge per area frequency response functions of transducers with 45vol % RuO_2 and 45vol% SWNT. (c) Micro-Strain per volt frequency response functions of transducers with 85vol% PANI, 50%vol PANI + 35vol % RuO_2, and 50vol% PANI + 35vol% SWNT. (d) Strain per charge per area frequency response functions of transducers with 85vol% PANI, 50%vol PANI + 35vol % RuO_2, and 50vol% PANI + 35vol% SWNT.

Modulus and damping ratios are computed according to equations (2.5), (2.7), and (2.8) and the results are shown in Table 4.7. Transducers with RuO_2 electrodes are stiffer than SWNT electrodes, while the damping ratio is higher in SWNT samples. The SWNT/RuO_2 hybrid is an outlier to the trend with a lower damping ratio.

4.7 Reliability of the DAP Method

In order to gauge the repeatability of the direct assembly process described in Section 2.6, three identical transducers are fabricated separately and fully characterized. The transducers were fabricated by painting 4 layers of RuO_2 / Nafion ink with a weight ratio of metal to polymer of 2.5 to 1. As can be seen in Figure 4.16, very little variation is observed in the microstrain per unit volt frequency response. The variation in the resonance peaks are attributed to some variations in electrode thickness and sample dimensions. Although more results are needed in order to obtain a standard deviation, this initial result shows that the

Table 4.7: Mechanical properties of five actuators fabricated for the SWNT/RuO_2 hybrid experiment.

	Elastic Modulus (MPa)	Damping Ratio (ξ) using curve fitting method	Damping Ratio (ξ) using half power method
45vol% SWNT	48	0.044	0.043
45vol% RuO_2	94	0.036	0.038
10vol% SWNT + 35vol% RuO_2	67	0.032	0.031
85vol% PANI	71	0.036	0.032
50vol% PANI + 35vol% RuO_2	54	0.048	0.052
50vol% PANI + 35vol% SWNT	75	0.056	0.060

direct assembly process is able to produce repeatable results.

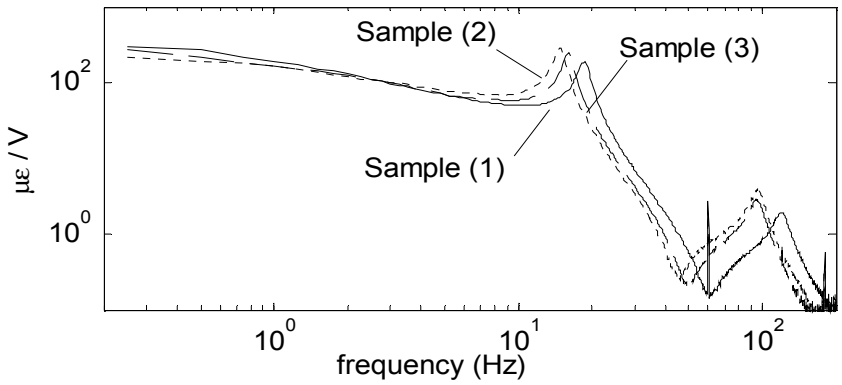

Figure 4.16: microstrain per volt frequency response for three pure RuO_2 samples.

In order to determine the long-term stability of the transducers, a reliability test is also performed on these three identical samples. The three samples were actuated continuously with a 1 Hz sine wave potential and the free strain generated in each sample was measured periodically. The effect of the peak amplitude of the applied potential on the long-term stability of the transducers is illustrated in Figure 4.17. As can be seen, the samples that were actuated with a 1 V and 2 V peak potential did not exhibit and degradation of the response after more than 250,000 cycles. It should be noted that the maximum generated strain in the samples is lower than the 20,000 microstrain these transducers are capable of because the samples are excited at 1Hz. In order to achieve strains on the order of 2% an input frequency of less than 0.04 Hz is required. This is due to the slow response speed of the devices fabricated with pure electrodes. However, the result demonstrates the

improved long-term stability of ionic polymer transducers that utilize ionic liquids instead of water as a diluent. By contrast, Bennett and Leo (2004) have shown that a water-swollen ionic polymer transducer would operate for about 2000 cycles in air. After 3600 cycles the motion decreased by 96% due to diluent evaporation.

Although the specific reason for the decrease in performance of the sample that was driven at +/- 3 V is unknown, a likely explanation is degradation of the ionic liquid. Cooper and O'Sullivan (1992) and Bonhote et al. (1996) have shown that the electrochemical stability window of the EMI-Tf ionic liquid is 4.1 V.

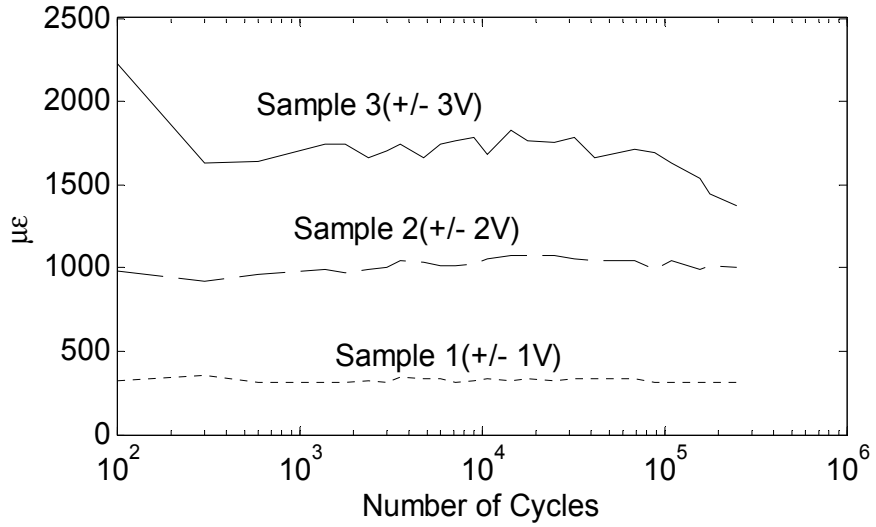

Figure 4.17: Reliability test on the three samples with +/-1V, +/-2V, +/-3V 1Hz sine wave applied on samples 1, 2, and 3 respectively.

4.8 Conclusions

The EmI-Tf ionic liquid diluent produces an environmentally stable transducer with moderate velocity. Formamide actuators could operate in air for several hours without significant loss of actuation performance and they exhibit a faster response time than ionic liquid transducers. Speed of response in ionic liquid transducers is correlated with the content of diluent uptake. Increasing the diluent uptake and decreasing the viscosity of ionic liquids leads to high speed transducers with excellent environmental stability. Tailoring the electrode composition is an effective method for achieving high strain transducers using ionomeric polymer materials. Our results demonstrate that surface area-to-volume ratio of

the metal particulate is a critical property in achieving large capacitance at low frequencies. Increasing the low-frequency capacitance increases the strain output of the transducer. The electrical conductivity through the electrode is also proved to be critical to the speed of response of the transducers. A trade off between high speed for gold particles and large strains for ruthenium dioxide particles is observed. Hybrid ionic transducers are fabricated and the electromechanical properties are characterized in terms of their peak strain output and strain rate due to an applied voltage. A study of electrode properties demonstrated that varying the particulate composition has a substantial impact on the strain output of the transducer. Electrodes fabricated with single-walled carbon nanotubes (SWNT) have an optimal performance at loadings around 30%, while polyaniline (PANI) electrodes are optimized at 95% loading. Due to low percolation threshold, SWNT actuators perform better at lower loading than other conducting powders. Adding SWNT tends to increase both the strain rate and the maximum strain. A SWNT/RuO_2 hybrid transducer was fabricated and achieved a strain rate of 1%/sec and a maximum attainable peak-to-peak strain of 9.38% when operated at +/- 2V. SWNT/PANI hybrid also increased both strain and strain rate but not as significant as with RuO_2.

In brief, this chapter shows the importance of the electrode architecture and composition on the performance of ionic polymer transducers. The conductivity and percolation threshold of the metal powders are proved to be crucial to the speed of response, while the amount of ionomer-conductor interfacial area and pseudocapacitance properties of the metal powder are correlated with the peak strain response of the transducer. Finally, conducting powders with large aspect ratio (low percolation threshold), high electrical conductivity, large surface area, and good pseudocapacitive properties are good candidates for electrode materials in ionic polymer transducers.

Chapter 5

Extensional and Bending Model

Experimental results from the previous chapter indicate that the electrode layer is a critical component that strongly influences transducer performance. Moreover, the results of Chapter 3 correlated the actuation properties of the transducer with the capacitance of the transducer. This result was consistent for ionomers with substantial difference in composition; therefore this result strongly suggests that charge accumulation at the polymer-metal interface is a determining factor in the strain and strain rate generated during actuation. This experimental result is supported by physics-based modeling efforts (Nemat-Nasser, 2002b; Leo et al., 2005) that highlight the role played by the boundary layer that forms at the interface of the electrode and the polymer. Although the understanding of fundamental actuation mechanisms in ionic polymer transducers is still under debate, our previous results and several other models relates such mechanisms to ion conduction across the membrane. Leo et al. (2005) modeled the electromechanical coupling by the expansion

$$\sigma(x,t) = \alpha\rho(x,t) + \beta\rho^2(x,t), \tag{5.1}$$

where α and β are coefficients that define the linear and quadratic terms of the transduction model, while σ represent the stress and ρ is the space-temporal charge density. In this thesis a similar approach is adopted and the electromechanical coupling model is assumed to be in the form

$$\epsilon = \alpha Q + \beta Q^2, \tag{5.2}$$

where ϵ represents the strain and Q is defined as the charge per unit area. This electromechanical model represents a coupling correlation between strain and charge suggested by

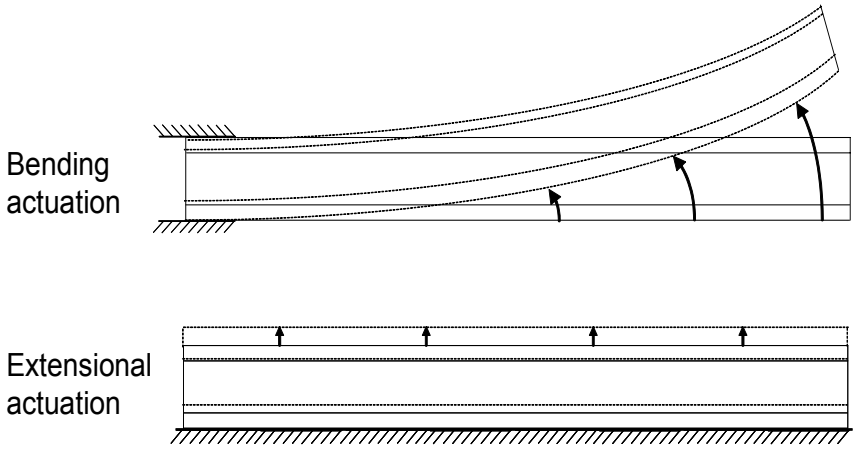

Figure 5.1: Bending and extensional actuation in a bimorph model of ionic polymer transducers.

previous experimental data represented in Chapters 3 and 4. The quadratic term in this model produces a 1st harmonic response for a sine wave voltage input. For ionic polymer transducers with symmetric electrodes this term generates a zero net bending moment due to the expansion of both active areas. If the actuation response is measured in the thickness direction, then the total strain in the transducer is the addition of strains in both electrodes. Hence, the positive βQ^2 term is cumulative in extensional actuation, and the expansion of both electrodes add to the total expansion of the transducer. Moreover, the linear term is canceled in extensional actuation of transducers with symmetric electrodes. Non-linear behavior in the bending actuation is reported in literature (Kothera and Leo, 2005). The quadratic term generates small 1st harmonic response in slightly assymetric electrodes. The bending and extensional actuation are elaborated in Figure 5.1

In this chapter transducers are characterized in bending and extensional actuation, and the results are explained using a bimorph model assuming the electrode as the active area, with Equation 5.2 for electromechanical coupling.

5.1 Modeling

The transducer is decomposed into three layers in this model, two active layers and one passive layer. The active layers are assumed to be the electrodes while the membrane is assumed to be a passive substrate. To justify this concept, we will demonstrate that most of the charges accumulate or deplete the assumed active areas. The electrode is a

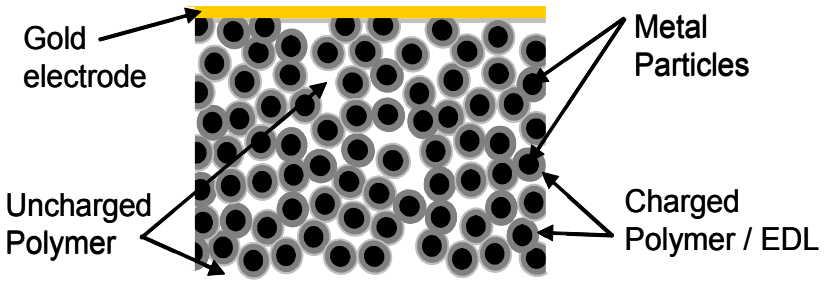

Figure 5.2: Schematic of a typical electrode in an ionic polymer transducer showing the particles surrounded by a charged sphere of ionomer.

metal-ionomer composite that is populated or depleted with the mobile cations upon the application of a potential across the transducer. The average thickness of the electrodes applied in this study is on the order of 10 to 100μm. Typical RuO_2 particles are 3 to 5 nm in diameter. The magnitude of the depleted or charged polymer is a couple of orders smaller than the electrode thickness. The Helmholtz electric double layer model demonstrates that ions approach the electrode to the distance of minimal approach known as the Stern layer, which is on the order of several Angstroms. While Gouy-Chapman model predict a larger length by including the diffuse layer, this length is typically smaller than 1 micron. This Nernst-Plank model is computed in Leo et al. (2005) for ionic polymer transducers and show that this distance is on the order of 0.1 to 1 μm. Figure 5.2 shows a schematic of a charged electrode and demonstrates that the charged volume is mostly bound to the electrode.

5.1.1 Active Areas Model: Simplified Bending

The transducer is modeled as two active electrodes and a passive substrate. A cross section of the model of an ionic polymer transducer is presented in Figure 5.3. This model is simplified by neglecting the nonlinear term in the electromechanical coupling model. The nonlinearities are neglected since they are not captured by the FRF analysis elaborated in chapter 2. This simplified bending model is used in the analysis of FRF bending experimental results, and specifically to extract and compare the values of α.

The equation of a beam in bending

$$EI\frac{d^2w}{dx^2} = M_{is} \tag{5.3}$$

where w is the displacement in the y direction, M_{is} is the internal moment generated by

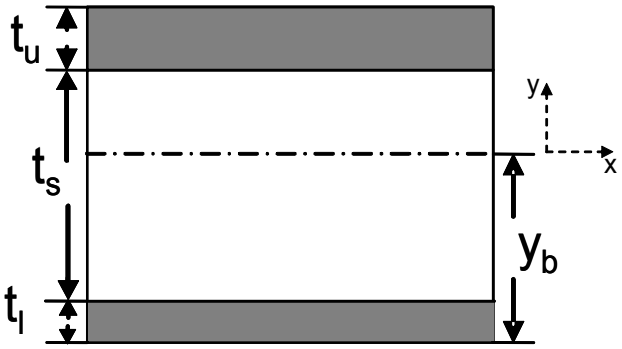

Figure 5.3: Schematic of an asymmetric transducer with an electrode on one side, where y_b represents the distance toward the neutral axis

the actuation of the active areas, and the equivalent EI is defined as

$$EI = \int_{T-y_b-t_u}^{T-y_b} bE_a z^2\,dz + \int_{-(y_b-t_l)}^{T-y_b-t_u} bE_s z^2\,dz + \int_{-y_b}^{-(y_b-t_l)} bE_a z^2\,dz \tag{5.4}$$

$$= bE_a(y_b^2(t_l+t_u) + y_b(-2t_lt_u - 2t_st_u - t_u^2 - t_l^2) + \frac{1}{3}t_u^3 + t_u^2t_l + t_ut_l^2$$

$$+2t_ut_lt_s + t_u^2t_s + t_ut_s^2 + \frac{1}{3}t_l^3) + bE_s(\frac{1}{3}t_s^3 + t_sy_b^2 - t_s^2y_b - 2t_lt_sy_b + t_l^2t_s + t_lt_s^2), \tag{5.5}$$

where T is the total thickness of the transducer:

$$T = t_u + t_s + t_l, \tag{5.6}$$

For a transducer with symmetrical electrodes where $t_u = t_l = t_a$ EI is expressed as

$$EI = \frac{1}{12}(6bE_at_s^2t_a + 12bE_at_st_a^2 + 8bE_aT_a^3 + bE_st_s^3), \tag{5.7}$$

and for a transducer with uni-sided electrode, that is one high surface area electrode on one side and a thin sheet of gold on the other side with negligible thickness and stiffness, EI is of the form:

$$EI = \int_{-y_b}^{t_s-y_b} bE_s z^2\,dz + \int_{t_s-y_b}^{t_s+t_a-y_b} -bE_a z^2\,dz \tag{5.8}$$

$$= \frac{bE_s}{3}(t_s^3 - 3t_s^2y_b + 3t_sy_b^2) + \frac{bE_a}{3}(t_a^3 + 3t_s^2t_a + 3t_st_a^2 - 3(t_a^2 + 2t_at_s)y_b + 3t_ay_b^2) \tag{5.9}$$

Therefore the average modulus of the composite transducer, which is the modulus computed from experimental results, is in the form:

$$\text{general} \quad E = \tfrac{12E_a}{T^3}(y_b^2(t_l+t_u) + y_b(-2t_lt_u - 2t_st_u - t_u^2 - t_l^2) + \tfrac{1}{3}t_u^3 + t_u^2t_l + t_ut_l^2 + 2t_ut_lt_s$$
$$+t_u^2t_s + t_ut_s^2 + \tfrac{1}{3}t_l^3) + \tfrac{12E_s}{T^3}(\tfrac{1}{3}t_s^3 + t_sy_b^2 - t_s^2y_b - 2t_lt_sy_b + t_l^2t_s + t_lt_s^2), \quad (5.10)$$

$$\text{symmetric} \qquad E = \tfrac{1}{T^3}(6E_at_s^2t_a + 12E_at_st_a^2 + 8E_aT_a^3 + E_st_s^3), \quad (5.11)$$

$$\text{single} - \text{sided} \qquad E = \tfrac{4E_s}{T^3}(t_s^3 - 3t_s^2y_b + 3t_sy_b^2),$$
$$+\tfrac{4E_a}{T^3}(t_a^3 + 3t_s^2t_a + 3t_st_a^2 - 3(t_a^2 + 2t_at_s)y_b + 3t_ay_b^2) \quad (5.12)$$

The neutral axis is determined by assuming that the cross section of the active area is a scaled width by the elasticity modulus ratio

$$n = \frac{E_a}{E_s}, \quad (5.13)$$

and hence the neutral axis is determined by

$$y_b = \frac{\sum_i A_iy_i}{\sum_i A_i} \quad (5.14)$$

$$= \frac{n(t_u^2 + t_l^2 + 2t_ut_l + 2t_ut_s) + 2t_st_l + t_s^2}{2n(t_u + t_l) + 2t_s} \quad (5.15)$$

for symmetrical and single sided electrodes y_b is defined as

$$y_b = \frac{2t_a + t_s}{2}, \quad (5.16)$$

$$y_b = \frac{t_s^2 + n(t_a^2 + 2t_at_s)}{2(t_s + nt_a)}, \quad (5.17)$$

Equations (2.1) and (2.2) computes the strain from the tip displacement of the actuator, and assumes the center line of the transducer to be the center of bending. Therefore bending is assumed to be around this middle line, and the internal strain moment is computed according to

$$M_{is} = \int_{T/2-t_u}^{T/2} \epsilon_u zbE_a\,dz + \int_{-T/2}^{-T/2+t_l} -\epsilon_l zbE_a\,dz$$
$$= \frac{E_ab}{2}(\epsilon_u(Tt_u - t_u^2) + \epsilon_l(Tt_l - t_l^2)) \quad (5.18)$$

In this simplified model the electrostatic term βQ^2 is neglected and therefore

$$\epsilon_u = \epsilon_l = \alpha Q, \quad (5.19)$$

and rewrite Equation 5.18 for the general case as

$$M_{is} = \frac{\alpha QE_ab}{2}(Tt_u - t_u^2 + Tt_l - t_l^2), \quad (5.20)$$

for symmetrical and single sided electrodes it is written as

$$M_{is} = \alpha Q b E_a t_a (t_s + t_a) \tag{5.21}$$

$$M_{is} = \frac{\alpha Q b E_a}{2}(T t_a - t_a^2) \tag{5.22}$$

Equations (2.1) and (2.2) represent the strain at the outer fibers of the transducers and therefore

$$\epsilon = \frac{d^2 w}{dx^2}\frac{T}{2} \tag{5.23}$$

where ϵ is the measured strain at the outer fibers and T represents the total thickness of the actuator. Equations 5.3 and 5.23 are combined to form

$$\epsilon = \frac{M_{is}}{EI}\frac{T}{2}. \tag{5.24}$$

Combining Equations 5.20, 5.21, and 5.22 with Equation 5.24 α is computed respectively for the general case, symmetric, and single sided electrodes

$$\text{general} \quad \alpha = \frac{4\epsilon EI}{QTbE_a(Tt_u - t_u^2 + Tt_l - t_l^2)}, \tag{5.25}$$

$$\text{symmetric} \quad \alpha = \frac{2\epsilon EI}{QTbE_a t_a (t_s + t_a))}, \tag{5.26}$$

$$\text{single} - \text{sided} \quad \alpha = \frac{4\epsilon EI}{QTbE_a(Tt_a - t_a^2)}, \tag{5.27}$$

5.1.2 Active Areas Model: Extensional model

In extension the ionomeric transducer is also modeled using three layers, two active layers and a passive substrate. As described in the experimental setup section the output is measured in the form of blocked force due to the difficulty of measuring sub-micron displacements at low frequencies. The transducer is relatively stiff in the thickness configuration and therefore the stiffness of the fixture is important and is accounted for in the model. The schematic of the three-layered polymer with the load cell is shown in Figure 5.4.

The model is developed at static equilibrium ignoring any dynamic effects. The experiments are done at a low frequency range of 0.1 to 100Hz. The first natural frequency of the transducer in extension is expected to be larger than this range. The equilibrium

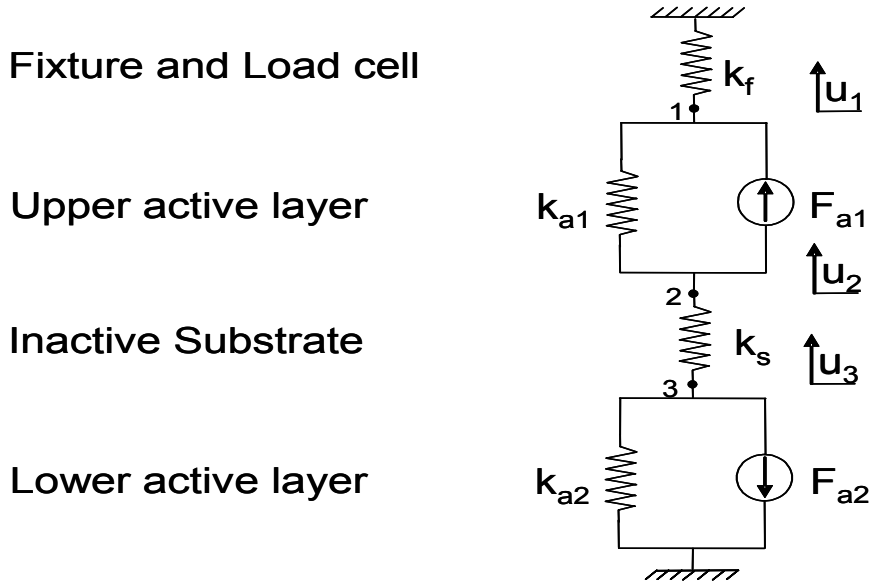

Figure 5.4: Schematic of the three-layered ionic polymer transducer in thickness configuration.

equations at the points 1, 2, and 3 respectively are

$$-k_f u_1 + F_{a1} - k_{a1}(u_1 - u_2) = 0 \tag{5.28}$$

$$-F_{a1} + k_{a1}(u_1 - u_2) - k_s(u_2 - u_3) = 0 \tag{5.29}$$

$$k_s(u_2 - u_3) - F_{a2} - k_{a2}u_3 = 0 \tag{5.30}$$

and the displacement at each point is

$$u_1 = k_s \frac{F_{a1}k_{a2} - k_{a1}F_{a2}}{k_{a1}k_s k_f + k_{a1}k_{a2}k_f + k_s k_{a2}k_{a1} + k_s k_{a2}k_f} \tag{5.31}$$

$$u_2 = -\frac{k_s F_{a1}k_f + k_s F_{a2}k_{a1} + k_s F_{a2}k_f + F_{a1}k_{a2}k_f}{k_{a1}k_s k_f + k_{a1}k_{a2}k_f + k_s k_{a2}k_{a1} + k_s k_{a2}k_f} \tag{5.32}$$

$$u_3 = -\frac{k_s F_{a1}k_f + k_s F_{a2}k_{a1} + k_{a1}F_{a2}k_f + k_s F_{a2}k_f}{k_{a1}k_s k_f + k_{a1}k_{a2}k_f + k_s k_{a2}k_{a1} + k_s k_{a2}k_f} \tag{5.33}$$

The stiffness of the active areas are defined as

$$k_{a1} = \frac{E_a A}{t_u} \tag{5.34}$$

$$k_{a2} = \frac{E_a A}{t_l} \tag{5.35}$$

where A is the area of the transducer. The passive substrate stiffness is defined as:

$$k_s = \frac{E_s A}{t_s} \tag{5.36}$$

The stiffness of the fixture and the load cell (k_f) was calibrated as demonstrated in Chapter 2 to be around $2.4N/\mu m$. Matching the theoretical model to the experimental data the active and substrate modulus are calibrated to be $E_a = 180MPa$ and $E_s = 30MPa$.

The free strain is computed from the electromechanical transduction model developed by Leo et al. (2005)

$$\epsilon_{a1} = \alpha Q + \beta Q^2 \tag{5.37}$$

$$\epsilon_{a2} = \alpha Q - \beta Q^2 \tag{5.38}$$

where Q is defined as the charge per unit area. The forcing functions in the active layers are defined as the free strain multiplied by the stiffness.

$$F_{a1} = E_a A \epsilon_{a1} \tag{5.39}$$

$$F_{a2} = E_a A \epsilon_{a2} \tag{5.40}$$

5.1.3 Active Areas Model: Bending with Electrostatic Expansion Term

The electrostatic attraction term βQ^2 is added to the simplified bending model. The electrostatic term always lead to positive strain or expansion in the active area. Therefore its net moment on perfectly symmetrical electrodes is expected to be zero, and largest on single sided electrodes. The average modulus and moment of inertia terms are computed similarly to the simplified model. The electrodes are also assumed to be the active areas and the bending is assumed to be around the center line of the transducer. Equation 5.18 is the same while the strain are modified as follows:

$$\epsilon_u = \alpha Q + \beta Q^2 \tag{5.41}$$

$$\epsilon_l = \alpha Q - \beta Q^2 \tag{5.42}$$

and the resulting moment is:

$$M_{is} = \frac{E_a b}{2} \alpha Q (T(t_u + t_l) - (t_u^2 + t_l^2)) + \frac{E_a b}{2} \beta Q^2 (T(t_u - t_l) - (t_u^2 - t_l^2)) \tag{5.43}$$

Equations 5.3, 5.23, and 5.43 are combined and the resulting strain equation:

$$\epsilon = \frac{T E_a b}{4EI} \left(\alpha Q (T(t_u + t_l) - (t_u^2 + t_l^2)) + \beta Q^2 (T(t_u - t_l) - (t_u^2 - t_l^2)) \right) \tag{5.44}$$

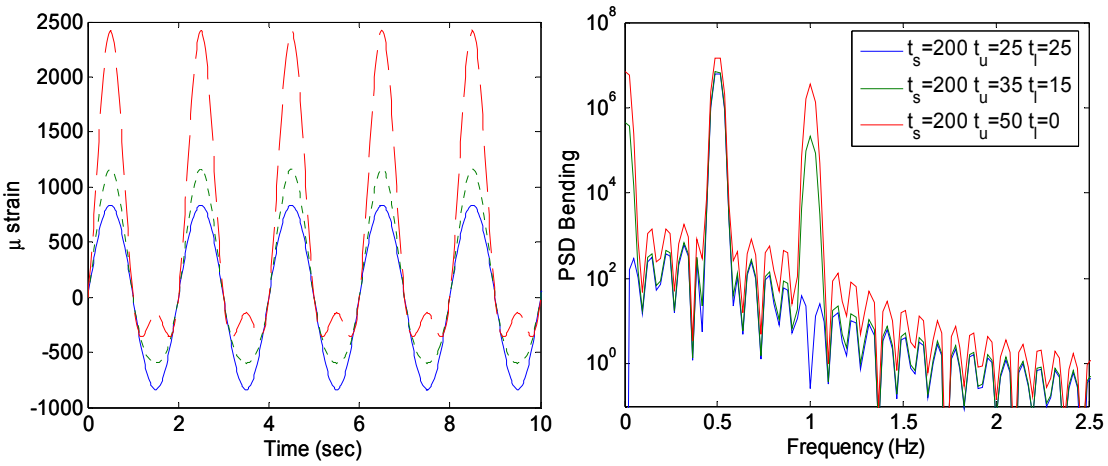

Figure 5.5: (a) Model simulation of the microstrain time response of three samples with different electrode configurations in bending mode. (b) Power spectrum of the time response.

α and β are computed by fitting equation 5.44 to time domain data of the transducer bending.

5.2 Model Simulations

Models of three transducers are built and simulated under typical actuation conditions. The three samples are made of $t_s = 200\mu m$ substrate and has an upper electrode thickness $t_u = 25\mu m,\ 35\mu m,\ and\ 50\mu m$, and a lower electrode thickness of $t_l = 25\mu m,\ 15\mu m,\ and\ 0\mu m$ respectively. These simulated transducers are named M1, M2, and M3 respectively. The geometries of these simulated transducers are similar to the experimentally tested transducers. The area for the extensional simulations is 3x3 mm^2 and 3x30 mm^2 in bending. Values for α and β are $2x10^{-6}$, $4x10^{-9}$ respectively. In this simulation we assume a sinusoidal charge density with amplitude of $450C/m^2$ is actuating the transducers at a frequency at 0.5Hz. Simulations of the time and frequency domain response of the transducers in bending are computed using Equation 5.44 and are shown in Figure 5.5(a) and (b) respectively. Time and frequency domain simulations in the extensional mode are computed according to Equation 5.31 and are shown in Figure 5.6(a) and (b) respectively. Model simulations demonstrate that distortion in the bending increases in the samples with greater assymetry. The first harmonic peak response increases from 1.5, 16, to 66 μstrain as the electrode

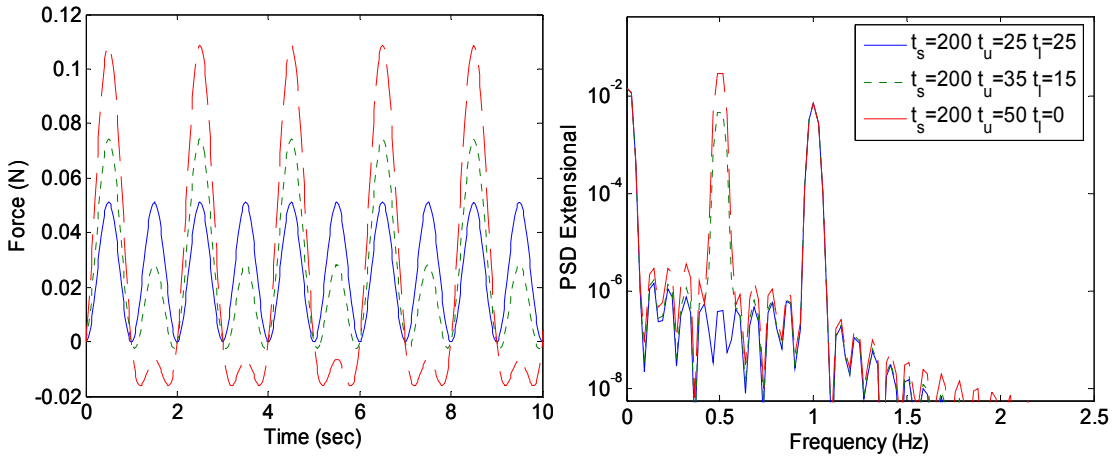

Figure 5.6: (a) Model simulation of the forcing time response of three samples with different electrode configurations in extensional mode. (b) Power spectrum of the time response.

symmetry decreases. The values of the fundamental frequency varies less and are 740, 770, and 1100 μstrain for models M1, M2, and M3 respectively.

The extensional mode simulations shows an opposite trend. Distortion or first harmonic response remains constant with electrode symmetry, while the fundamental frequency response decrease to the noise flour for symmetric electrodes. The response of models M1, M2, and M3 on the fundamental frequency are 0.2, 20, and 51 mN respectively. The first harmoninc response is constant at 30mN for all the models.

Simulations demonstrate that the ratio of the first harmonic to the fundamental frequency response is a representation of distortion in the actuator. This ratio is presented in Figure 5.7 for the simulations of bending and extensional mode actuation response. The model predicts larger values of distortion in the extensional mode compared to that of the bending reponse. The maximum distortion in the symmeteric transducer extentional mode actuation is around 16 compared 0.06 maximum distortion in the assymetric transducer for the extentional mode. This simulation result justify the reason that distortion is not reported frequently in bending, while it is very prominent in extensional mode as our results will show later. Furthermore, this graph asserts the previous result that distortion increases in bending with increasing assymetry, and decreases in the extensional mode.

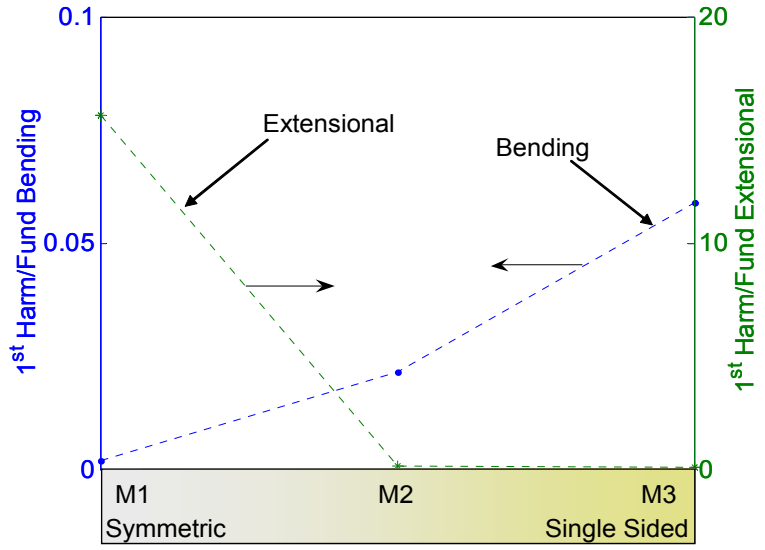

Figure 5.7: 1^{st} Harmonic/ Fundamental frequency response as a function of electrode symmetry in bending and extensional modes.

5.3 Experimental Results

Several transducers are prepared and their electromechanical properties are measured in bending and thickness. The ionic polymer transducers varied in membrane thickness and electrode thickness on each side. Four single sided electrode transducers are also prepared and characterized.

5.3.1 Simplified Bending Model: FRF Analysis

Seven samples are prepared, three samples had a targeted electrode thickness of 25 μm thick electrode on each side and membranes of 50, 90, and 125μm (S2, S3, and S4). Three other samples had different electrode thicknesses on an 180 μm membrane. Two other samples had 10 μm and 50 μm electrodes on each side of a 180 μm membrane (S5, S6, and S7). The seventh transducer had 25 μm electrode on a single side of a 180 μm membrane and is labeled S1. The effective thickness measured under the microscope at three different points across the actuator are shown in Table 5.1.

Prior to measuring α the modulus of the active electrode and the substrate are calibrated. In Chapter 2, Section 2.1 we presented two methods of measuring the modulus of the transducer according to Equations 2.5 and 2.9. Table 5.3.1 is a comparison of stiff-

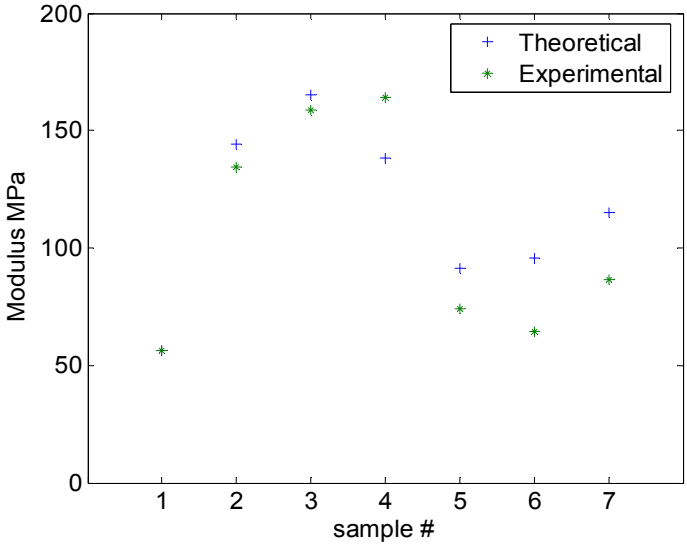

Figure 5.8: Modulus calibration of samples

Table 5.1: Thickness measurements of the upper electrode, polymer substrate, and lower electrode for samples S1 through S7.

	S1	S2	S3	S4	S5	S6	S7
t_u	22	55	30	47	55	45	30
t_l	0	32	20	37	37	37	22
t_s	242	65	105	120	220	207	230

nesses of samples S1 through S4 computed using the natural frequency and direct stiffness measurement methods. The maximum variation is around 26%.

Modulus of elasticity of samples S1 through S7 are computed from the resonance peaks of the FRFs in Figure 5.9(b) according to equation 2.5. Equations 5.10, 5.11, and 5.12 are fitted to the experimental data and the modulus of the electrode and the membrane are calibrated to be 180MPa and 30MPa respectively. Figure 5.8 shows the experimentally measured effective modulus compared to the model prediction of the seven samples.

The strain per unit volt FRF results demonstrates large variation between the performance of the samples. The single sided electrode actuator performed worst at 140 μm at 0.25Hz compared to 1560 μm for 90 μm membrane transducer (see Figure 5.9 (a)). The strain per volt was normalized with respect to charge per area. The resulting FRF shows less variations of 2 to 6 μstrain/(C/m^2), moreover the frequency roll-off is eliminated and

Table 5.2: Stiffness of four samples computed from the natural frequencies and directly from the fixed-sliding beam experiment.

	S1	S2	S3	S4
Stiffness from natural frequency (MPa)	57	135	156	164
Stiffness from direct measurement (MPa)	54	166	124	191
Error	5.1%	23.1%	25.6%	16.7%

the response in flat in the 0.25 - 10 Hz range (see Figure 5.9 (b)). The strain per charge data is inserted in the simplified bending model and the value of α was computed as function of frequency according to Equations 5.25, 5.26, and 5.27 for each sample. The charge (Q) is computed by integrating the measured actuation current per volt FRF. At 0.25Hz the maximum variation of α is from 3.1x10^{-6} to 5.2x10^{-6} strain/(C/m^2) (see Figure 5.9 (b). This demonstrates that the active areas model collapsed the data from a maximum variation of 200% for the strain per charge to less than 68% for α.

5.3.2 Extensional Actuation Results

The extensional response of ionic polymer transducers due to a sine wave potential input is a distorted sine wave containing the fundamental frequency and several harmonics. The first harmonic is usually dominant over the remaining harmonics. The βQ^2 in the electromechanical model represents the electrostatic repulsion forces between ions in the charged electrode and depleted regions. The quadratic charge term introduced a first harmonic signal in the response. The square of a sine wave is a positive cosine signal with double the frequency:

$$(\sin \omega t)^2 = \frac{1 - \cos 2\omega t}{2}, \tag{5.45}$$

This model is capable of predicting the first and second peak. Due to the existence of harmonics in the charge input to the actuator, some of the higher harmonics are also fitted. In this section the experimental data is analyzed in the frequency domain. The power spectral density (PSD) estimate of the blocked force and charge density signals are estimated according to the Welch's method (Welch, 1967). The data was initial filtered with a Hanning window. The model is fitted to the first two frequency peaks in the experimental

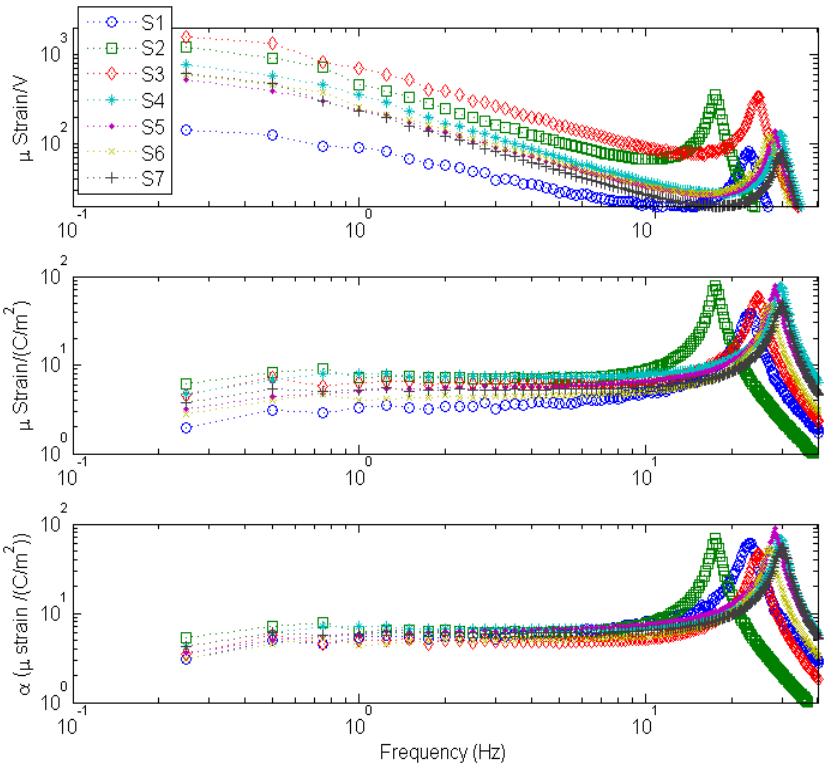

Figure 5.9: (a) FRF of the strain per volt, (b) FRF of the strain per charge per area, and (c) FRF of the α computed from the simplified bending moment model.

data by selecting the appropriate values for α and β. A mamdani fuzzy logic controller is built for the purpose of automatically fitting the fundamental and 1st harmonic peaks. The membership functions and the rules of the fuzzy controller were tailored to follow the trends in the data. The α coefficient controls the fundamental frequency in the response of the model, and β coefficients fits the 1st harmonic. Little coupling exist between the two terms, and it is mostly significant when the charge density signal contains strong harmonics.

Shown in Figure 5.10 are the values of α and β for the model to fit the experimental data for seven different ionic polymer transducers in the frequency range of 0.5 to 10Hz. The values of α varies from approximately 5 μstrain/(C/m^2) to 20 μstrain/(C/m^2) and it is fairly constant with frequency in the 2Hz to 10Hz range. However β is not constant but rather shows an increasing linear trend with frequency. Values at 0.5Hz varied from 3x10^{-3}μstrain/(C/m^2)^2 to 13x10^{-3}μstrain/(C/m^2)^2. The range at 10Hz is between 0.35μstrain/(C/m^2)^2 to 3.7μstrain/(C/m^2)^2 or two orders of magnitude larger. The sample

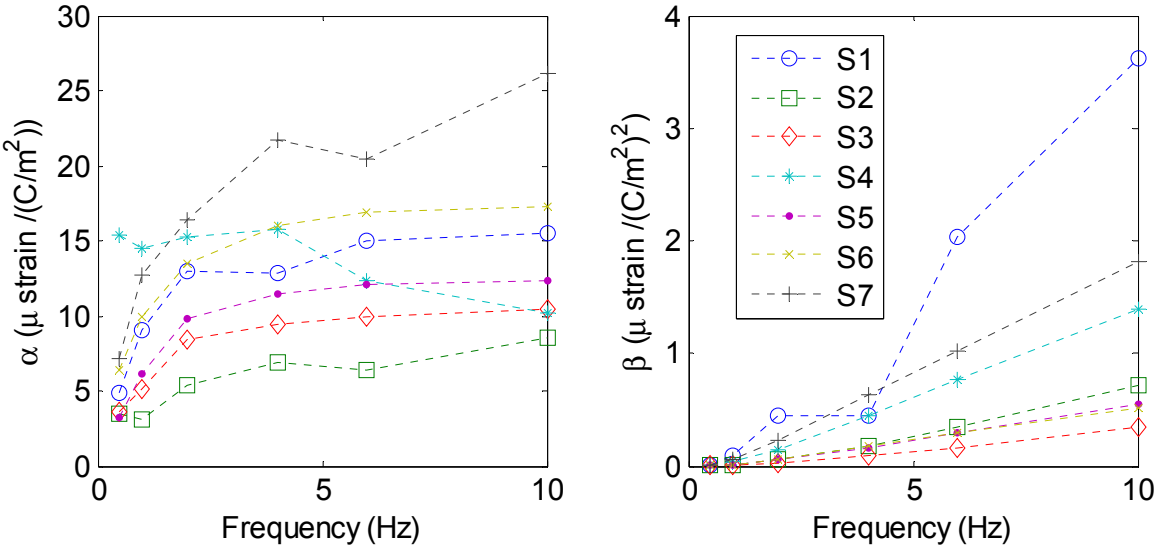

Figure 5.10: Values of the α and β for the model to fit the experimental data for seven different ionic polymer transducers in the frequency range of 0.5 to 10Hz.

to sample variation of the α and β values are believed to be due to non-uniformity in the electrodes and the large tolerances in the measurements that are reported in Table 5.1.

Figure 5.11 (a) and (b) shows respectively the typical response of the time and frequency domain blocked pressure and model fit for a sample with 25μm electrodes on each side on a 180 μm membrane, actuated with a 2V 0.5Hz sine wave. Notice the doubling in frequency that is more dominant than the fundamental frequency response. The stiffness of this sample is estimated experimentally to be around 90MPa and therefore the corresponding strain to 10kPa is estimated to be 110 μstrain.

5.3.3 Bending with Electrostatic Expansion Term

In this section the values of α and β computed from the through-thickness actuation data are incorporated in the fully developed bending model to predict the response in bending of the corresponding transducer.

Shown in Figure 5.12 (a) is the ratio of the 1st harmonic to the fundamental frequency in the strain response computed from experimental results. Figure 5.12 (c) shows the model's prediction of these ratios which match within 70% error on the 0.5 Hz while the error increase drastically at higher frequency. In the time domain the model predicts

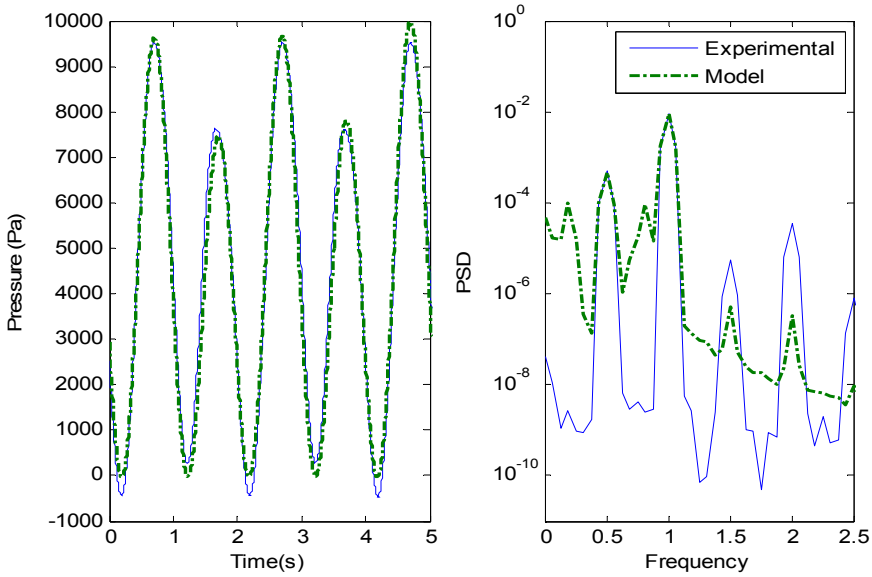

Figure 5.11: (a) Typical blocked pressure response and model fit for a sample with 25μm electrodes on each side on a 180 μm membrane, actuated with a 2V 0.5Hz sine wave. (b) Measured and model prediction psd for the same sample.

Table 5.3: Thickness measurements of the upper electrode, polymer substrate, and lower electrode for samples L1 through L6.

	L1	L2	L3	L4	L5	L6
t_u	20	40	40	40	48	30
t_l	0	0	0	0	30	25
t_s	260	150	115	68	260	260

the response at low frequency (see Figure 5.13) but over-predicts the harmonics at higher frequencies. Furthermore, the model well predicts the trends in the amount of distortion between samples. S1 and S2 are samples with most assymetrical electrodes. Experimentally the bending response of these samples has the most distortion, and this well predicted by our model as shown in Figure 5.12 (c). More details on these trends are presented in later sections.

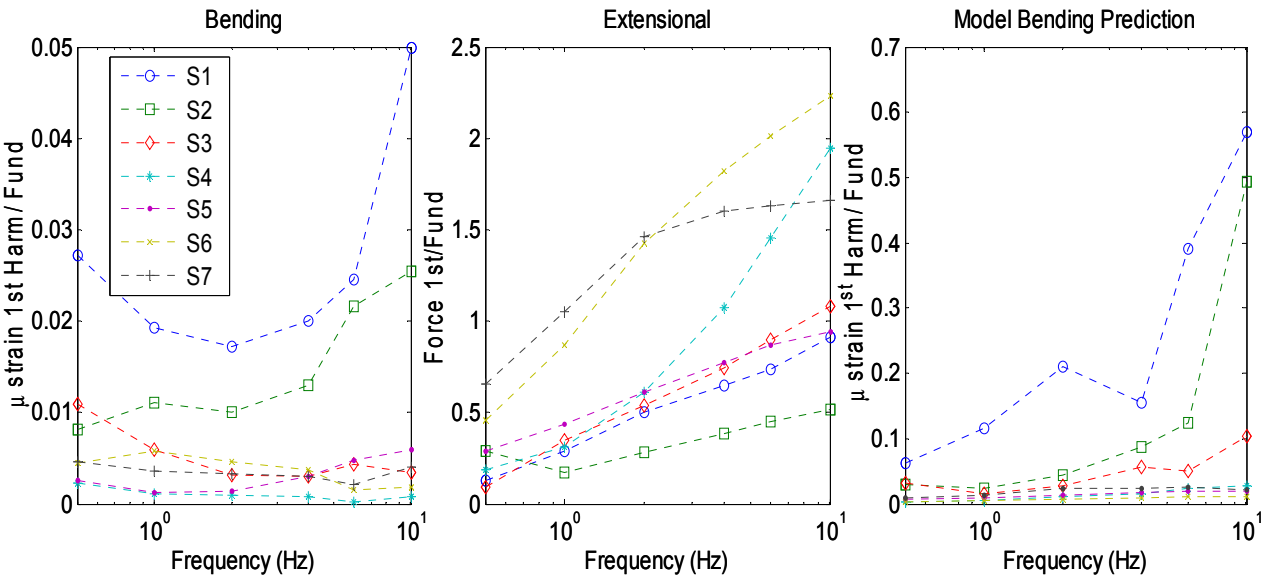

Figure 5.12: (a) Experimental ratio of the 1st harmonic to the fundamental frequency in the strain response under 2V sine waves (b) The distortion ratio in extensional actuation (c) Model prediction of this ratio

5.4 Discussion and Model Verification

A series of six transducers is built and characterized for the purpose of verifying the model and confirming previous analysis. Four of the samples are painted with single sided electrodes of approximately 25 μm on membranes of 50, 90, 125, and 180μm thick and are labeled L1, L2, L3, and L4 respectively. The other two transducers have two symmetric electrodes of different thicknesses and are labeled L5 and L6. Measurement of the actual thicknesses under the microscope are presented in Table 5.4. The six samples are built and characterized similar to the process presented in the previous sections. The values of α and β from either thickness or bending experiments are within the range of the previous set of transducers (see Figure 5.14).

5.4.1 Dependency on the Potential

Charge injection into the ionic polymer transducer increases with the applied voltage across the membrane. As mentioned earlier the fundamental frequency in the response is due to the αQ term while the first harmonic response is mainly due to the βQ^2 term. Therefore the harmonic is expected to increase as a function of charge, which in turn is a function of the applied voltage. This could be verified in Figure 5.15.

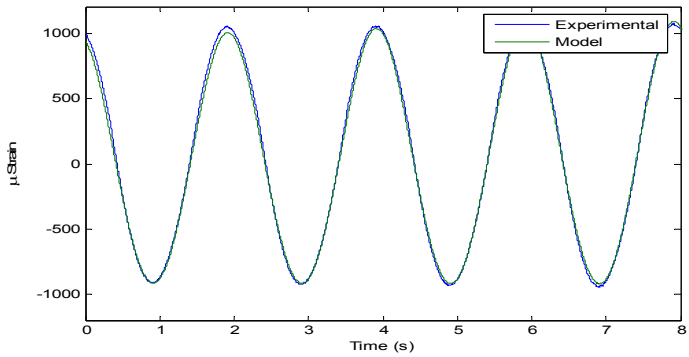

Figure 5.13: Experimental and modeling of a two sided transducer time response due to 2V 0.5Hz **sine wave in bending.**

Furthermore, Figure 5.14 (b) and (d) demonstrates that the model was able to account for the dependency on Q^2 and the computed value of β didn't vary significantly from 1V to 2V.

5.4.2 Model Discussion and Trends

The nonlinear quadratic term in the electromechanical model produces a 1^{st} harmonic response for a sine wave actuation input. For transducers with symmetric electrodes this term generates a zero net bending moment as predicted in the model simulation section. Figure 5.12 (a) represents the ratio of the 1^{st} harmonic to the fundamental frequency bending response for the seven transducers presented in the results section. The value of this ratio is largest for the single sided electrode and S2 which has the most assymetric electrode (see Table 5.3.1). Figure 5.12 (b) represents this ratio for the extensional actuation response. The magnitude of the 1^{st} harmonic to the fundamental response is almost 50x larger. The samples with highest bending distortion (S1 and S2) had the lowest extensional distortion (Figure 5.12 (b)). Figure 5.12 (c) demonstrates that our model is predicting these trends.

Numerical (Leo et al., 2005) and analytical (Farinholt et al., 2005) solutions of the Nernst-Plank equation on ion selective membrane with mobile cations and bonded anions indicates the development of an assymetrical charge profile at low frequency and large voltage (in the order 1Hz and 1V). Leo et al. (2005) observed that this charge profile becomes symmetrical at high frequencies and low voltages. Figure 5.16 represents the schematic of the space charge density across the transducer at low and large frequencies. The square of

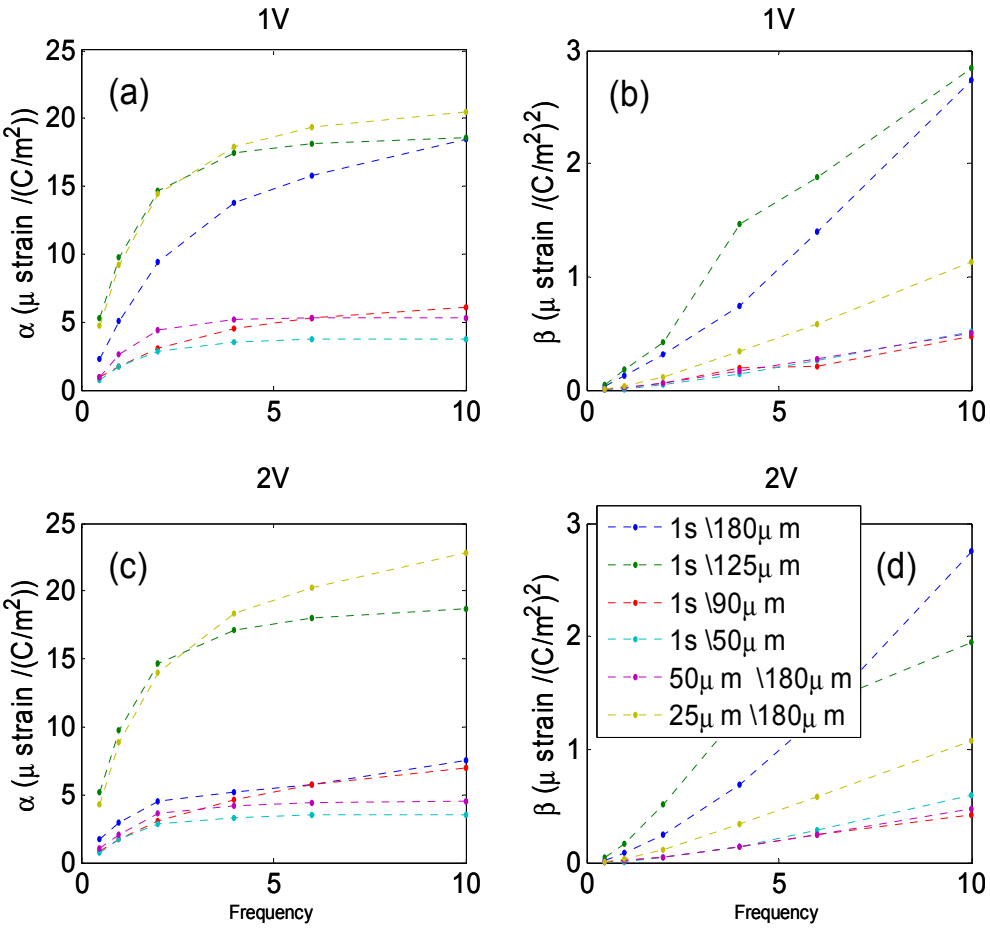

Figure 5.14: (a)Values for α under 1V (b) Values for β under 1V (c) Values for α under 2V (d) Values for β under 2V

the charge distribution are also estimated in the schematics.

At high frequency a symmetrical profile is developed. The Q^2 term result in a zero bending moment for symmetrical electrodes. However at low frequency Q^2 the assymetric profile is expected to produce a larger bending moment due to the difference in thickness and magnitude. In our model Q^2 is detected from the 1st harmonic and therefore a decrease in the distortion is expected with the increase in frequency. This is verified in Figure 5.12(a) which represents the ratio of the first harmonic peak to the fundamental peak. Moreover Figure 5.12(b) demonstrates that the distortion increases as a function of frequency in extention. This behavior is also expected because the magnitude of the charge density Q is less distributed and have higher magnitude at smaller area. Therefore the Q^2 term

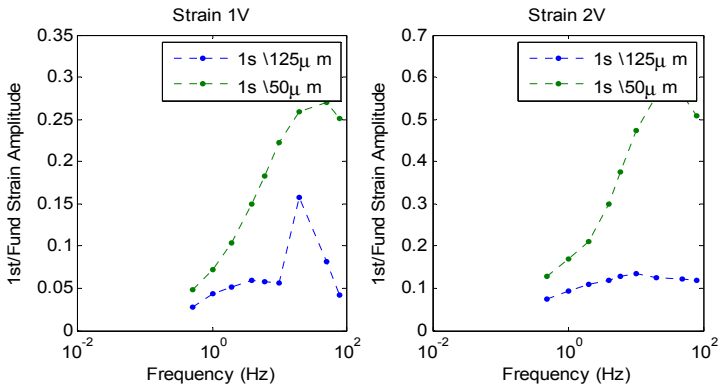

Figure 5.15: (a) Ratio of the 1^{st} harmonic to the fundamental frequency in the strain response under 1V sine wave, and (b) 2V sine wave

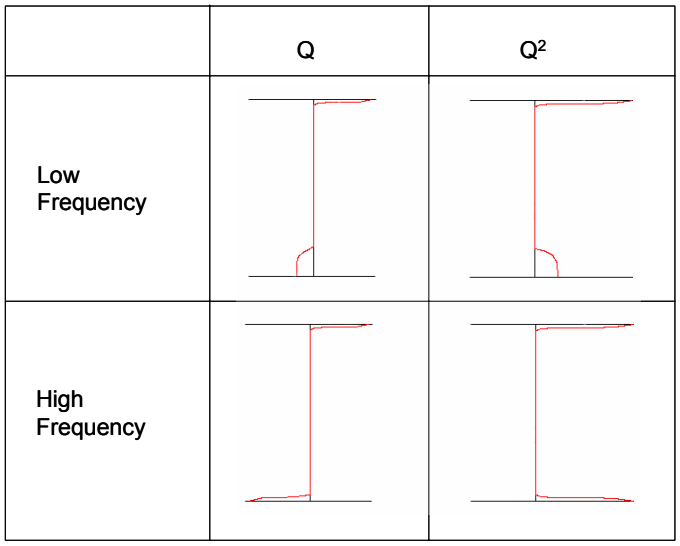

Figure 5.16: Charge density profile in a cross section of an ionic polymer transducer at low frequency and high frequency.

increases with symmetric profile. Since our model is frequency independent those effects might explain the increase in β which is not predicted by our fixed active area model.

5.5 Conclusions

In this chapter we reported actuation through the thickness of the membrane, leading to the potential of a new actuation mechanism for ionomeric polymer materials. To our knowledge this is the first report of this actuation behavior. Several experiments were performed to compare bending actuation with the extensional actuation. Experimental

results demonstrates strain on the order of 110 μstrain in the thickness direction compared to 1700 μstrain peak to peak on the external fibers for the same transducer when it is allowed to bend under +/-2V potential at 0.5 Hz. A bimorph model is presented and used to assess the effect of electrode thickness on the strain. An electromechanical coupling model with a linear and a quadratic term determined the strain in the active areas as a function of the charge. The linear term computed from the simplified demonstrated a decrease in variation between the samples. The values of α and β from the thickness were incorporated in the model to predict the bending response. The prediction was relatively good at low frequency while it was very poor at higher frequencies due to the linear increase in the values of β. This study demonstrated that β is independent of the electric potential while the 1^{st} harmonic response increase with it. This lends further support to existence of a quadratic term in actuation. Experimental results support the prediction of the model that assymetric electrodes has most distortion in bending while least in extensional direction.

Chapter 6

Summary and Conclusions

In this chapter a brief summary of the dissertation is provided. The contributions to the field are presented and major conclusions are drawn. Finally recommendations for future work will be presented.

6.1 Dissertation Summary

In this dissertation we have developed, optimized, and characterized a novel ionic polymer transducer fabrication technique named the direct assembly process (DAP). This process provided good control on the electrode morphology and architecture of the transducer, which enabled us to study the effect of the electric double layer on actuation in ionic polymer transducers. The direct assembly process was inspired from large capacitance devices known as supercapacitors. An initial motivation study indicated that the strain response of an ionomeric transducer is strongly correlated with the capacitance of the plated material. The Direct Assembly Process was developed in collaboration with Dr. Kenton Wiles and Dr. James E. McGrath at Virginia Tech. In this study we reported for the first time actuation through the thickness of the membrane, leading to the potential of a new actuation mechanism for ionomeric polymer materials. Electromechanical characterization setup are built to measure the bending actuation with the extensional actuation response.

In this dissertation, we studied the transducer performance of several different ionomers from three ionomer families. Results demonstrate that there is an approximately linear relationship between strain response per unit voltage and the capacitance of the transducer.

This relationship indicates that the strain output per unit electric displacement is approximately constant for all of the polymers tested. Our experiments indicate that this value ranged between 9.8 $\frac{\mu strain}{\frac{C}{m^2}}$ and 15 $\frac{\mu strain}{\frac{C}{m^2}}$ for the polymers tested in this work, and that this value was consistent with data presented previously by other researchers.

These results suggest a strong relationship between charge accumulation at the polymer-metal interface and transducer performance. It is known that the low-frequency capacitance of an ionomeric material is due to blocking electrode effects, therefore a strong correlation between capacitance and strain indicates that charge accumulation at the interface between the electrode and the polymer is responsible for mechanical deformation. Although this has been suggested in the literature before, our results demonstrate that the amount of strain produced by this charge accumulation is approximately the same for a wide range of ionomer materials that have substantially different properties.

The EmI-Tf ionic liquid diluent produces an environmentally stable transducer with moderate velocity. Five organic diluents are studied in this dissertation. PolyEthylene Glycols (PEG) are polar alcohols with relatively high boiling point. PEG with four molecular weights (MW) are explored. Ethylene Glycol (EG) is the basic unit, diethylene glycol (DEG) is a two repeating units, triethylene glycol (TEG) is three , PEG 200 is an average of 4.2 repeating units, and finally Formamide a highly polar and low viscosity diluent are incorporated in transducers. These organic diluents actuators could operate in air for several hours without significant loss of actuation performance and they exhibit a faster response time than ionic liquid transducers. The speed of response is correlated to the viscosity and polarity of the organic diluent. Formamide attained the highest speed of 1%strain/sec averaged on the first 2 seconds of a 2V step response. Speed of response in ionic liquid transducers is correlated with the content of diluent uptake. Increasing the diluent uptake and decreasing the viscosity of ionic liquids could lead into high speed transducers with excellent environmental stability.

Tailoring the electrode composition is an effective method for achieving high strain transducers using ionomeric polymer materials. Our results demonstrate that surface area-to-volume ratio of the metal particulate is a critical property in achieving large capacitance at low frequencies. Increasing the low-frequency capacitance increases the strain output of the transducer. The electrical conductivity through the electrode is also proved to be critical to the speed of response of the transducers. A trade off between high speed for gold particles

and large strains for ruthenium dioxide particles is observed. The electrode composition and morphology of ionic polymer transducers is manipulated, and evidence of electric double layer formation at the electrode-polymer interface is proposed. The actuation mechanism is charge driven, and the slow diffusion of ions toward the electrode is critical to speed of response.

Electrodes fabricated with RuO_2 high surface area metal particles have an optimal performance at 42% metal loading. The increasing part of the curve is determined by the percolation theory in a conductor-insulator matrix. The percolation threshold of RuO_2 in Nafion was measured to be around 19%. The decreasing part of the curve is attributed to the absence of ionomer and the slow diffusion of ions into the electrode.

Hybrid ionic transducers are also fabricated and the electromechanical properties are characterized in terms of their peak strain output and strain rate due to an applied voltage. A study of electrode properties demonstrated that varying the particulate composition has a substantial impact on the strain output of the transducer. Electrodes fabricated with single-walled carbon nanotubes (SWNT) have an optimal performance at loadings around 30%, while polyaniline (PANI) electrodes are optimized at 95% loading. Due to low percolation threshold, SWNT actuators perform better at lower loading than other conducting powders. Adding SWNT tends to increase both the strain rate and the maximum strain. A SWNT/RuO_2 hybrid transducer has a strain rate of 1%/sec and a maximum attainable peak-to-peak strain of 9.38% when operated at +/- 2V. This is over 50x enhancement from strains achieved in transducers using traditional fabrication techniques. SWNT/PANI hybrid also increased both strain and strain rate but not as significant as with RuO2. PANI/RuO2 actuator had an overwhelming back relaxation under the application of a DC electric field.

Experimental results demonstrates strain on the order of 110 μstrain in the thickness direction compared to 1700 μstrain peak to peak on the external fibers for the same transducer when it is allowed to bend under +/-2V potential at 0.5 Hz. A bimorph model is presented and used to assess the effect of electrode thickness on the strain. An electromechanical coupling model with a linear and a quadratic term determined the strain in the active areas as a function of the charge. The alpha term computed from the simplified demonstrated a decrease in variation between the samples. The values of α and β from the thickness were incorporated in the model to predict the bending response. The prediction

was relatively good at low frequency while it was very poor at higher frequencies due to the linear increase in the values of β. This study demonstrated that β is independent of the electric potential while the 1^{st} harmonic response increase with it. This lends further support to existance of a quadratic term in actuation. Experimental results supports the prediction of the model that assymetric electrodes has most distortion in bending while least in extensional direction.

6.2 Contributions

This dissertation has three major contributions to the field of ionic polymer transducers. These contributions enhances the performance of ionic polymer transducers, provide tools to the fabrication and characterization of the actuators, and finally highlights some physic based actuation concepts through models and correlations. The following is a list of these contributions:

- The first major contribution is the determination of a correlation between capacitance and mechanical strain. This correlation indicates that the actuation response in ionic polymers is directly related to the charge displacement in the material. This result has a major impact on the modeling and on the understanding of the actuation mechanisms.

- The second major contribution is the development of a fabrication process which allows good control on the composition of ionic polymer transducers. This process, called the Direct Assembly Process, facilitates the study of different diluents in ionomeric actuators. This resulted in a dry actuator with EmI-Tf ionic liquid diluents that can operate in air for over 250000 cycles. The DAP allows the variation in the electrode architecture which enabled us to fabricate dry transducers with 50x better performance compared to transducers made using the impregnation-reduction technique. DAP fabricated transducers achieved a strain of 9.38% at a strain rate of 1%/s. This DAP allows variation of several other transducer parameters including the ionomer used leading to more performance.

- Finally, an extensional actuation mechanism in ionomeric polymer transducers is reported for the first time in this dissertation. This actuation mechanism enables a new

class of ionic polymer transducers with large force and small displacement. Furthermore this actuation mechanism leads to the development of an active areas model that emphasizes the importance of the boundary layer on the conductor-ionomer interfacial area.

6.3 Future Work

Three main recommendations for future works will be presented in this section.

- The first recommendation is to further optimize the DAP process by studying different ionic liquids as diluents with less viscosity. We can further increase the conductivity of the electrode by adding other materials and enhance their dispersion especially in the case of the SWNT.

- A second idea is to apply a similar study to the sensing properties in ionic polymer transducers. In this dissertation we focused solely on the actuation side of the transducers; while mechanical deformation sensing is a very important application area for such transducers.

- The last future work recommendation is to further understand the physical actuation mechanism by exploring the active area model especially in the extensional mode. Several electrode material could be incorporated using the DAP process and study their effect on the charge strain correlation. Also further optimizing this model we should be able to produce bending and extensional ionic polymer transducers with increased energy densities.

6.4 Conclusions

Actuation in ionic polymer transducers is charge driven. Increasing the capacitance of the actuator increases the bending response of the transducer. Capacitance in such polymers is electric double layer and therefore increased by increasing the conductor-ionomer interfacial surface area. Strain rate in ionic polymer actuators correlates to the speed of injection of cations in and out of the electrode area. This is controlled by the conductivity of the electrode that is modeled using percolation theory. Viscosity and polarity of the diluent

in the transducer is critical to the speed of response. An electromechanical model with a quadratic term is proved to model the actuation response in ionic polymer transducers. This model is associated with a bimorph model that assumes the electrodes to be the active areas. Such model emphasized the importance of the boundary layer area. First harmonic distortion in the bending response increases for assymetric electrode and eliminated for perfectly symmetric electrode.

Bibliography

Akle, B. J., Bennett, M. D., and Leo, D. J., 2004a, "High-strain ionomeric - ionic liquid composites via electrode tailoring," in: *Proceedings of the 2004 ASME International Mechanical Engineering Congress (Submitted to sensors and actuators A: physical)*, Vol. 2004-61246.

Akle, B. J., Hickner, M. A., Leo, D. J., and McGrath, J. E., 2005, "Correlation of Capacitance and Actuation in Ionomeric Polymer Transducers," *Journal of Material Science*, Vol. 40, pp. 3715–3724.

Akle, B. J. and Leo, D. J., 2003, "Consideration of Ionic Polymer Materials as Flapping Mechanisms for Micro-Air Vehicles," in: *Proceedings of the 44th AIAA/ASME/ASCE/AHS/ASC Structures, Structural Dynamics, and Materials Conference*, Vol. 2003-1438.

Akle, B. J., Wiles, K., Leo, D. J., and McGrath, J. E., 2004b, "Effects of Electrode Morphology on The Performance of BPSH and PATS Ionic Polymer Transducers," in: *Proceeding of the EAP Actuators And Devices. SPIE*, Vol. 5385-73.

Asaka, K., Fujiwara, N., Oguro, K., Onishi, K., and Sewa, S., 2001a, "State of water and ionic conductivity of solid polymer electrolyte membranes in relation to polymer actuators," *Journal of Electroanalytical Chemistry*, Vol. 505, pp. 24–32.

Asaka, K., Fujiwara, N., Oguro, K., Onishi, K., and Sewa, S., 2001b, "State of water and ionic conductivity of solid polymer electrolyte membranes in relation to polymer actuators," *Journal of Electromechanical Chemistry*, Vol. 505, pp. 24–32.

Bar-Cohen, Y., ed., 2001, *Electroactive Polymer Actuators as Artificial Muscles*, SPIE Press, Bellingham, WA.

Barisci, J. N., Spinks, G. M., Wallace, G. G., Madden, J. D., and Baughman, B. H., 2003, "Increased actuation rate of electromechanical carbon nanotube actuators using potential pulses with resistance compensation," *Smart Materials and Structures*, Vol. 12 (4), pp. 549–555.

Baughman, R. H., Chanxing, C., Zakhidov, A. A., Iqbal, Z., Barisci, J. N., Spinks, G. M., Wallace, G. G., Mazzoldi, A., Rossi, D. D., Rinzler, A. G., Jaschinski, O., Roth, S., , and Kertesz, M., 1999, "Carbon nanotube actuators," *Science*, Vol. 284, pp. 1340–1344.

Bennett, M. and Leo, D. J., 2003, "Manufacture and characterization of ionic polymer transducers employing non-precious metal electrodes," *Smart Materials and Structures*, Vol. 12, pp. 424 436.

Bennett, M. and Leo, D. J., 2005, "Morphological and electromechanical characterization of ionic liquid/Nafion polymer composites," in: *Proceeding of the EAP Actuators And Devices. SPIE*, Vol. 5759, pp. 506–517.

Bennett, M. D. and Leo, D. J., 2004, "Ionic Liquids as Solvents for Ionic Polymer Transducers," *Sensors and Actuators A: Physical*, Vol. 115, pp. 79–90.

Bockris, J., Devanathan, M., and Muller, K., 1963, "On the structure of charged interfaces," *Proc. R. Soc. London A*, Vol. 274, pp. 55 79.

Bonhote, P., Dias, A. P., Papageorgiou, N., Kalyanasundaram, K., and Gr tzel, M., 1996, "Hydrophobic, highly conductive ambient-temperature molten salts," *Inorganic Chemistry*, Vol. 35, pp. 1168–1178.

Broadbent, S., 1954, "Discussion on symposium on Monte Carloo methods," *Journal of Royal Statistics Society B*, Vol. 68.

Broadbent, S. R. and Hammersley, J. M., 1957, "Percolation processes. Crystals and mazes," *Proceedings Cambridge Philosophy Society*, Vol. 53, pp. 629–641.

Buechler, M. A. and Leo, D. J., 2004, "Electromechanical Model of an Active Polymer Thin Circular Disk," in: *Proceeding of the ASME Dynamic Systems and Controls Division: 2004 IMECE*, Vol. IMECE 2004-61477.

Cahan, B. and Wainwright, J., 1993, "AC Impedance Investigations of Proton Conduction in Nafion," *Journal of the Electrochemical Society*, Vol. 140, No. 12, pp. L185–L186.

Chapman, D., 1913, "A contribution to the theory of electrocapillarity," *Philos. Mag.*, Vol. 25, pp. 475 481.

Cheng, Z., Bharti, V., Xu, T., Xu, H., Mai, T., and Zhang, Q. M., 2001, "Electrostrictive P(VDF-TrFE) Copolymers," *Sensors and Actuators A-Phys.*, Vol. 90, pp. 138–147.

Conway, B. E., 1999, *Electrochemical Supercapacitors: Scientific Fundamentals and Technological Applications*, Kluwer Academic/ Plenum Publishers.

Conway, B. E., Birss, V., and Wojtowicz, J., 1997, "The role and utilization of pseudocapacitance for energy storage by supercapacitors," *Journal of Power Sources*, Vol. 66, pp. 1–14.

Cooper, E. I. and O'Sullivan, E. J., 1992, "New,Stable, Ambient- Temperature Molten Salts," *In Proceedings of the Eighth Interational Symposium on Molten Salts, The Electrochemical Society*, pp. 386–396.

Cross, L. E. and Rossetti, G. A., 1991, "Origin of the first-order phase change at the Curie temperature in KNbO[sub 3]," *Journal of Applied Physics*, Vol. 69, No. 2, pp. 896–898.

Daniel, V. V., 1967, *Dielectric Relaxation*, Academic Press.

de Gennes, P., Okumura, K., Shahinpoor, M., and Kim, K. J., 2000, "Mechanoelectric Effects in Ionic Gels," *Europhysics Letters*, Vol. 50, No. 4, pp. 513–518.

de Gennes, P. and Seances, C., 1975, *Acad. Sci.*, Vol. Ser. B 281, No. 101, pp. L185–L186.

Ding, J., Liu, L., Spinks, G. M., Zhou, D., Wallace, G. G., and Gillespie, J., 2003, "High performance conducting polymer actuators utilizing a tubular geometry and helical wire interconnects," *Synthetic Metals*, Vol. 138(3), pp. 391–398.

Domb, C., 1983, *The Percolation Transition*, Chap. 2, Annals of the Israel Physical Society.

Dow, 2005a, "Tetraethylene Glycol Product Guide," *The Dow Chemical Company*, Vol. http://www.dow.com/ethyleneglycol/resources/index.htm, pp. 612–00005–0704X.

Dow, 2005b, "Triethylene Glycol Product Guide," *The Dow Chemical Company, http://www.dow.com/ethyleneglycol/resources/index.htm*, Vol. www.dow.com, pp. 612–00004–0704X8.

Endo, M., Takeda, T., Kim, Y. J., Koshiba, K., and Ishii, K., 2001, "High power electric double layer capacitor (EDLC's); from operating principle to pore size control in advanced activated carbons," *Carbon science*, Vol. 1, pp. 117–128.

Etebari, A., Akle, B. J., Farinholt, K., Bennett, M., Leo, D. J., and Vlachos, P. P., 2004, "The use of active ionic polymers in Dynamic skin friction measurements," in: *Proceedings of the 2004 Heat Transfer/Fluids Engineering Conference*, Vol. HT-FED2004-56837.

Ewins, D., 2000, *Model Testing theory, practice and application*, Research Studies Press LTD, 2nd Edition, England.

Farinholt, K. and Leo, D., 2002, "Modeling of Electromechanical Charge Sensing in Ionic Polymer Transducers," *to appear in Mechanics of Materials.*

Farinholt, K. M., Leo, D. J., and Vlachos, P. P., 2005, "Electrical impedance modeling of ionic polymer transducers," in: *Proceedings of the 2005 Heat EAP SPIE Conference*, Vol. 5761-10.

Fontanella, J., McLin, M., Wintersgill, M., Calame, J., and Greenbaum, S., 1993, "Electrical impedance studies of acid form Nafion membranes," *Solid State Ionics*, Vol. 66, pp. 1–4.

Frackowiak, E. and Beguin, F., 2001, "Review: Carbon materials for the electrochemical storage of energy in capacitors," *Carbon* ., Vol. 39, pp. 937 950.

Fujiwara, N., Asaka, K., Nishimura, Y., Oguro, K., and Torikai, E., 2000, "Preparation of Gold-Solid Polymer Electrolyte Composites As Electric Stimuli-Responsive Materials," *Chem. Mater.*, Vol. 12, pp. 1750–1754.

Funakubo, H., 1987, *Shape Memory Alloys*, Gordon and Breach, New York.

Gouy, G., 1910, "Constitution of the electric charge at the surface of an electrolyte," *J Physique*, Vol. 9, pp. 457 467.

Grahame, D., 1947, "The electrical double layer and the theory of electrocapillarity," *Chem*, Vol. Rev 41, pp. 79–85.

Gray, M., 1987, *Polymer Electrolyte Reviews-1*, edited by J. R. MacCallum and C. A. Vincent Kluwer Academic, Dordrecht, p. 139.

Grzeszczuk, M. and Poks, P., 1995, "Analysis of charge transport impedance in the reduction of thin films of conducting polyaniline in aqueous trichloroacetic acid solutions," *Journal of Electroanalytical Chemistry*, Vol. 387, pp. 441 501.

Hickner, M., Kim, Y., Wang, F., Zawodzinski, T., and McGrath, J., 2001, in: *Proceedings of the American Society for Composites, Sixteenth Technical Conference*, pp. 323–336.

Inman, D. J., 2000, *Engineering Vibration*, Prentice-Hall, New Jersey.

Kim, K. J. and Shahinpoor, M., 2003, "Ionic polymer-metal composites: II. Manufacturing techniques," *Smart Materials and Structures*, Vol. 12, pp. 65–79.

Kim, Y., Dong, L., Hickner, M., Glass, T., Webb, V., and McGrath, J., 2003, "State of Water in Disulfonated Poly(arylene ether sulfone) Copolymers and a Perfluorosulfonic Acid Copolymer (Nafion) and Its Effect on Physical and Electrochemical Properties," *Macromolecules*, Vol. 36, No. 17.

Kitahara, A. and Watanabe, A., 1984, *Electrical phenomena at interfaces : fundamentals, measurements, and applications*, Vol. 15, M. Dekker, New York.

Kornbluh, R., Perline, R., Joseph, J., Heydt, R., Pei, Q., and Chiba, S., 1999, "High-field electrostriction of elastomeric polymer dielectrics for actuation,," *International Symposium on Smart Structures and Materials: Electroactive polymer actuator and devices, (EAPAD) in SPIE proceeding*, Vol. 3669, pp. 149–161.

Kothera, C. S. and Leo, D. J., 2005, "Identification of the Nonlinear Response of Ionic Polymer Actuators using the Volterra Series," *Journal of Vibration and Control*, Vol. 11(4), pp. 519–541.

Kotz, R. and Carlen, M., 2000, "Principles and applications of electrochemical capacitors," *Electrochim. Acta*, Vol. 45, pp. 2483 2498.

Lendlein, A. and Langer, R., 2002, "Biodegradable, Elastic Shape-Memory Polymers for Potential Biomedical Applications," *Science*, Vol. 296(5573), pp. 1673–1676.

Leo, D. J., 2001, "ME5984: Smart Structures/ Active Material Systems," *Virginia Tech courses*, Vol. 1, No. 1.

Leo, D. J., Farinholt, K., and Wallmersperger, T., 2005, "Computational models of ionic transport and electromechanical transduction in ionomeric polymer transducers," in: *Proceeding of the SPIE Smart Structures and Materials 2005: Electroactive Polymer Actuators and Devices (EAPAD)*, Vol. 5759, pp. 170–181.

Leo, D. J., Kothera, C., and Farinholt, K., 2003, "Constitutive Equations for an Induced-strain Bending Actuator with a Variable Substrate," *Journal of Intelligent Material Systems and Structurs*, Vol. 14, pp. 707–718.

Levitsky, I. A., Kanelos, P. T., and Euler, W. B., 2004, "Novel Actuating System Based on a Composite of Single-Walled Carbon Nanotubes and an Ionomeric Polymer," in: *Materials Research Society Symposium Proceedings*, Vol. 785.

Liang, C. and Rogers, C., 1992, "Multi-dimensional constitutive model for shape memory alloys," *Journal of Engineering Mathematics*, Vol. 26 (3), pp. 429–443.

Lindler, J. and Wereley, N., 1999, "Double adjustable shock absorbers using electrorheological fluid," *Journal of Intelligent Material Systems and Structures*, Vol. 10 (8), pp. 652–657.

Madden, J. D., Madden, P. G., and Hunter, I. W., 2002, "Conducting polymer actuators as engineering materials," in: *Proceeding of SPIE Smart Structures and Materials*, no. 4695, pp. 176–190.

Madden, J. D., Vandesteeg, N., Anquetil, P. A., Madden, P. G., Takshi, A., Pytel, R. R., Lafontaine, S. R., Wieringa, P. A., and Hunter, I. W., 2004, "Artificial Muscle Technology: Physical Principles and Naval Prospects," .

Mauritz, K., 1989, "Dielectric Relaxation Studies of Ion Motions in Electrolyte-Containing Perfluorosulfonate Ionomers. 4.Long-Range Ion Transport," *Macromolecules*, Vol. 22, pp. 4483–4488.

Mauritz, K. and Fu, R., 1988, "Dielectric Relaxation Studies of Ion Motions in Electrolyte-Containing Perfluorosulfonate Ionomers. 1. NaOH and NaCl Systems," *Macromolecules*, Vol. 21, pp. 1324–1333.

Mauritz, K. and Yun, H., 1988, "Dielectric Relaxation Studies of Ion Motions in Electrolyte-Containing Perfluorosulfonate Ionomers. 2. CH3COONa, KC1, and KI Systems," *Macromolecules*, Vol. 21, pp. 2738–2743.

MeGlobal, 2005, "Diethylene GlycolProduct Guide," http : //www.meglobal.biz/literature/product_guides/MEGlobal_DEG.pdf.

Mozga, W., 2005, "Physiochemical Properties of Popular Liquids," http : //www.trimen.pl/witek/ciecze/old$_{l}$iquids.html.

Nemat-Nasser, S., 2002a, "Micro-mechanics of Actuation of Ionic Polymer-metal Composites," *Journal of Applied Physics*, Vol. 92, No. 5, pp. 2899–2915.

Nemat-Nasser, S., 2002b, "Micromechanics of Actuation of Ionic Polymer-metal Composites," *Journal of Applied Physics*, Vol. 92, No. 5.

Nemat-Nasser, S. and Li, J., 2000, "Electromechanical Response of Ionic Polymer Metal Composites," in: *Proceedings of the SPIE*, Vol. 3987, pp. 82–91.

Nemat-Nasser, S. and Thomas, C. W., 2001, "Ionomeric Polymer-Metal Composites," in: *Electroactive Polymer Actuators as Artificial Muscles*, Chap. 6, SPIE Press, Bellingham, WA, pp. 139–191.

Nemat-Nasser, S. and Wu, Y., 2003a, "Comparative experimental study of ionic polymer metal composites with different backbone ionomers and in various cation forms," *Journal of Applied Physics*, Vol. 93, No. 9, pp. 5255–5267.

Nemat-Nasser, S. and Wu, Y., 2003b, "Comparative experimental study of ionic polymer metal composites with different backbone ionomers and in various cation forms," *Journal of Applied Physics*, Vol. 93 (9), pp. 5255–5267.

Newbury, K. M. and Leo, D. J., 2002, "Electromechanical Modeling and Characterization of Ionic Polymer Benders," *Journal of Intelligent Material Systems and Structures*, Vol. 13, No. 1, pp. 51–60.

Newbury, K. M. and Leo, D. J., 2003a, "Linear Electromechanical Model of Ionic Polymer Transducers Part I: Model Development," *Journal of Intelligent Material Systems and Structures*, Vol. 14, No. 6, pp. 333–342.

Newbury, K. M. and Leo, D. J., 2003b, "Linear Electromechanical Model of Ionic Polymer Transducers Part II: Experimental Validation," *Journal of Intelligent Material Systems and Structures*, Vol. 14, No. 6, pp. 343–358.

Oguro, K., Fujiwara, N., Asaka, K., Onishi, K., and Sewa, S., 1999, "Polymer electrolyte actuator with gold electrodes," in: *Proceedings of the SPIE*, Vol. 3669, pp. 63–71.

Oguro, K., Kawami, Y., and Takenaka, H., 1992, "Bending of an Ion-Conducting Polymer Film-Electrode Composite by an Electric Stimulus at Low Voltage," *Journal of Micromachine Society*, Vol. 5, pp. 27–30.

Osada, Y., Okuzaki, H., and Hori, H., 1992, "A polymer gel with electrically driven motility," *Nature*, Vol. 355, pp. 242–244.

Park, C., Ounaies, Z., Watson, K. A., Pawlowski, K., Lowther, S., Connell, J., Siochi, E., Harrison, J. S., and Clair, T. L. S., 2002a, "Polymer-Single Wall Carbon Nanotube Composites for Potential Spacecraft Applications," in: *Materials Research Society Symposium Proceedings*, Vol. 706.

Park, C., Ounaies, Z., Watson, K. A., Pawlowski, K., Lowther, S. E., Connell, J. W., Siochi, E. J., Harrison, J. S., and Clair, T. L. S., 2002b, "Polymer-Single Wall Carbon Nanotube Composites for Potential Spacecraft Applications," in: *Proceedings of Materials Research Society Symposium*, Vol. 706.

Pelrine, R., Kornbluh, R., Pei, Q., and Joseph, J., 2000, "High-Speed Electrically Actuated Elastomers with Strain Greater Than 100%," *Science*, Vol. 287, No. 5454, pp. 836–839.

Prasad, K. R. and Munichandraiah, N., 2002, "Fabrication and evaluation of 450 F electrochemical redox supercapacitors using inexpensive and high-performance, polyaniline coated, stainless-steel electrodes," *Journal of Power Sources*, Vol. 112, pp. 443 451.

Sadeghipour, K., Salomon, R., and Neogi, S., 1992, "Development of a Novel Electrochemically Active Membrane and Smart Material based Vibration Damper," *Smart Materials and Structures*, Vol. 1, pp. 3445–3447.

Shahinpoor, M., 1994, "Continuum Electromechanics of Ionic Polymeric Gels as Artificial Muscles for Robotic Applications," *Smart Structures and Materials*, Vol. 3, pp. 367–372.

Shahinpoor, M., Bar-Cohen, Y., Simpson, J., and Smith, J., 1998, "Ionic Polymer-Metal Composites (IPMCs) as Biomimetic Sensors, Actuators and Artificial Muscles - a Review," *Smart Materials and Structures*, Vol. 7, No. 6, pp. R15–R30.

Shahinpoor, M. and Kim, K. J., 2002a, "Novel Ionic Polymer-metal composites equipped with physically loaded particulate electrodes as biomimetic sensors, actuators and artificial muscles," *Sensors and Actuators A*, Vol. 96, pp. 125–132.

Shahinpoor, M. and Kim, K. J., 2002b, "A novel method of manufacturing three-dimensional ionic polymer-metal composites (IPMCs) biomimetic sensors, actuators and artificial muscles," *Polymer*, Vol. 43, pp. 797–802.

Shahinpoor, M. and Kim, K. J., 2002c, "Solid-state soft actuator exhibiting large electromechanical effect," *Applied Physics Letters*, Vol. 80, No. 18, pp. 91–94.

Sparnaay, M., 1972, Vol. 4 of *first edition*, Pergamon Press(Australia) Pty. Ltd., Sydney.

Stauffer, D. and Aharony, A., 1992, Vol. 4, Taylor and Francis, London.

Stern, O., 1924, "Zur theorie der elektrolytischen doppelschicht," *Z Elektrochem*, Vol. 30, pp. 508 516.

Sugimoto, W., Kizaki, T., Yokoshima, K., Murakami, Y., and Takasu, Y., 2004, "Evaluation of the pseudocapacitance in RuO2 with a RuO_2/GC thin film electrode," *Electrochimica Acta*, Vol. 49, pp. 313 320.

Supriya, L., Akle, B. J., Leo, D. J., and O.Claus, R., 2005, "Assembly of Au Electrodes on Polymeric Sensors and Actuators using a Poly(urethane urea) Linking Agent," *submitted to the IEEE Sensors Journal*.

Taegeun, N., Suk, T. Y., Jae-Do, N., Wook, J. J., Mo, K. H., Hyoukryeol, C., and Sik, B. S., 2001, "Development of large-surface Nafion-metal composite actuator and its electrochemical characterization," in: *Proceedings of the SPIE*, Vol. 4329, pp. 458–465.

Tamagawa, H., Nogata, F., Watanabe, T., Abe, A., Yagasaki, K., and Jin, J. Y., 2003, "Influence of metal plating treatment on the electric response of Nafion," *Journal of Materials Science*, Vol. 38, pp. 1039 1044.

von Helmholtz, H. L. F., 1853, "Ueber einige gesetze der vertheilung elektrischer strome in korperlichen leitern mit anwendung auf die thierisch-elektrischen versuche," *Ann. Phys. Chem.*, Vol. (Ser.1) 89, No. 4, pp. 211 233.

Wang, F., Hikner, M., Kim, Y., Zawodzinski, T., and McGrath, J., 2002, "Direct polymerization of sulfonated poly(arylene ether sulfone) random (statistical) copolymers: candidates for new proton exchange membranes," *J. Membr. Sci*, Vol. 197, pp. 231–242.

Watanabe, M., Suzuki, M., Hirako, Y., Shirai, H., and Hirai, T., 2001, "Hysteresis in Bending Electrostriction of Polyurethane Films," *Journal of Applied Polymer Science*, Vol. 79, pp. 1121– 1126.

Welch, P. D., 1967, "The Use of Fast Fourier Transform for the Estimation of Power Spectra: A Method Based on Time Averaging Over Short, Modified Periodograms," *IEEE Trans. Audio Electroacoustics*, Vol. AU-15, pp. 70–73.

Wesley, F. J., 2003, "Electromechanical Modeling of Encapsulated Ionic Polymer Transducers," *Masters Thesis Virginia Tech.*

Wiles, K., Bhanu, V., Wang, F., and J.E.McGrath, 2002, "Synthesis and Characterization of Poly(arylene sulfide sulfone) Copolymers as Candidates for Proton Exchange Membranes," *Polymer Preprints*, Vol. 43(2), pp. 993–994.

Wintersgill, M. C. and Fontanella, J. J., 1997, "Complex Impedance Measurements on Nafion," *Electrochimica Acta*, Vol. 43, pp. 1533–1538.

Zallen, R., 1983, *Introduction To Percolation: A Model For All Seasons*, Chap. 1, Annals of the Israel Physical Society.

Zhang, Q. M., 1998, "Displacement properties of RAINBOW and THUNDER piezoelectric actuators," *Sensors and Actuators A*, Vol. 69, pp. 33–38.

Vita

Barbar J. Akle was born in Zgharta, Lebanon, on July 31, 1978. He received a BE in Mechanical Engineering with distinction from the American University of Beirut in 2001. After graduation he moved to Virginia Tech where he received a Master of Science in June of 2003 and Doctoral degree in July 2005 both in Mechanical Engineering under the supervision of Dr. Donald Leo in the Center for Intelligent Material Systems and Structures. Recent research accomplishments include the development of the Direct Assembly Process, characterization of extensional actuation in ionic polymer transducers and enhancing their bending actuation response. Furthermore, Barbar has studied their possible employment in applications such as flapping mechanisms for micro air vehicles or as fluid shear sensors. Barbar has authored five journal papers and more than fifteen conference proceedings presented at highly respected conferences in the area of active materials. He is the receiver of the creative achievement award from the American University of Beirut in 2001. Barbar is currently pursuing his work as a research scientist in the Center for Intelligent Material Systems and Structures. Other than the topics presented in this dissertation, his research interests include biologicaly inspired systems and self healing structures.

Permanent Address: 300 Durham Hall
Blacksburg, VA 24061, USA

This dissertation was typeset with LaTeX 2$_\varepsilon$[1] by the author.

[1] LaTeX 2$_\varepsilon$ is an extension of LaTeX. LaTeX is a collection of macros for TeX. TeX is a trademark of the American Mathematical Society. The macros used in formatting this dissertation were written by Greg Walker, Department of Mechanical Engineering, Virginia Tech.